

# **Advanced Calibration for Device Simulation User Guide**

---

Version T-2022.03, March 2022

**SYNOPSYS®**

# Copyright and Proprietary Information Notice

© 2022 Synopsys, Inc. This Synopsys software and all associated documentation are proprietary to Synopsys, Inc. and may only be used pursuant to the terms and conditions of a written license agreement with Synopsys, Inc. All other use, reproduction, modification, or distribution of the Synopsys software or the associated documentation is strictly prohibited.

## Destination Control Statement

All technical data contained in this publication is subject to the export control laws of the United States of America. Disclosure to nationals of other countries contrary to United States law is prohibited. It is the reader's responsibility to determine the applicable regulations and to comply with them.

## Disclaimer

SYNOPSYS, INC., AND ITS LICENSORS MAKE NO WARRANTY OF ANY KIND, EXPRESS OR IMPLIED, WITH REGARD TO THIS MATERIAL, INCLUDING, BUT NOT LIMITED TO, THE IMPLIED WARRANTIES OF MERCHANTABILITY AND FITNESS FOR A PARTICULAR PURPOSE.

## Trademarks

Synopsys and certain Synopsys product names are trademarks of Synopsys, as set forth at <https://www.synopsys.com/company/legal/trademarks-brands.html>.

All other product or company names may be trademarks of their respective owners.

## Free and Open-Source Licensing Notices

If applicable, Free and Open-Source Software (FOSS) licensing notices are available in the product installation.

## Third-Party Links

Any links to third-party websites included in this document are for your convenience only. Synopsys does not endorse and is not responsible for such websites and their practices, including privacy practices, availability, and content.

[www.synopsys.com](http://www.synopsys.com)

# Contents

---

Conventions . . . . .	6
Customer Support . . . . .	7
<hr/>	
<b>1. Introduction to Advanced Calibration Device . . . . .</b>	8
Overview of Advanced Calibration Device . . . . .	8
Location of Advanced Calibration Device Files . . . . .	8
Target Devices and Technologies . . . . .	9
Content of Parameter Files . . . . .	9
Special Parameter Files . . . . .	19
Using Advanced Calibration Device . . . . .	20
<hr/>	
<b>2. Guide to Device Simulations . . . . .</b>	21
Specifying Simulation Cases . . . . .	21
Accessing Parameter Files and Model Frameworks . . . . .	22
Path A: Basic CMOS Simulation Command File Sections . . . . .	22
Path B: Add Influence of Mechanical Stress to Physics Section Shown in Path A . . . . .	23
Path C: Add High-k Mobility Degradation to Physics Section Shown in Path B . . . . .	25
Path D: Thin-Layer MOS Simulations Including Thin-Film Effects . . . . .	26
Path E: FinFET Simulations . . . . .	27
Path F: Smart-Power HVMOS and LDMOS Devices . . . . .	28
Path G: GaN HEMT Simulations . . . . .	29
Path H: SiC Diode Simulations . . . . .	30
Path I: InGaAs FinFET Simulations . . . . .	32
References . . . . .	34
<hr/>	
<b>3. Calibration Methodology for Device Simulations . . . . .</b>	35
Calibration of CMOS Devices . . . . .	35
C–V Calibration . . . . .	35

## Contents

---

I <sub>d</sub> –V <sub>g</sub> Mobility Calibration . . . . .	37
Calibration of Parasitic Series Resistance . . . . .	39
I <sub>d</sub> –V <sub>g</sub> Mobility Calibration at Low-Drain Bias Voltage . . . . .	40
I <sub>d</sub> –V <sub>g</sub> Mobility Calibration at High-Drain Bias Voltage . . . . .	41
References . . . . .	42
<hr/>	
<b>4. Descriptions of Models . . . . .</b>	43
Overview of Models . . . . .	43
CMOS Devices . . . . .	43
Unstrained Band Structure and Electrostatics . . . . .	43
Strained Band Structure and Electrostatics . . . . .	43
Unstrained Low-Field Mobility . . . . .	44
Strained Low-Field Mobility . . . . .	47
Influence of Mechanical Stress . . . . .	47
First-Order (Linear) Piezoresistance Mobility Model . . . . .	49
Second-Order Piezoresistance Mobility Model . . . . .	50
Nonlinear Piezoresistance Models for Electrons and Holes (MCmob and SBmob) . . . . .	50
Intel Stress-Induced Hole Mobility Model (hSixBand) . . . . .	51
eSubband Model for Electrons . . . . .	51
hSubband Model for Holes . . . . .	52
Unstrained High-Field Mobility . . . . .	52
Strained High-Field Mobility . . . . .	53
Gallium Nitride HEMTs . . . . .	54
Silicon Carbide Devices . . . . .	54
Silicon Smart-Power Devices . . . . .	54
<hr/>	
<b>5. Quality of Fitting and Extraction . . . . .</b>	55
Low-Field Mobility of Planar CMOS Devices With Silicon Channel . . . . .	55
Oxide–Silicon Interface . . . . .	55
Influence of Metal Gate on Inversion Layer Mobility . . . . .	62
Influence of High-k Gate Stack on Inversion Layer Mobility . . . . .	63
Extraction of Contact Resistance Parameters . . . . .	64
Extraction of Parameters for Mobility Models in Accumulation Regime . . . . .	65
Basic Properties of Silicon Carbide Devices . . . . .	66
Basic Properties of Gallium Nitride Devices . . . . .	74

## Contents

Basic Properties of Indium Gallium Arsenide Devices . . . . .	75
Permittivity . . . . .	75
Lattice Heat Capacity . . . . .	75
Thermal Conductivity . . . . .	76
Band Gap and Electron Affinity . . . . .	76
Density-of-States . . . . .	77
Bandgap Narrowing . . . . .	79
Quantization Effects . . . . .	80
Low-Field Bulk Mobility and Its Doping Dependency . . . . .	83
Philips Unified Mobility Model . . . . .	85
Inversion Layer Mobility . . . . .	86
Inversion and Accumulation Layer Mobility Model . . . . .	86
Interface Charge Mobility Model . . . . .	88
Strained Low-Field Mobility . . . . .	89
Multivalley Electron Mobility Model . . . . .	89
Piezoresistance Mobility Model . . . . .	90
Basic Properties of Silicon Germanium Devices . . . . .	90
Permittivity . . . . .	90
Thermal Conductivity . . . . .	90
Band Structure . . . . .	91
Bulk Low-Field Mobility . . . . .	93
Ballistic Mobility . . . . .	94
References . . . . .	96
<hr/>	
A. Physical Model Interface Models . . . . .	103
Features of the MCmob and SBmob Models . . . . .	103
Parameters . . . . .	104
Specifying Device Coordinate Systems . . . . .	108
Specifying Local Coordinate Systems . . . . .	108
Using Parameters . . . . .	110
Parameter Interface . . . . .	111
Parameter Interface and Equations of SBmob Model . . . . .	112
PMI for Calculating the Sheet Resistance . . . . .	114

# About This Guide

---

The Synopsys® Sentaurus™ Device tool is a quantum drift-diffusion device simulator that solves semiconductor equations in one, two, or three spatial dimensions.

Extensions for hydrodynamic transport, solving the heat conduction equation, and many other features are also available. Because of the many models and corresponding model parameters and their dependency on fabrication processes and device types, it is difficult to derive automatically a well-adjusted device simulation environment for specific simulation tasks. Therefore, preselection of models and precalibration of parameter sets are necessary. Advanced Calibration Device refers to the preselection of models and the precalibration of parameter sets.

This user guide describes the contents and use of the Advanced Calibration Device files and is designed to give users fast access to parameter sets and model selections needed for device simulation. This user guide is intended for users who are familiar with Sentaurus Device and want to achieve a higher accuracy in device simulation. See the *Sentaurus™ Device User Guide*.

For additional information, see:

- The TCAD Sentaurus release notes, available on the Synopsys SolvNetPlus support site (see [Accessing SolvNetPlus on page 7](#))
- Documentation available on the SolvNetPlus support site

---

## Conventions

The following conventions are used in Synopsys documentation.

Convention	Description
Courier font	Identifies text that is displayed on the screen or that the user must type. It identifies the names of files, directories, paths, parameters, keywords, and variables.
<i>Italicized text</i>	Used for emphasis, the titles of books and journals, and non-English words. It also identifies components of an equation or a formula, a placeholder, or an identifier.

## Customer Support

Customer support is available through the Synopsys SolvNetPlus support site and by contacting the Synopsys support center.

---

### Accessing SolvNetPlus

The SolvNetPlus support site includes an electronic knowledge base of technical articles and answers to frequently asked questions about Synopsys tools. The site also gives you access to a wide range of Synopsys online services, which include downloading software, viewing documentation, and entering a call to the Support Center.

To access the SolvNetPlus site:

1. Go to <https://solvnetplus.synopsys.com>.
  2. Enter your user name and password. (If you do not have a Synopsys user name and password, follow the instructions to register.)
- 

### Contacting Synopsys Support

If you have problems, questions, or suggestions, you can contact Synopsys support in the following ways:

- Go to the Synopsys [Global Support Centers](#) site on [www.synopsys.com](http://www.synopsys.com). There you can find email addresses and telephone numbers for Synopsys support centers throughout the world.
  - Go to either the Synopsys SolvNetPlus site or the Synopsys Global Support Centers site and open a case (Synopsys user name and password required).
- 

### Contacting Your Local TCAD Support Team Directly

Send an email message to:

- [support-tcad-us@synopsys.com](mailto:support-tcad-us@synopsys.com) from within North America and South America
- [support-tcad-eu@synopsys.com](mailto:support-tcad-eu@synopsys.com) from within Europe
- [support-tcad-ap@synopsys.com](mailto:support-tcad-ap@synopsys.com) from within Asia Pacific (China, Taiwan, Singapore, Malaysia, India, Australia)
- [support-tcad-kr@synopsys.com](mailto:support-tcad-kr@synopsys.com) from Korea
- [support-tcad-jp@synopsys.com](mailto:support-tcad-jp@synopsys.com) from Japan

# 1

## Introduction to Advanced Calibration Device

---

*This chapter introduces the use of Advanced Calibration Device in Sentaurus Device simulations.*

---

### Overview of Advanced Calibration Device

Advanced Calibration Device is a set of models and parameters that is recommended for device simulations of certain device types and technologies. This set of models and parameters is contained in text files, which standard text editors can open.

You select the standard Synopsys calibration by starting Sentaurus Device with the corresponding Advanced Calibration Device command file section and by loading the Advanced Calibration Device parameter file from that command file.

For more information about how to use the command file that defines models and the parameter file that defines the parameters of the models selected in the command file, see the *Sentaurus™ Device User Guide*.

This user guide describes the parameter file and command file sections for Advanced Calibration Device.

---

### Location of Advanced Calibration Device Files

Each release of TCAD Sentaurus provides new Advanced Calibration Device files that include the latest set of models and parameters. The `MaterialDB` folder of the standard installation of Sentaurus Device stores the parameter files and is located at:

`$STROOT/tcad/$STRELEASE/lib/sdevice/``MaterialDB`

See [Table 1 on page 11](#) for a list of the available material-related parameter files.

## Target Devices and Technologies

Advanced Calibration Device provides a set of parameters for CMOS technologies from micrometer dimensions down to the 7 nm node, including planar gate-first and gate-last technologies, nonplanar technologies for the 14 nm node, and technologies beyond 14 nm likely based on novel channel materials (silicon, SiGe, Ge, and III-V).

In addition, Advanced Calibration Device provides parameters and models for silicon smart-power and power devices (IGBT, LDMOS, NMOS, and PMOS), GaN HEMTs, InGaAs channel devices, SiC diodes, and SiC FETs.

The main process features of planar and nonplanar bulk and SOI technology nodes covered by the model and parameter sets are:

- Stress and crystallographic orientation engineering
- Poly/SiON or SiO<sub>2</sub> gate stacks and metal/HfO<sub>2</sub>/SiON or SiO<sub>2</sub> gate stacks
- Gate-first and gate-last technologies
- Silicon, germanium, SiGe, or InGaAs channels

For these devices and technologies, Advanced Calibration Device provides model selections and parameter sets for the simulation of the following device properties:

- Electrostatic properties and quantization
- Low-field and high-field mobility
- Stress dependency of mobility
- Ballistic resistance

**Note:**

The parameter sets must be considered as initial parameter sets, that is, starting points for further calibration.

---

## Content of Parameter Files

The information presented here relates to the models presented in [Chapter 2 on page 21](#) and to the files stored in the `MaterialDB` folder of Sentaurus Device.

[Table 1 on page 11](#) lists the content and features of the material-related parameter files. References and additional comments for the parameters can be found in the parameter files.

## **Chapter 1: Introduction to Advanced Calibration Device**

### Content of Parameter Files

When simulating silicon or SiGe CMOS, or silicon smart-power or power devices, you must load one or more of the following files:

- Silicon.par
- Germanium.par
- SiliconGermanium.par
- Siliconcl00.par
- Siliconcl10.par
- SiliconGermaniumc100.par
- SiliconGermaniumc110.par

When simulating wide-bandgap devices, depending on the material, you must load one or more of the following files:

- AlGaN.par, AlInGaN.par, AlInN.par, AlN.par
- Diamond.par
- Ga2O3.par
- GaN.par
- InGaN.par, InN.par

When simulating III–V arsenide devices, you must load one or more of the following files:

- AlAs.par
- AlGaAs.par
- GaAs.par
- InAs.par
- InGaAs.par

When simulating SiC devices, you must load one of the following files:

- SiliconCarbide.par
- 4H-SiC.par/4HSiC.par/SiC\_4H.par
- 6H-SiC.par

## Chapter 1: Introduction to Advanced Calibration Device

### Content of Parameter Files

Table 1 Parameter files in MaterialDB folder of Sentaurus Device

Parameter file	Material	Parameters
AlAs.par	AlAs	<ul style="list-style-type: none"><li>• Permittivity</li><li>• Heat capacitance</li><li>• Thermal conductivity</li><li>• Band gap and affinity</li><li>• Density-of-states</li><li>• Parameters in Multivalley section</li><li>• Optical parameters</li></ul> <p>Other model parameter sections are available in the parameter file but are not yet updated and reviewed.</p>
AlGaAs.par	AlGaAs	<ul style="list-style-type: none"><li>• Permittivity</li><li>• Heat capacitance</li><li>• Thermal conductivity</li><li>• Band gap and affinity</li><li>• Density-of-states</li><li>• Parameters in Multivalley section</li><li>• Optical parameters</li></ul> <p>Other model parameter sections are available in the parameter file but are not yet updated and reviewed.</p>

## Chapter 1: Introduction to Advanced Calibration Device

### Content of Parameter Files

Table 1 Parameter files in MaterialDB folder of Sentaurus Device (Continued)

Parameter file	Material	Parameters
AlGaN.par	AlGaN	<ul style="list-style-type: none"><li>For most models, mole fraction dependency is interpolated linearly between the corner materials GaN and AlN</li><li>U-shape of thermal conductivity is described by a piecewise linear spline function in the parameter file</li><li>Mole fraction-dependent band gap (parabolic interpolation)</li><li>Mole fraction-dependent mass is interpolated linearly between GaN and AlN for density-of-states calculation</li><li>Mole fraction-dependent mobility with doping dependency is described by a piecewise linear spline function in the parameter file</li><li>Mole fraction-dependent high field dependency is described by a piecewise linear spline function in the parameter file</li><li>Mole fraction-dependent impact ionization is described by a piecewise linear spline function in the parameter file</li></ul>
AlInGaN.par	AlInGaN	<ul style="list-style-type: none"><li>For most models, mole fraction dependency is interpolated linearly between the corner materials AlN, GaN, and InN</li></ul>
AlInN.par	AlInN	<ul style="list-style-type: none"><li>For most models, mole fraction dependency is interpolated linearly between the corner materials AlN and InN</li></ul>

## Chapter 1: Introduction to Advanced Calibration Device

### Content of Parameter Files

Table 1 Parameter files in MaterialDB folder of Sentaurus Device (Continued)

Parameter file	Material	Parameters
AlN.par	AlN	<ul style="list-style-type: none"><li>• Isotropic and anisotropic permittivity</li><li>• Thermal conductivity</li><li>• Lattice heat capacity</li><li>• Band gap and affinity</li><li>• Density-of-states and masses</li><li>• Mobility with doping dependency</li><li>• High field dependency</li><li>• Shockley–Read–Hall</li><li>• Auger</li><li>• Impact ionization</li><li>• Piezoelectric polarization</li><li>• Optical material properties</li><li>• Mechanical compliance parameters</li></ul>
CobaltSilicide.par	CoSi/CoSi <sub>2</sub>	<ul style="list-style-type: none"><li>• Permittivity</li><li>• Thermal conductivity</li><li>• Lattice heat capacity</li><li>• Resistivity</li><li>• Optical material parameters</li></ul>
Diamond.par	Diamond	<ul style="list-style-type: none"><li>• Isotropic and anisotropic permittivity</li><li>• Thermal conductivity</li><li>• Incomplete ionization</li><li>• Band gap and affinity</li><li>• Density-of-states</li><li>• Constant mobility</li><li>• High field dependency</li><li>• Impact ionization</li></ul>
Ga2O3.par	Ga <sub>2</sub> O <sub>3</sub>	<ul style="list-style-type: none"><li>• Permittivity</li><li>• Heat capacitance</li><li>• Thermal conductivity</li><li>• Band structure (band gap and affinity)</li><li>• Density-of-states for electrons</li><li>• High-field saturation</li><li>• Impact ionization</li></ul>

## Chapter 1: Introduction to Advanced Calibration Device

### Content of Parameter Files

Table 1 Parameter files in MaterialDB folder of Sentaurus Device (Continued)

Parameter file	Material	Parameters
GaAs.par	GaAs	<ul style="list-style-type: none"><li>• Permittivity</li><li>• Heat capacitance</li><li>• Thermal conductivity</li><li>• Band structure (band gap, affinity, and parameters for the Multivalley section)</li><li>• Bandgap narrowing</li><li>• Density-of-states</li><li>• Bulk and inversion mobility for different surface and channel orientations</li><li>• Quantization parameters</li><li>• Optical properties</li></ul> <p>Other model parameter sections are available in the parameter file but are not yet updated and reviewed.</p>
GaAsSb.par	GaAsSb	<ul style="list-style-type: none"><li>• Permittivity</li><li>• Heat capacitance</li><li>• Thermal conductivity</li><li>• Band gap and affinity</li><li>• Density-of-states</li><li>• Parameters in Multivalley section</li></ul>
GaInSb.par	GaInSb	<ul style="list-style-type: none"><li>• Permittivity</li><li>• Heat capacitance</li><li>• Thermal conductivity</li><li>• Band gap and affinity</li><li>• Density-of-states</li><li>• Parameters in Multivalley section</li></ul>

## Chapter 1: Introduction to Advanced Calibration Device

### Content of Parameter Files

Table 1 Parameter files in MaterialDB folder of Sentaurus Device (Continued)

Parameter file	Material	Parameters
GaN.par	GaN	<ul style="list-style-type: none"><li>• Isotropic and anisotropic permittivity</li><li>• Thermal conductivity</li><li>• Lattice heat capacity</li><li>• Band gap and affinity</li><li>• Density-of-states and masses</li><li>• Bulk mobility with doping dependence</li><li>• Inversion layer mobility (<math>\text{IALMob}</math>)</li><li>• High field dependency</li><li>• Shockley–Read–Hall</li><li>• Auger</li><li>• Radiative recombination</li><li>• Impact ionization</li><li>• Piezoelectric polarization</li><li>• Optical material properties</li><li>• Mechanical compliance parameters</li></ul>
GaSb.par	GaSb	<ul style="list-style-type: none"><li>• Permittivity</li><li>• Heat capacitance</li><li>• Thermal conductivity</li><li>• Band gap and affinity</li><li>• Density-of-states</li><li>• Parameters in Multivalley section</li></ul>
Germanium.par	Germanium	<ul style="list-style-type: none"><li>• Permittivity</li><li>• Heat capacitance</li><li>• Thermal conductivity</li><li>• Band gap and bandgap narrowing</li><li>• Density-of-states</li><li>• Bulk mobility</li><li>• High field dependency</li><li>• Optical properties</li></ul> <p>Other model parameter sections are available in the parameter file but are not yet updated and reviewed.</p>

## Chapter 1: Introduction to Advanced Calibration Device

### Content of Parameter Files

Table 1 Parameter files in MaterialDB folder of Sentaurus Device (Continued)

Parameter file	Material	Parameters
InAs.par	InAs	<ul style="list-style-type: none"><li>• Permittivity</li><li>• Heat capacitance</li><li>• Thermal conductivity</li><li>• Band structure (band gap, affinity, and parameters for the Multivalley section)</li><li>• Bandgap narrowing</li><li>• Density-of-states</li><li>• Bulk and inversion mobility for different surface and channel orientations</li><li>• Quantization parameters</li><li>• Optical properties</li></ul> <p>Other model parameter sections are available in the parameter file but are not yet updated and reviewed.</p>
InGaAs.par	InGaAs	<ul style="list-style-type: none"><li>• Permittivity</li><li>• Heat capacitance</li><li>• Thermal conductivity</li><li>• Band structure (band gap, affinity, and parameters for the Multivalley section)</li><li>• Bandgap narrowing</li><li>• Density-of-states</li><li>• Bulk and inversion mobility for different surface and channel orientations</li><li>• Quantization parameters</li><li>• Optical properties</li></ul> <p>Other model parameter sections are available in the parameter file but are not yet updated and reviewed.</p>
InGaN.par	InGaN	<ul style="list-style-type: none"><li>• For most models, mole fraction dependency is interpolated linearly between the corner materials GaN and InN</li></ul>

## Chapter 1: Introduction to Advanced Calibration Device

### Content of Parameter Files

Table 1 Parameter files in MaterialDB folder of Sentaurus Device (Continued)

Parameter file	Material	Parameters
InN.par	InN	<ul style="list-style-type: none"><li>• Isotropic and anisotropic permittivity</li><li>• Heat capacitance</li><li>• Thermal conductivity</li><li>• Band gap and affinity</li><li>• Density-of-states</li><li>• Mobility with doping dependency</li><li>• High field dependency</li><li>• Impact ionization</li><li>• Piezoelectric polarization</li><li>• Mechanical compliance parameters</li></ul>
InSb.par	InSb	<ul style="list-style-type: none"><li>• Permittivity</li><li>• Heat capacitance</li><li>• Thermal conductivity</li><li>• Band gap and affinity</li><li>• Density-of-states</li><li>• Parameters in Multivalley section</li></ul>
Silicon.par Siliconc100.par Siliconc110.par	Si	<ul style="list-style-type: none"><li>• Permittivity</li><li>• Heat capacitance</li><li>• Thermal conductivity</li><li>• Band gap and bandgap narrowing</li><li>• Density-of-states</li><li>• Quantization</li><li>• Bulk and inversion mobility for different surface and channel orientations, and film thicknesses</li><li>• High field dependency</li></ul> <p>Other model parameter sections are available in the parameter file but are not yet updated and reviewed.</p>

## Chapter 1: Introduction to Advanced Calibration Device

### Content of Parameter Files

Table 1 Parameter files in MaterialDB folder of Sentaurus Device (Continued)

Parameter file	Material	Parameters
SiliconCarbide.par 4H-SiC.par/4HSiC.par/ SiC_4H.par 6H-SiC.par	SiC	<ul style="list-style-type: none"><li>• Isotropic and anisotropic permittivity</li><li>• Isotropic and anisotropic thermal conductivity</li><li>• Heat capacitance</li><li>• Band gap and bandgap narrowing</li><li>• Density-of-states</li><li>• Bulk mobility with doping dependence</li><li>• Inversion layer mobility (<math>E_{n\text{ormal}}</math>)</li><li>• Inversion layer mobility (<math>I_{AL\text{Mob}}</math>)</li><li>• Anisotropic mobility</li><li>• Isotropic and anisotropic high field dependency</li><li>• Shockley–Read–Hall</li><li>• Auger</li><li>• Isotropic and anisotropic impact ionization</li><li>• Incomplete ionization</li></ul>
SiliconGermanium.par SiliconGermaniumc100.par SiliconGermaniumc110.par	SiGe (0–100%) can be used for Ge as well	<ul style="list-style-type: none"><li>• All models are mole fraction dependent</li><li>• Permittivity</li><li>• Heat capacitance</li><li>• Thermal conductivity</li><li>• Band gap and bandgap narrowing</li><li>• Density-of-states</li><li>• Quantization</li><li>• Bulk and inversion mobility for different surface and channel orientations, and film thicknesses</li><li>• High field dependency</li><li>• Auger</li></ul> <p>Other model parameter sections are available in the parameter file but are not yet updated and reviewed.</p>

## Special Parameter Files

The `MaterialDB/custom` directory of Sentaurus Device contains the following special parameter files that reflect certain application cases:

- `GaAs_DEEPEN.par`, `InAs_DEEPEN.par`, and `InGaAs_DEEPEN.par` contain parameters in the `Bandgap` and `Multivalley` sections extracted from hybrid functional calculations within the scope of the European Union DEEPEN project.
- For `AlN_DEEPEN.par`, `GaN_DEEPEN.par`, and `InN_DEEPEN.par`, the parameters in the `Piezoelectric_Polarization` section are included, based on the results of hybrid functional calculations. In addition, the bowing parameters are updated in the `Bandgap` section for the `AlGaN_DEEPEN.par`, `AlInN_DEEPEN.par`, and `InGaN_DEEPEN.par` files.
- `GatePolySilicon.par` is for the polysilicon gate of FETs.
- `mcmob.par` and `sbmob.par` contain the default parameter set for the `MCmob` and `SBmob` models (see [Appendix A on page 103](#)).
- `StrainedSi_SiGe.par` contains in-plane transport parameters at 300 K for silicon under biaxial tensile strain present when a thin silicon film is grown on top of a relaxed SiGe substrate (*in-plane* refers to charge transport that is parallel to the interface to SiGe as is the case for MOSFETs). This parameter file defines parameters for the materials `StrainedSilicon`, `Silicon`, and `Oxide`. Further explanation can be found in the header of this parameter file.

**Note:**

This parameter file is outdated and no longer maintained or supported.

- `SiGeHBT.par` contains transport parameters at 300 K for SiGe under biaxial compressive strain present when a thin SiGe film is grown on top of a relaxed silicon substrate, such as occurs in the base of npn-SiGe heterojunction bipolar transistors. The electron parameters refer to the out-of-plane direction (that is, perpendicular to the SiGe–silicon interface), and the hole parameters refer to the in-plane direction (that is, parallel to the SiGe–silicon interface). The transport parameters have been obtained from full-band Monte Carlo simulations. Further explanation can be found in the header of this parameter file.

**Note:**

This parameter file is outdated and no longer maintained or supported.

- `StrainedSilicon.par` contains the same parameters as `StrainedSi_SiGe.par` for a strained silicon material, but it does not contain the corresponding material sections for `Silicon` and `Oxide`.

**Note:**

This parameter file is outdated and no longer maintained or supported.

## Chapter 1: Introduction to Advanced Calibration Device

### Using Advanced Calibration Device

- `Silicon_kvm.par` and `SiliconGermanium_kvm.par` contain calibrated kinetic velocity model (KVM) parameters for better simulation of ballistic effects in short-channel devices (see the *Sentaurus™ Device User Guide*).
- `In52Al48As.par`, `In53Ga47As.par`, and `In52Al48As_In53Ga47As.par` contain material parameters specifically for  $\text{In}_{0.52}\text{Al}_{0.48}\text{As}$ ,  $\text{In}_{0.53}\text{Ga}_{0.47}\text{As}$ , and  $(\text{In}_{0.52}\text{Al}_{0.48}\text{As})_x(\text{In}_{0.53}\text{Ga}_{0.47}\text{As})_{1-x}$  alloys, respectively, which are lattice matched to InP material. To be recognized in Sentaurus Device, these material names can be added manually to the `datexcodes.txt` file:

```
Materials {
    In52Al48As {
        label      = "In52Al48As"
        group     = Semiconductor
    }
    In53Ga47As {
        label      = "In53Ga47As"
        group     = Semiconductor
    }
    In52Al48As_In53Ga47As {
        label      = "In52Al48As_In53Ga47As"
        group     = Semiconductor
    }
}
```

The mole fraction-dependent material  $(\text{In}_{0.52}\text{Al}_{0.48}\text{As})_x(\text{In}_{0.53}\text{Ga}_{0.47}\text{As})_{1-x}$  must be defined as well in the `Molefraction.txt` file:

```
#(In52Al48As)(x)(In53Ga47As)(1-x)
In52Al48As_In53Ga47As (x=0) = In53Ga47As
In52Al48As_In53Ga47As (x=1) = In52Al48As
```

---

## Using Advanced Calibration Device

To use Advanced Calibration Device, you can look up the parameter files and the command files that are best suited for your device and technology requirements in [Chapter 2 on page 21](#).

The European Union projects DEEPEN and III-V-MOS have generated additional parameter sets that complement the general parameter files of Advanced Calibration Device. The parameter files from the DEEPEN project are stored in the `MaterialDB/custom` folder for AlGaN, AlInN, AlN, GaAs, GaN, InAs, InGaAs, InGaN, and InN (see [Special Parameter Files on page 19](#)).

In Version T-2022.03, parameter sets and experience have accumulated for the simulation of band-to-band tunneling in silicon and SiGe devices using the dynamic nonlocal path band-to-band tunneling model. These parameter sets can be delivered on request.

# 2

## Guide to Device Simulations

---

*This chapter provides a guide for the quick selection of parameter sets and device models.*

---

### Specifying Simulation Cases

[Table 2](#) and [Table 3 on page 22](#) present typical simulation cases, where a path is defined that you can use to select the proper device simulation parameter set and the appropriate `Physics` section for the command file. In the tables, the characters `A` to `E` indicate different paths that are described in subsequent sections.

*Table 2 Specifying the simulation case: CMOS*

	Node																
	> 130 nm	32–130 nm			14–32 nm			< 14 nm									
Selection path	A	B	C	C	B	C	C	C	E	D	E	E	I	I	E	E	E
Planar bulk and SOI	X	X	X	X	X	X	X	X									
FinFET									X		X	X	X				
Nanowire													X	X	X	X	
Thin-layer SOI										X							
Si	X	X	X		X	X		X	X	X				X			
SiGe				X			X			X				X		X	
Ge											X					X	
InGaAs												X	X				
Gate-first	X	X			X												

*Table 2 Specifying the simulation case: CMOS (Continued)*

	Node											
	> 130 nm	32–130 nm			14–32 nm			< 14 nm				
Selection path	A	B	C	C	B	C	C	E	D	E	E	I
Gate-first with metal gate			X	X		X	X					
Gate-last with metal gate								X	X	X	X	X
Without stress	X										X	X
With stress		X	X	X	X	X	X	X	X	X		X

*Table 3 Specifying the simulation case: Smart power and power*

	Device				
	HVMOS	LDMOS	HEMT	Diode	IGBT
Selection path	F	F	G	H	F
Si	X	X			X
SiC	X			X	
GaN			X		

## Accessing Parameter Files and Model Frameworks

The following sections describe the parameter files and the model frameworks. For information about handling and loading parameter files, see the *Sentaurus™ Device User Guide*.

### Path A: Basic CMOS Simulation Command File Sections

Quantization uses the density gradient model of Sentaurus Device (`eQuantumPotential` and `hQuantumPotential`). However, for technologies with gate oxide thicknesses greater

than 3 nm, you can neglect quantum correction without greatly affecting the simulation of the gate capacitance.

The orientation of the conducting interface is detected automatically. However, you must define the channel or the current flow direction manually using the correct mobility parameter file. The corresponding parameter files are located in the `MaterialDB` folder.

For the `<110>` channel direction, you must load the `Siliconc110.par` file. For the `<100>` channel direction, you must load the `Siliconc100.par` file.

```
Physics {Fermi}
  Physics (Material="Silicon") {
    eQuantumPotential(AutoOrientation density)
    hQuantumPotential(AutoOrientation density)
    Mobility (Enormal (IALMob(AutoOrientation)) HighFieldSaturation)
    # For PMOS, it is useful to use PhononCombination=2 in the IALMob.
    EffectiveIntrinsicDensity(OldSlotboom)
    Recombination(SRH)
    # Recombination(SRH Band2Band(Model=NonlocalPath))
      # For off-current calculation, band-to-band
      # tunneling models must be switched on.
  }
}
```

---

## Path B: Add Influence of Mechanical Stress to Physics Section Shown in Path A

Taking into account mechanical stress, you must combine the low-field mobility model with a model describing the stress influence. You can model the mobility change by mechanical stress in one of the following ways:

- Use the `eSubband` and `hSubband` models for a more physics-based calculation of the mobility enhancement by mechanical stress in silicon devices that is directly based on band structure and subbands. For the subband models, you must set the channel direction in the command file when it is *not* the `<110>` channel.
- Use the `MCmob` physical model interface (PMI) model (parameters are extracted from Sentaurus Device Monte Carlo) or the `SBmob` PMI model (parameters are extracted from Sentaurus Band Structure). For the `MCmob` and `SBmob` models, you must set the channel direction in the parameter file (see [Appendix A on page 103](#)).

The orientation of the conducting interface is detected automatically. However, you must define the channel or the current flow direction manually using the correct mobility parameter file. The corresponding parameter files are located in the `MaterialDB` folder.

For the `<110>` channel direction, you must load the `Siliconc110.par` file. For the `<100>` channel direction, you must load the `Siliconc100.par` file.

With subband models, you must use the following syntax:

```

Physics {Fermi}
Physics (Material="Silicon") {
    eQuantumPotential(AutoOrientation density)
    hQuantumPotential(AutoOrientation density)
    Mobility (Enormal (IALMob(AutoOrientation)) HighFieldSaturation)
        # For the inclusion of ballistic effects, you can use the command
        # BalMob(KVM(Full) Frenksley Fermi) in the Mobility statement.
        # For PMOS, it is useful to use PhononCombination=2 in the IALMob.
    EffectiveIntrinsicDensity(OldSlotboom)
    Recombination(SRH)
        # Recombination(SRH Band2Band(Model=NonlocalPath))
            # For off-current calculation, band-to-band
            # tunneling models must be switched on.

    eMultivalley(MLDA kpDOS -density) # hMultivalley for holes.
        # For holes, defining kpDOS and parfile
        # together results in double-counting
        # for holes when gamma hole valleys are
        # defined in the parameter file.

    Piezo (
        Model (
            Mobility (
                saturationfactor=0.2
                eSubband(Fermi EffectiveMass Scattering(MLDA))
                # eSubband(Fermi EffectiveMass Scattering(MLDA) -RelChDir110)
                # for <100> channel.
                # hSubband(Fermi EffectiveMass Scattering(MLDA)) for holes
                # For holes, the replacement of the option Fermi by the
                # option Doping can result in speedup of the simulation.
            )
            DOS(eMass hMass)
            DeformationPotential(Minimum ekp hkp)
        )
    )
}

```

With the MCmob model or SBmob model, you must use the following syntax:

```

Physics {Fermi}

Physics (Material="Silicon") {
    eQuantumPotential(AutoOrientation density)
    hQuantumPotential(AutoOrientation density)
    Mobility (Enormal (IALMob(AutoOrientation)) HighFieldSaturation)
        # For PMOS, it is useful to use PhononCombination=2 in the IALMob.
    EffectiveIntrinsicDensity(OldSlotboom)
    Recombination(SRH)
        # Recombination(SRH Band2Band(Model=NonlocalPath))
            # For off-current calculation, band-to-band
            # tunneling models must be switched on.

```

```

Piezo (
    Model (
        Mobility (
            saturationfactor=0.2
            efactor(Kanda sfactor=SBmob(Type=0))      # Type=1 for holes
            #efactor(Kanda sfactor=MCmob(Type=0))      # when using MCmob.
        )
        DOS(eMass hMass)
        DeformationPotential(Minimum ekp hkp)
    )
)
}
    
```

These command file sections are designed for electron transport (NMOS). For hole transport (PMOS), replace `eSubband` with `hSubband`, `eMultivalley` with `hMultivalley`, and specify `Type=1` for `MCmob` and `SBmob`.

## Path C: Add High-k Mobility Degradation to Physics Section Shown in Path B

The orientation of the conducting interface is detected automatically. However, you must define the channel or the current flow direction manually using the correct mobility parameter file. The corresponding parameter files are located in the `MaterialDB` folder.

You must load the following parameter files for the corresponding channel direction:

- For the silicon <100> channel direction, load the `Siliconc100.par` file.
- For the silicon <110> channel direction, load the `Siliconc110.par` file.
- For the SiGe <100> channel direction, load the `SiliconGermaniumc100.par` file.
- For the SiGe <110> channel direction, load the `SiliconGermaniumc110.par` file.

```

Physics {Fermi}

Physics (Material="Silicon") {
#or Physics (Material="SiliconGermanium") {
    eQuantumPotential(AutoOrientation density)
    hQuantumPotential(AutoOrientation density)
    Mobility (
        Enormal (
            IALMob(AutoOrientation)
            # For PMOS, it is useful to use PhononCombination=2 in IALMob.
            RPS                      # Used for remote phonon scattering (RPS).
            NegInterfaceCharge (SurfaceName="s1")
                # Used for remote Coulomb scattering (RCS)
                # and remote dipole scattering (RDS).
            PosInterfaceCharge (SurfaceName="s1")
                # Used for RCS and RDS.
        )
    )
}
    
```

```

        )
    HighFieldSaturation)    # To include ballistic effects, you can
                            # use the BalMob(KVM(Full) Frenksley Fermi)
                            # command in the Mobility statement.
    EffectiveIntrinsicDensity(OldSlotboom)
                            # For SiGe with high Ge mole fraction or for pure
                            # Ge, it is recommended to switch off the Fermi
                            # correction and to use
                            # EffectiveIntrinsicDensity(OldSlotboom NoFermi)
    Recombination(SRH)
    # Recombination(SRH Band2Band)  # For off-current calculation,
                                    # band-to-band tunneling models
                                    # must be switched on.

    eMultivalley(MLDA kpDOS -density)  # hMultivalley for holes.
                                    # For SiGe, use eMultivalley(MLDA kpDOS parfile -density)

    Piezo (
        Model (
            Mobility (
                saturationfactor=0.2
                eSubband(Fermi EffectiveMass Scattering(MLDA))
                # eSubband(Fermi EffectiveMass Scattering(MLDA) -RelChDir110)
                # for <100> channel.
                # hSubband(Fermi EffectiveMass Scattering(MLDA)) for holes
                # For holes, the replacement of the option Fermi by the
                # option Doping can result in speedup of the simulation.
            )
            DOS(eMass hMass)
            DeformationPotential(Minimum ekp hkp)
        )
    )
}

```

The surface name specifies the surface or interface that causes the mobility degradation, for example, the HfO<sub>2</sub>–oxide interface in the high-k gate stack of a MOS transistor. The surface must be defined in the `Math` section of the command file. For more information about high-k mobility degradation models, see [Unstrained Low-Field Mobility on page 44](#).

---

## Path D: Thin-Layer MOS Simulations Including Thin-Film Effects

The `Mobility` command in the `Physics` section of Path C must be replaced by:

```

Mobility (
    ThinLayer (IALMob(AutoOrientation))
    # For PMOS, it is useful to use PhononCombination=2 in IALMob.
    Enormal (
        RPS                      # Used for remote phonon scattering (RPS).
        NegInterfaceCharge (SurfaceName="s1")
                                # Used for remote Coulomb scattering (RCS)
                                # and remote dipole scattering (RDS).

```

```

        PosInterfaceCharge (SurfaceName="s1") # Used for RCS and RDS.
    )
    HighFieldSaturation)

```

All other options and statements remain the same.

## Path E: FinFET Simulations

You can use the same Physics section as shown in Path C. The `AutoOrientation` option for the density gradient model must be switched on. As a starting point for calibration, the same parameter files `Siliconc100.par`, `Siliconc110.par`, `SiliconGermaniumc100.par`, and `SiliconGermaniumc110.par` can also be used. However, because the interface quality of the fin sidewalls can be very different from the interface quality of a planar transistor, parameter adjustments are often necessary.

In general, the electron inversion mobility of FinFETs is higher at the (110) sidewalls than in planar (110) transistors [1].

[Table 4](#) and [Table 5](#) show the approach for modeling planar and nonplanar FinFET devices regarding orientation-related parameters.

*Table 4 Parameter files for planar FETs and FinFETs with silicon channel*

Device	Number of conducting planes	Conducting plane orientation	Channel orientation	Parameter file to load
Planar MOS	1	(100)	<100>	Siliconc100.par
Planar MOS	1	(110)	<100>	Siliconc100.par
Planar MOS	1	(100)	<110>	Siliconc110.par
Planar MOS	1	(110)	<110>	Siliconc110.par
FinFET	3	(100)	<100>	Siliconc100.par
FinFET	3	(100) (110)	<110> <110>	Siliconc110.par

**Table 5** Parameter files for planar FETs and FinFETs with SiGe channel

Device	Number of conducting planes	Conducting plane orientation	Channel orientation	Parameter file to load
Planar MOS	1	(100)	<100>	SiliconGermaniumc100.par
Planar MOS	1	(110)	<100>	SiliconGermaniumc100.par
Planar MOS	1	(100)	<110>	SiliconGermaniumc110.par
Planar MOS	1	(110)	<110>	SiliconGermaniumc110.par
FinFET	3	(100)	<100>	SiliconGermaniumc100.par
FinFET	3	(100) (110)	<110> <110>	SiliconGermaniumc110.par

For very short gate lengths (less than 15 nm), the isotropic density gradient model can overestimate the leakage current in the transport direction and quantization effects at doping and mole fraction gradients. In those cases, the `alpha` parameter in the density gradient model can help to suppress artificial source/drain leakage and quantization effects in the transport direction. For FinFET simulations with a gate length below 15 nm, using an `alpha` in the transport direction smaller than 0.1 is a good starting point. For more information about handling and using the anisotropic density gradient model, see the *Sentaurus™ Device User Guide*.

When using `EparallelToInterface` as a driving force in the high-field saturation model, the electric field components that are normal to the channel direction and in-plane with the fin cross section can lower the mobility. This is an artifact and makes the use of this driving force very questionable.

**Note:**

Using the `DOS(eMass hMass)` model in the `Piezo` section and the temperature equation at the same time might result in convergence problems. Using the `NumericalIntegration` option, for example, `DOS(hMass(NumericalIntegration))`, can improve the numeric behavior.

---

## Path F: Smart-Power HVMOS and LDMOS Devices

In principle, you should use Path A for silicon-based smart-power devices exhibiting a traditional polysilicon/oxide gate stack when no mechanical stress occurs in the structure. When mechanical stress occurs in the structure, you must use Path B. However, in many

cases, the linear piezoresistance model might be sufficient because the mechanical stress is relatively low. For complex devices or 3D simulation structures, you might need to simplify the model complexity to reduce simulation time or to achieve convergence. You can use the following simplified `Physics` section in those cases:

```
Physics {Fermi}

Physics (Material="Silicon") {
    Mobility (Enormal (IALMob(AutoOrientation)) HighFieldSaturation)
        # For PMOS, it is useful to use PhononCombination=2 in IALMob.
    EffectiveIntrinsicDensity(OldSlotboom)
    Recombination (Auger SRH(DopingDep TemDep))
        # Recombination(Auger SRH(DopingDep TemDep) Band2Band)
            # For off-current calculation, band-to-band tunneling models
            # must be switched on.
}
```

Quantum correction is neglected here, resulting in better simulation performance. The loss of accuracy can mostly be compensated by a corresponding workfunction shift and a reduction of the gate isolation permittivity. For devices with a gate isolation oxide thickness greater than 3 nm, the influence of quantum correction decreases. The `Physics` section above is designed for  $I_d-V_d$  and  $I_d-V_g$  simulations, but it does not include the models for breakdown, substrate current, and complex electrostatic discharge simulation. In addition, you must switch on the commands needed to account for self-heating.

Parameter files and the model section have been tested for LDMOS devices. No tests or investigations have been conducted for IGBTs, thyristors, or bipolar devices.

---

## Path G: GaN HEMT Simulations

For numeric reasons, the well-known extended Canali model is used to simulate high-field effects. The use of the transferred electron models, which are physically more suited to the simulation of GaN HEMTs, is limited because of poor convergence.

It is known that additional mobility degradation mechanisms at interfaces to the GaN channel influence the channel mobility. However, no model is included for mobility in the 2D electron gas because of missing model parameters.

Typically, you should use the density gradient model for quantum correction. However, no model for quantum correction is included because of missing parameters.

The values for the trap concentration and the energy level given here are typical for nitride-passivated GaN HEMTs. However, the actual values depend on the device and might differ from the values presented here. In addition to the interface traps shown in the command file `Physics` section here, bulk traps are important and must be implemented in the simulation, for example, when investigating current collapse effects.

For III-V nitride wide-bandgap materials, you must load the parameter files `GaN.par`, `AlGaN.par`, `AlN.par`, `InGaN.par`, and `InN.par`, which contain the material parameters.

The following Physics section should be used together with the parameter files:

```
Physics {
    Mobility (
        DopingDependence(Arora) # Masetti model can be used as well.
                                    # Model parameters are in the parameter
                                    # files GaN.par, AlGaN.par, and AlN.par.
        HighFieldSaturation
    )
    EffectiveIntrinsicDensity(noBandGapNarrowing)
    Piezoelectric_Polarization(strain)
    Recombination(Radiative)
    Fermi
    Thermodynamic
    Thermionic
    HeteroInterface
    eBarrierTunneling "STUN"      # For tunneling at the source contact,
                                    # you must define a nonlocal mesh in
                                    # the Math section.
    eBarrierTunneling "DTUN"      # For tunneling at the drain contact,
                                    # you must define a nonlocal mesh in
                                    # the Math section.
}
Physics (MaterialInterface="AlGaN/Nitride") {
    Traps(Donor Level Conc=1E13 EnergyMid=0.4 FromMidBandGap)
        # The values for the trap concentration and the energy
        # are calibration parameters as well as the trap
        # location and the trap type. Several combinations
        # of different trap distributions are usually
        # necessary to reproduce measured results.
    Piezoelectric_Polarization(strain activation=0)
}
```

---

## Path H: SiC Diode Simulations

The parameter files `4H-SiC.par` and `6H-SiC.par` contain the material parameters for SiC-based wide-bandgap materials.

The following Physics section should be used together with the parameter files:

```
Physics {
    eMobility (
        DopingDependence(Arora)      # For 6H-SiC, Arora parameters are not
                                    # available in the parameter file.
                                    # Therefore, it is recommended to
                                    # switch to the Masetti model.
        HighFieldSaturation
}
```

## Chapter 2: Guide to Device Simulations

### Accessing Parameter Files and Model Frameworks

```
)  
hMobility (  
    DopingDependence(Arora)      # For 6H-SiC, Arora parameters are not  
                                    # available in the parameter file.  
                                    # Therefore, it is recommended to  
                                    # switch to the Masetti model.  
    HighFieldSaturation  
)  
EffectiveIntrinsicDensity(Slotboom NoFermi)  
IncompleteIonization  
Recombination(SRH(DopingDep TempDep Tunneling) Band2Band Avalanche  
    (Okuto))  
                                    # For forward characteristics, you can  
                                    # neglect the commands Band2Band and  
                                    # Tunneling. This can improve  
                                    # convergence behavior.  
Fermi  
#Thermodynamic          # Add for thermodynamic simulations.  
#AnalyticTEP            # Add for thermodynamic simulations.  
Temperature=300.0  
eBarrierTunneling "NLM" (Twoband Transmission)  
                    # Nonlocal mesh definition in Math section necessary.  
Traps (  
    Donor Level EnergyMid=1.0 FromConductionband Conc=1e14  
    eXSection=1.0e-12 hXSection=1.0e-12 PooleFrenkel  
    TrapVolume=1.0e-9  
    HuangRhys=0.1 PhononEnergy=0.05 eBarrierTunneling (Twoband)  
)  
                    # Bulk traps are often necessary for the physically  
                    # correct calculation of the thermal behavior of the  
                    # reverse leakage current.  
}  
  
Physics (Electrode="top") {  
    #MSPeltierHeat          # Add for thermodynamic simulations.  
    Schottky BarrierLowering  
}
```

Depending on how the mobility model was calibrated, that is, whether or not the total chemical concentration or the active concentration was used, you can add IncompleteIonization to the Mobility statement. For holes, the suggested parameters for the Arora model in the 4H-SiC.par file have been calibrated to the total acceptor concentration. In addition, scattering on the neutral impurities is often comparable to scattering on the ionized impurities for 4H-SiC p-type layers.

**Note:**

Using the IncompleteIonization model might cause convergence problems.

To distinguish between cubic and hexagonal 4H-SiC lattice sites, you can activate the following option in the `IncompleteIonization` statement of the `Physics` section of the command file:

```
IncompleteIonization(Split (Doping="NitrogenActive" Weights=(0.5 0.5)))
```

The corresponding parameters must be defined in the parameter file. Precalibrated values are in the `4H-SiC.par` and `6H-SiC.par` files for phosphorus and nitrogen. For phosphorus, the parameters corresponding to hexagonal sites are active, and modification of the `datexcodes.txt` file is necessary to treat both sites.

The values for the trap concentration, the energy levels, and other parameters in the `Traps` command are typical. However, the actual values depend on the device and might differ from the values presented here. Especially for the leakage current in reverse mode, tunneling by defect traps can play an important role and should be investigated.

The use of the `NoFermi` option depends on the extraction of the parameters for the bandgap narrowing model. This option is applied if you use parameters for bandgap narrowing that have been extracted assuming Fermi statistics.

When including heat generation and conduction, a lumped model (thermal network) using the thermal resistance of layers and material regions that are not included in the simulation can improve the simulation results.

You can use an alternative model, the `JainRoulston` model, which is physically more suited for bandgap narrowing.

For 2D and 3D structures, anisotropic material properties for mobility, permittivity, thermal conductivity, and impact ionization must be taken into account in the simulation. This can be performed by the following statement in the `Physics` section:

```
Aniso (Mobility Poisson Temperature Avalanche)
```

The corresponding parameters must be defined in the parameter file. Precalibrated values are in the `4H-SiC.par` (same as `SiliconCarbide.par`) and `6H-SiC.par` files for mobility, permittivity, thermal conductivity, impact ionization, incomplete ionization, high-field saturation, and other models.

---

## Path I: InGaAs FinFET Simulations

For InGaAs FinFET devices with a gate width less than 10 nm, the following quantization models of Sentaurus Device are available to model quantized distributions of carriers:

- Use the modified local-density approximation (MLDA) model with the `ThinLayer` option specified in the command file to activate size quantization with the multivalley model. For a 2D structure, the layer thickness can be extracted automatically, and the depletion at corner regions corresponds better to the results of the Schrödinger equation using the

MaxFit option. Setting `MaxFitWeight=0.35` is advisable to start with, although an adjustment might be required depending on fin geometries.

- Use the density gradient model with the multivalley model. The quantization parameter ( $\gamma$ -parameter) of the density gradient model depends on the layer thickness and the fin geometry. Therefore, it is advisable to calibrate the solutions from the Schrödinger equation in test structures with a similar channel geometry.

In addition, the inversion and accumulation layer mobility (`IALMob`) model is available to model inversion-type n-channel InGaAs FinFETs. The parameters have been calibrated to available experimental data under the condition of `PhononCombination=1`.

The parameter files `GaAs.par`, `InGaAs.par`, and `InAs.par` contain the material parameters for III–V arsenide materials.

For the MLDA model, you must use the following `Physics` section with the parameter files:

```
Physics {Fermi}

Physics (Material="InGaAs") {
    Mobility (
        eHighFieldSaturation # In case of convergence issues, you can use
                             # eHighFieldSaturation(EparallelToInterface).
        Enormal(IALMob(PhononCombination=1))
    )
    EffectiveIntrinsicDensity(BandGapNarrowing(JainRoulston) NoFermi)
    Recombination(SRH Auger)
    eMultiValley(MLDA Nonparabolicity ThinLayer)
    LayerThickness(MaxFitWeight=0.35)
}
```

For the density gradient model, you must use the following `Physics` section with the parameter files:

```
Physics {Fermi}

Physics (Material="InGaAs") {
    Mobility (
        eHighFieldSaturation # In case of convergence issues, you can use
                             # eHighFieldSaturation(EparallelToInterface).
        Enormal(IALMob(PhononCombination=1))
    )
    EffectiveIntrinsicDensity(BandGapNarrowing(JainRoulston) NoFermi)
    Recombination(SRH Auger)
    eMultiValley(Nonparabolicity)
    eQuantumPotential(Density)      #  $\gamma$ -parameter requires calibration.
}
```

## References

- [1] C. D. Young *et al.*, "(110) and (100) Sidewall-oriented FinFETs: A performance and reliability investigation," *Solid-State Electronics*, vol. 78, pp. 2–10, December 2012.

# 3

## Calibration Methodology for Device Simulations

---

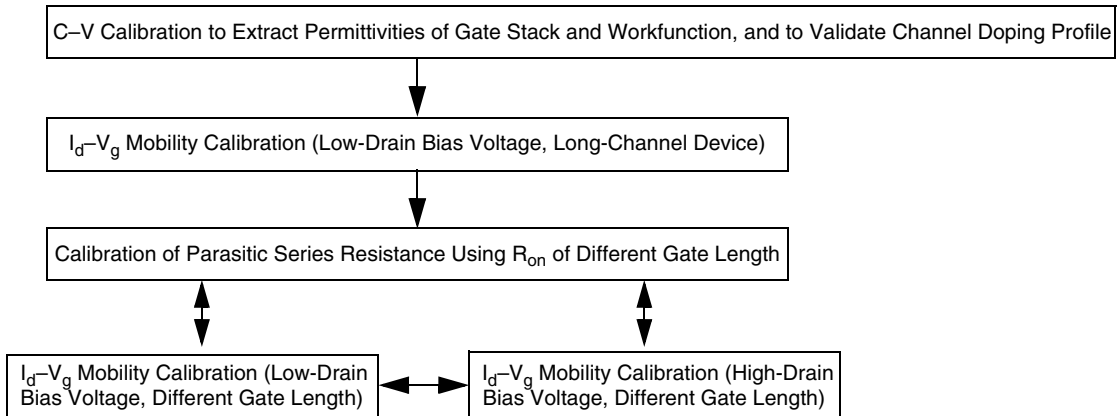
*This chapter describes the basic calibration methodology used to improve the accuracy of CMOS device simulations.*

---

### Calibration of CMOS Devices

Figure 1 shows a general flow of the calibration methodology used for CMOS devices. Different measurements and layout configurations allow you to separate device simulation model parameters. However, in many cases, iterations are necessary.

Figure 1     *Calibration methodology used for CMOS devices ( $I_d-V_g$  calibration can be complemented by involving mobility measurements)*



The next sections describe this calibration methodology in detail. It is assumed that all process calibration issues are solved beforehand and the doping profile is correct.

---

### C–V Calibration

Capacitance–voltage (C–V) calibration is the first step in the device calibration and is strongly connected to the doping profile and to process simulation or calibration. Because it

## Chapter 3: Calibration Methodology for Device Simulations

### Calibration of CMOS Devices

is assumed that the doping profile is correct, the bottom of the C–V curve (marked in [Figure 2](#)) fits the experiment already.

C–V calibration is performed on large-area MOS transistors or MOS capacitor test structures at low frequency. Therefore, in some cases, you can have slightly different workfunctions compared to smaller transistor devices.

*Figure 2 C–V calibration methodology (NMOS)*

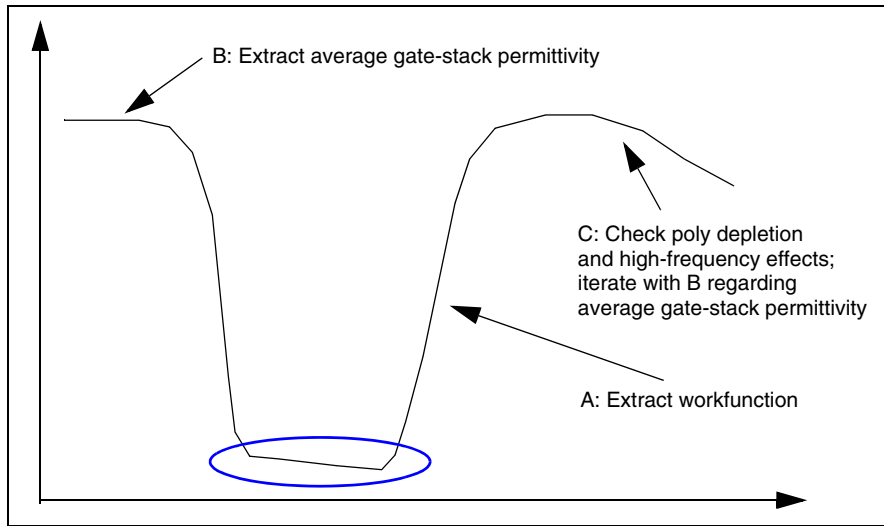


*Table 6 Main steps and extracted parameters of C–V calibration*

Step	Target	Parameter to extract	Validity range of parameter	Comments
A	Region of weak or moderate inversion	Workfunction	Metal gate workfunction: NMOS (4.0–4.7 eV) PMOS (4.5–5.2 eV) Polygate barrier: –0.2 V – 0.2 V	Workfunction or barrier voltages extracted from C–V and used for long-channel I–V simulation can require corrections, particularly when special C–V test structures are used.
B	Accumulation part of C–V	Average permittivity of gate isolation	Permittivity of high-k material: 14–25 Permittivity of interfacial oxide: 3.9–6	For high-k gate stacks with several material layers, first the permittivity of the interfacial oxide layer is adjusted. Second, the permittivity of the high-k material is calibrated.
C	Inversion part of C–V	Poly doping in case of polygate	Depends on process conditions	–

## $I_d - V_g$ Mobility Calibration

The calibration of long-channel devices is necessary to extract low-field mobility parameters. Typically, for this, you use the  $I_d - V_g$  characteristics of devices with a gate length greater than 500 nm, at a low-drain bias voltage smaller than 100 mV. An iterative process extracts the parameters of the mobility model in different voltage regions (see [Figure 3](#), [Figure 4](#), and [Table 7 on page 38](#)).

*Figure 3 Long-channel  $I_d - V_g$  mobility calibration methodology in linear scale*

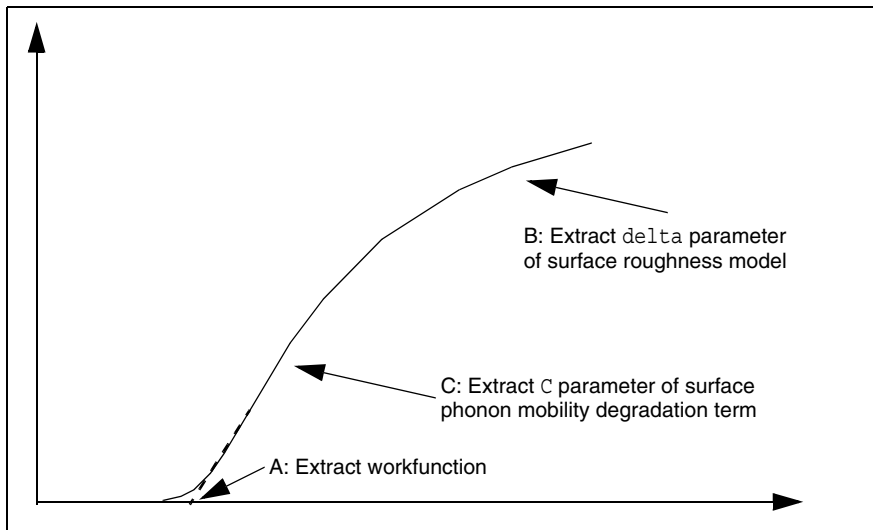
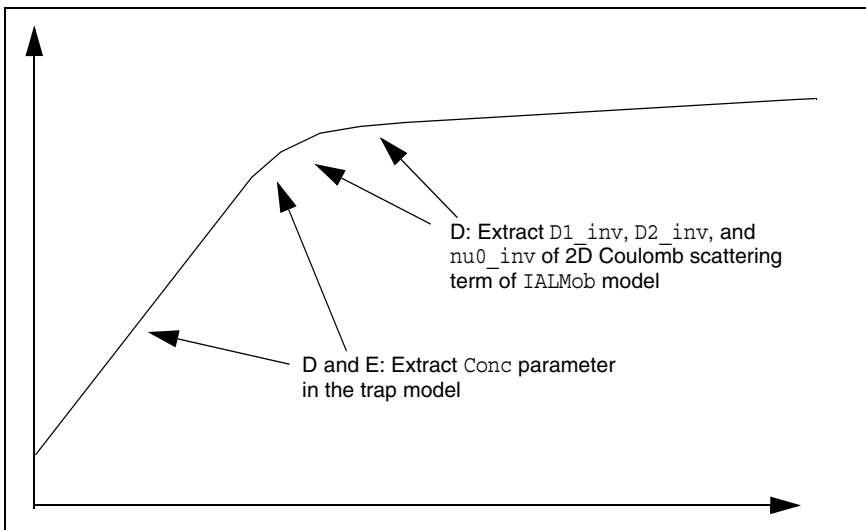


*Figure 4 Long-channel  $I_d - V_g$  mobility calibration methodology in logarithmic scale*



## Chapter 3: Calibration Methodology for Device Simulations

### Calibration of CMOS Devices

**Table 7 Main steps and extracted parameters of long-channel  $I_d$ - $V_g$  mobility calibration**

Step	Target	Parameter to extract	Validity range of parameter	Comments
A	Threshold voltage	Workfunction	Depends on gate material. Stress in the metal gate, grain sizes, and orientations influence the workfunction and can result in a dependency on gate length and geometric parameters.	Typically, metal gate workfunctions of 4.1 eV for NMOS and 4.9 eV for PMOS are used. Take initial value from C-V calibration. Note there can be an influence of remote Coulomb or dipole scattering (RCS or RDS), or 2D impurity Coulomb scattering on the threshold voltage, which couples workfunction and mobility extraction.
B	Strong inversion – high gate bias voltage	$\delta$ parameter of surface roughness model	Depends on process conditions and other parameters. No validity range is known.	Surface roughness can change when changing process conditions and surface orientations. Fine-tuning is always necessary to fit $I_d$ - $V_g$ characteristics.
C	Linear region of $I_d$ - $V_g$ curve	c parameter of surface phonon mobility degradation term	Depends on process conditions and other parameters. No validity range is known.	Extraction requires mostly an iteration between steps B and C and, sometimes, even between steps B, C, and D. Interface properties and material composition at the interface can change when changing process conditions. Fine-tuning is always necessary to fit $I_d$ - $V_g$ characteristics.

## Chapter 3: Calibration Methodology for Device Simulations

### Calibration of CMOS Devices

**Table 7** Main steps and extracted parameters of long-channel  $I_d$ – $V_g$  mobility calibration

Step	Target	Parameter to extract	Validity range of parameter	Comments
D	Transition between logarithmic and linear slope – threshold voltage region	1. Parameters of 2D Coulomb mobility degradation term 2. Parameters of InterfaceCharge model	1. No validity range is known 2. Parameters of InterfaceCharge mode	Calibration focuses on the Coulomb roll-off visible in the $\mu(E_{\text{eff}})$ curve, but it also can be done to the bending of the $I_d$ – $V_g$ curve between subthreshold and linear region. These mobility degradation terms also affect the threshold voltage and the drain-induced barrier lowering (DIBL) of the device.
E	Subthreshold region	Parameters of InterfaceCharge model	No validity range is known	Calibration focuses on the Coulomb roll-off visible in the $\mu(E_{\text{eff}})$ curve, but it also can be done to the subthreshold region. This mobility degradation term also affects the threshold voltage and the DIBL of the device.

---

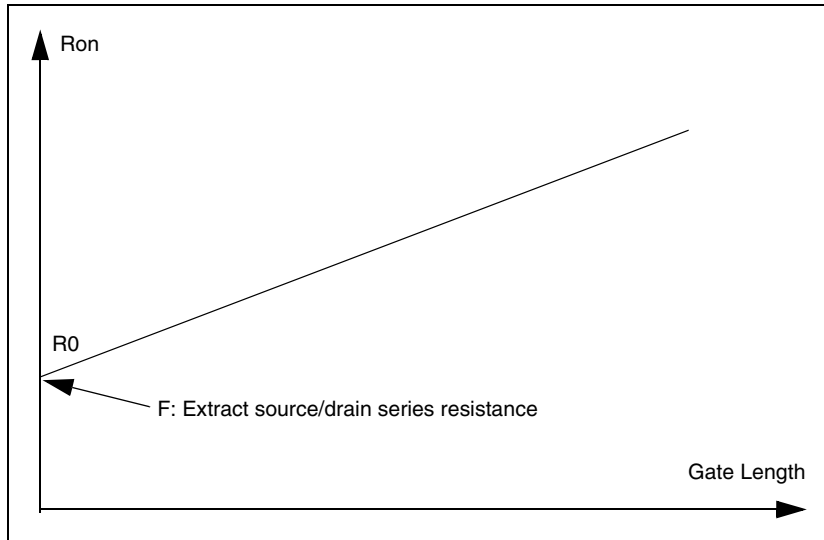
## Calibration of Parasitic Series Resistance

With the inclusion of a ballistic mobility model that gives a finite resistance for an infinitely small channel length, the calibration of the channel mobility is coupled to the calibration of the source/drain channel series resistance. Therefore, the extraction of this series resistance is most important for the calibration of the parameters of the ballistic mobility model. Iterations might be needed to update the extracted series resistance when changing parameters of the ballistic mobility model in the calibration of the channel mobility.

## Chapter 3: Calibration Methodology for Device Simulations

### Calibration of CMOS Devices

**Figure 5** Extraction methodology of source/drain series resistance



Equation 1 shows the parameters  $R_0$  and  $R_s$  forming the on-resistance:

$$R_{\text{on}} = R_0 + Lg \cdot R_s \quad (1)$$

**Table 8** Main step and extracted parameter of source/drain series resistance

Step	Target	Parameter to extract	Validity range of parameter	Comments
F	Measured dependency of on-resistance at low-drain bias voltage on gate length	On-resistance at zero gate length $R_0$ (in Equation 1)	$R_0$ is determined by contact and source/drain series resistance. The value depends on the technology node and device type, and can vary greatly. No validity range is known.	$R_0$ extraction is especially important for step G (extraction of "ballistic" resistance).

### $I_d$ - $V_g$ Mobility Calibration at Low-Drain Bias Voltage

Reference [1] discusses a possible overestimation of the current response close to equilibrium when having strong electrical built-in fields, for example, caused by p-n junctions. This effect might be connected to deviations from the Einstein relation in certain situations, but it is not considered in the calibration methodology because of convergence

## Chapter 3: Calibration Methodology for Device Simulations

### Calibration of CMOS Devices

issues. This means, to some extent, that the calibration of the parameters of the ballistic mobility model includes this physically different effect.

**Figure 6** Short-channel  $I_d$ - $V_g$  mobility calibration methodology in linear scale, with low-drain bias voltage

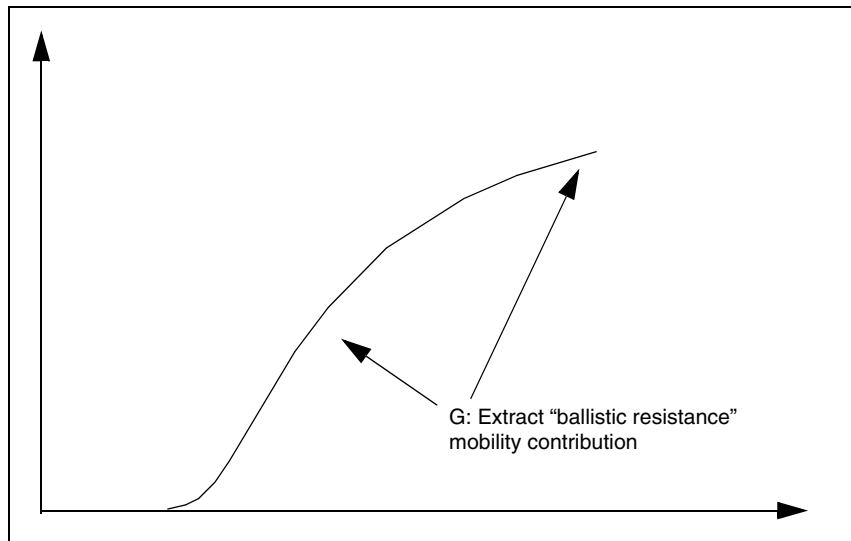


**Table 9** Main step and extracted parameter of  $I_d$ - $V_g$  mobility calibration at low-drain bias voltage

Step	Target	Parameter to extract	Validity range of parameter	Comments
G	Moderate and strong inversion	Adjust “ballistic resistance” mobility contribution using parameters of the ballistic mobility models in Sentaurus Device	No validity range	This involves iteration with step F.

### $I_d$ - $V_g$ Mobility Calibration at High-Drain Bias Voltage

This step extracts the saturation velocity. The extraction of  $v_{sat0}$  from  $I_{dsat}$  roll-off data or  $I_d$ - $V_g$  curves at large drain bias voltage, using experiments or Monte Carlo simulation, is straightforward. However, the calibration of both  $I_{dsat}$  and  $I_{dlin}$  at the same time using  $v_{sat0}$ , source/drain resistance, and ballistic mobility parameters is more challenging.

Nevertheless, it is mostly possible to achieve a good agreement during the device calibration because of the inclusion of the ballistic mobility model [2].

**Figure 7** Short-channel  $I_d$ - $V_g$  mobility calibration methodology in linear scale, with high-drain bias voltage

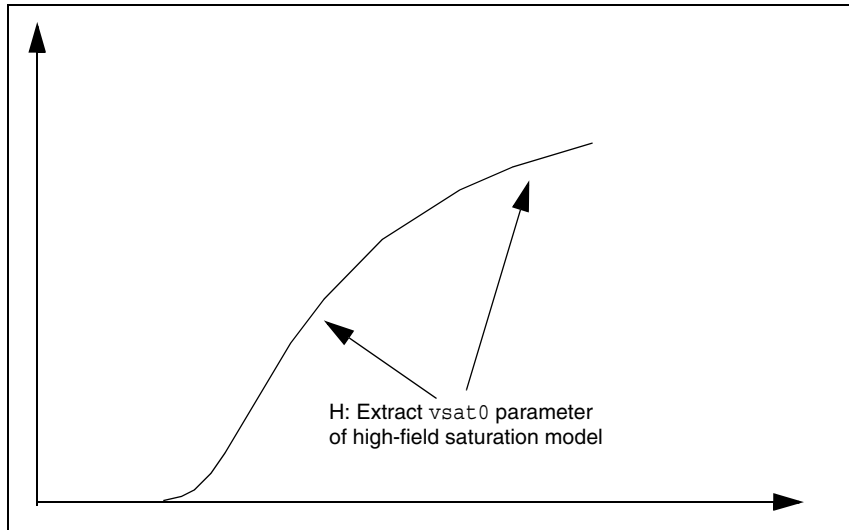


**Table 10** Main step and extracted parameter of  $I_d$ - $V_g$  mobility calibration at high-drain bias voltage

Step	Target	Parameter to extract	Validity range of parameter	Comments
H	Whole $I_d$ - $V_g$ curve and $I_{dsat}$	Adjust $vsat0$	For silicon: < 5e7 cm/s	This might involve iteration with steps F and G.

## References

- [1] A. T. Pham, C. Jungemann, and B. Meinerzhagen, "Modeling and validation of piezoresistive coefficients in Si hole inversion layers," *Solid-State Electronics*, vol. 53, no. 12, pp. 1325–1333, 2009.
- [2] A. Erlebach, K. H. Lee, and F. M. Bufler, "Empirical Ballistic Mobility Model for Drift-Diffusion Simulation," in *Proceedings of the 46th European Solid-State Device Research Conference (ESSDERC)*, Lausanne, Switzerland, pp. 420–423, September 2016.

# 4

## Descriptions of Models

---

*This chapter presents a review of selected models of Sentaurus Device.*

---

### Overview of Models

Given the many models implemented in Sentaurus Device for the simulation of device characteristics, it is often difficult to quickly design appropriate command files for device simulation. Therefore, this chapter presents a review of selected models, which are evaluated with respect to their capabilities in simulating certain device aspects.

In the quantum drift-diffusion (QDD) approximation, electron and hole mobilities determine charge carrier transport. Advanced Calibration Device focuses on low-field mobility and high-field mobility, with and without mechanical stress, for planar and nonplanar silicon and SiGe FETs. In addition, there is a discussion of models and parameters for InGaAs, AlGaN, and SiC devices.

---

### CMOS Devices

This section discusses models relevant to CMOS devices.

---

#### Unstrained Band Structure and Electrostatics

In Sentaurus Device, the band gap, the electron affinity, the bandgap narrowing, and the density-of-states define the bulk band structure. The temperature dependency of these quantities and the doping dependency of the bandgap narrowing are represented by empirical functions.

---

#### Strained Band Structure and Electrostatics

The band structure changes with the mechanical stress in the device. The dependency of the conduction and valence bands and, therefore, of the band gap and electron affinity, on

## Chapter 4: Descriptions of Models

### CMOS Devices

the mechanical stress or strain is described by the deformation potential model where the band structure information comes from the  $k \cdot p$  calculation. You can also extract the stress dependency of the density-of-states from the  $k \cdot p$  calculation.

---

## Unstrained Low-Field Mobility

In the limit of low-driving fields, several mechanisms can degrade mobility. Typically, MISFET simulation takes into account mobility degradation by ionized dopants, surface roughness scattering, surface phonon scattering, and bulk phonon scattering. For high-k gate stacks, you must consider additional remote scattering mechanisms such as remote Coulomb scattering (RCS), remote phonon scattering (RPS), and remote dipole scattering (RDS). A crucial point is the transition between bulk mobility and inversion or accumulation layer mobility. Because of the transition from 3D to 2D charge carrier gas, the scattering behavior of electrons and holes changes and screening becomes different. Furthermore, the mobility model must include dependency on the channel material (for example, the germanium mole fraction), the channel direction, and the surface orientation. For thin silicon films in the range of a few nanometers, additional contributions come into effect that cause a dependency of the mobility on the film thickness.

In summary, a drift-diffusion or QDD low-field mobility model for the simulation of SiON/SiO<sub>2</sub> or high-k gate stack FETs without mechanical stress should have the following features:

- Mobility degradation by ionized impurities – impurity Coulomb scattering (ICS)
- Mobility degradation by the roughness of the surface or interface – surface roughness scattering (SRS)
- Mobility degradation by interaction with bulk phonons – bulk phonon scattering (BPS)
- Mobility degradation by interaction with surface phonons – surface phonon scattering (SPS)
- Mobility degradation by charges in the gate isolator (high-k gate stack) (RCS)
- Mobility degradation by different permittivity in the gate isolator (high-k gate stack) (RPS)
- Mobility degradation by dipole configurations in the gate isolator (high-k gate stack) (RDS)
- Mole fraction dependency of the low-field mobility model parameters (for example, alloy scattering)
- Transition between bulk scattering and scattering in 2D charge carrier gas for ICS
- Parameters for different channel and surface or interface orientations; channel: <100> and <110>; surface: (100) and (110)

## Chapter 4: Descriptions of Models

### CMOS Devices

- Mobility degradation for very thin silicon films
- Mobility in thin films, including influence of quantization

Sentaurus Device offers the following low-field mobility degradation models for MISFET simulation:

- Bulk phonon-limited mobility model (BPS):

```
Physics { ConstantMobility }
```

- Mobility degradation by ionized impurities (in some cases, it contains bulk phonon-limited mobility, in the low-doping limit) (ICS):

- Masetti model provides mole fraction–dependent model parameters:

```
Physics { Mobility ( DopingDependence (Masetti) ) }
```

- Arora model provides mole fraction–dependent model parameters:

```
Physics { Mobility ( DopingDependence (Arora) ) }
```

- Philips unified mobility model includes screening and carrier–carrier scattering, and provides mole fraction–dependent model parameters:

```
Physics { Mobility ( PhuMob ) }
```

- University of Bologna bulk mobility model is specially calibrated for an extended temperature range and provides mole fraction–dependent model parameters:

```
Physics { Mobility ( DopingDependence (UniBo) ) }
```

- Carrier–carrier scattering models (Conwell–Weisskopf and Brooks–Herring):

```
Physics { Mobility ( CarrierCarrierScattering ) }
```

- Mobility degradation at interfaces:

- Enhanced Lombardi model includes automatic detection of surface orientation and provides mole fraction–dependent model parameters:

```
Physics { Mobility ( Enormal (Lombardi) ) }
```

- Inversion and accumulation layer mobility model includes automatic detection of surface orientation, provides mole fraction–dependent model parameters, and contains the Philips unified mobility model, the enhanced Lombardi model, and additional terms for Coulomb scattering in 2D electron gas:

```
Physics { Mobility ( Enormal (IALMob) ) }
```

- University of Bologna surface mobility model is specially calibrated for an extended temperature range, includes screening of bulk ICS, no special model for ICS in 2D

## Chapter 4: Descriptions of Models

### CMOS Devices

charge carrier gas, and simplified Lombardi-style model for acoustic phonon and surface roughness scattering:

```
Physics { Mobility ( Enormal (UniBo) ) }
```

- 2D Coulomb scattering model for ionized impurities, which must not be used with the PhuMob model or any other DopingDependence model because mobility degradation is counted twice, is designed for Coulomb scattering (ICS) in 2D charge carrier gas:

```
Physics { Mobility ( Enormal (Lombardi Coulomb2D) ) }
```

- 2D Coulomb scattering models for positive and negative charges at remote interfaces allow you to distinguish between RCS and RDS:

```
Physics { Mobility ( Enormal (Lombardi NegInterfaceCharge  
PosInterfaceCharge) ) }
```

- Thin-layer mobility model describes mobility degradation due to finite silicon film thickness, includes dependency of phonon scattering on quantization as well as additional empirical mobility degradation terms, and includes automatic detection of surface orientation. The model can be combined with Enormal-like models:

```
Physics { Mobility (ThinLayer) }
```

Because of the use of Matthiessen's rule, several combinations of these mobility models are possible. For MISFETs, you usually need to combine bulk phonon and Coulomb scattering with scattering at interfaces and surfaces. Historically, the following combinations have been used:

1. DopingDependence(Masetti) + Lombardi
2. PhuMob + Lombardi
3. IALMob
4. IALMob + RPS + NegInterfaceCharge + PosInterfaceCharge
5. RPS + NegInterfaceCharge + PosInterfaceCharge + ThinLayer(IALMob)

Combination 2 has been the standard for a long time. However, several problems require a change to another low-field mobility model. First, the transition between 3D bulk Coulomb scattering and Coulomb scattering in the inversion layer is not described correctly because the PhuMob model, which is a bulk model, is used for the mobility degradation by scattering at ionized impurities from accumulation to strong inversion. This causes problems in describing the onset of moderate or strong inversion around the threshold voltage in the  $I_d - V_g$  curve. Second, in thin silicon layers, it is mandatory to include the dependency on the film thickness.

## Chapter 4: Descriptions of Models

### CMOS Devices

#### Note:

For these reasons, you must change the low-field mobility framework and switch to combination 3, 4, or 5. For MISFET simulation, the recommended models are combination 3 (devices without high-k gate stacks), combination 4 (devices with high-k gate stacks), and combination 5 (thin films).

---

## Strained Low-Field Mobility

This section discusses strained low-field mobility.

### Influence of Mechanical Stress

Modeling the influence of stress on the channel mobility must deal with several typical cases. These cases must be simulated accurately to minimize additional device calibration. The typical cases are as follows:

- Planar silicon channel PMOS with compressive stress between 0.5 GPa and 2 GPa in the channel direction and up to 2 GPa tensile stress normal to the silicon surface (gate-first with SiGe pockets and dual stress liner (DSL))
- Planar silicon channel PMOS with compressive stress between 1 GPa and 3 GPa in the channel direction and less than 500 MPa normal to the silicon surface (gate-last with SiGe pockets)
- Planar silicon channel NMOS with tensile stress between 1 GPa and 2 GPa in the channel direction and less than 500 MPa normal to the silicon surface (gate-last with SiC pockets)
- Planar silicon channel NMOS with tensile stress between 300 MPa and 1.5 GPa in the channel direction and up to 2 GPa compressive stress in the normal direction (gate-first with DSL and stress memorization technique)
- Planar PMOS channel with biaxial strained SiGe channel and stress between 1 MPa and 4 GPa in the channel direction and up to 2 GPa tensile stress in the normal direction (gate-first with DSL and SiGe pockets)
- Nonplanar silicon channel NMOS (FinFET) with mixed compressive or tensile stress components of up to 2 GPa depending on the configuration (for example, with SiC pockets wrapped around the fin and metal gate as a liner replacement)
- Nonplanar silicon channel PMOS (FinFET) with mixed compressive or tensile stress components of up to 2 GPa depending on the configuration (for example, with SiGe pockets wrapped around the fin and metal gate as a liner replacement)

## Chapter 4: Descriptions of Models

### CMOS Devices

- Nonplanar SiGe or Ge channel NMOS (FinFET) with mixed compressive or tensile stress components of up to 4 GPa depending on the configuration
- Nonplanar SiGe or Ge channel PMOS (FinFET) with mixed compressive or tensile stress components of up to 4 GPa depending on the configuration

You must simulate stress configurations for several wafer orientations (such as (001) and (110)), channel directions (such as <100> and <110>), and channel materials (such as silicon and SiGe). Typically, all three stress components ( $s_{xx}$ ,  $s_{yy}$ , and  $s_{zz}$ ) are important. A model validity check, which is limited to uniaxial or biaxial stress configurations, is not sufficient. In addition, the response of mobility degradation components (such as phonon scattering, Coulomb scattering, and remote scattering) to mechanical stress differs and requires the separate treatment of each component.

Typically, in Sentaurus Device, the total mobility is scaled with a stress enhancement factor calculated with the models discussed here. The following models in Sentaurus Device describe the influence of stress on mobility:

- Piezoresistance mobility models:
  - [First-Order \(Linear\) Piezoresistance Mobility Model](#)
  - [Second-Order Piezoresistance Mobility Model](#)
  - [Nonlinear Piezoresistance Models for Electrons and Holes \(MCmob and SBmob\)](#)
- Occupation-based and band structure-based models:
  - [Intel Stress-Induced Hole Mobility Model \(hSixBand\)](#)
  - [eSubband Model for Electrons](#)
  - [hSubband Model for Holes](#)

You can choose several additional options. For the piezoresistance mobility models, the Kanda option includes the dependency of the stress-induced mobility change on doping concentration. Differences in the influence of mechanical stress on minority and majority carriers can be considered by an additional fitting parameter. You can also calibrate the influence of the normal electric field in a metal–insulator–semiconductor (MIS) structure and of the germanium mole fraction on the first-order piezoresistive coefficients. Because the first-order and second-order piezoresistance mobility models are bulk models, the default piezoresistive coefficients are not accurate for inversion layers and must be adjusted. The first-order and second-order piezoresistance mobility models can be used as factor models or tensor models, thereby introducing anisotropic properties.

## Chapter 4: Descriptions of Models

### CMOS Devices

You can fine-tune the influence of the saturation velocity on stress-dependent mobility by setting the `SaturationFactor` parameter that controls how strongly the saturation velocity depends on stress as follows:

- Setting `SaturationFactor=0` means the mobility change is applied to the low-field mobility only.
- Setting `SaturationFactor=1` means the mobility change applies to the total mobility. This is the default in Sentaurus Device.

Because it is known from Monte Carlo simulation and from experiments that short-channel transistors show a much lower mobility enhancement due to mechanical stress, it is better to apply the mobility change to the low-field mobility only. Further adjustment of this parameter should be performed with good references only.

The occupation-based and band structure-based models characterize the dependency of occupation and band structure on mechanical stress for the calculation of the mobility. These models have their own dependency on the doping concentration, and a Kanda-like option is not necessary. In addition, the electric field dependency should be a result of the model itself.

## First-Order (Linear) Piezoresistance Mobility Model

This model uses the piezoresistance tensor with constant coefficients to calculate the stress-induced mobility change.

### Options

The model can be used as a factor (isotropic) model or a tensor (anisotropic) model. The piezoresistive coefficients can depend on the normal electric field in an inversion layer. Minority and majority charge carrier transport can be distinguished. You can include dependency on the doping concentration. Calibration of dependency of the influence of mechanical stress on the saturation velocity is possible.

### Advantages

The model is well adjusted to measurements for the bulk case. It is fully transformable, so it can consider all stress configurations and current directions in a bulk situation. It is easy to use and to calibrate.

### Disadvantages

It is accurate for low stress only (< 200 MPa). Tensor symmetry is broken for nonbulk conditions as in an inversion layer, which is not reflected by the model. The default piezoresistive coefficients are not accurate for inversion layers.

## **Second-Order Piezoresistance Mobility Model**

This model uses the 6th-grade piezoresistance tensor with constant coefficients to calculate the stress-induced mobility change.

### **Options**

The model can be used as a factor (isotropic) model or a tensor (anisotropic) model. Minority and majority charge carrier transport can be distinguished. You can include dependency on the doping concentration. Calibration of dependency of the influence of mechanical stress on the saturation velocity is possible.

### **Advantages**

Parameters are available for the bulk case. The model is fully transformable, so it can consider all stress configurations and current directions in a bulk situation.

### **Disadvantages**

It is accurate for low and moderate stress values only (< 500 MPa). Tensor symmetry is broken for nonbulk conditions as in an inversion layer, which is not reflected by the model. The default piezoresistive coefficients are not accurate for inversion layers.

## **Nonlinear Piezoresistance Models for Electrons and Holes (MCmob and SBmob)**

These models use nonlinear piezoresistive coefficients and higher-order cross-term corrections that are extracted from Monte Carlo simulation, Sentaurus Band Structure simulation, or other sources (experiments and simulations available from the literature).

### **Options**

Minority and majority charge carrier transport can be distinguished. You can include dependency on the doping concentration. Calibration of dependency of the influence of mechanical stress on the saturation velocity is possible. Germanium mole fraction dependency of the model coefficients can be switched on. Parameters for different orientations can be used and an auto-orientation option is available. You can load complete parameter sets using the Sentaurus Device parameter file.

### **Advantages**

Parameters are available for strong inversion and for different channel materials (silicon and SiGe). The model can be extended to other conditions when there are reference tools such as Monte Carlo simulations or experiments. The model is available for different channel and wafer orientations. It is fast and can be calibrated easily.

### **Disadvantages**

Interpolation especially for untypical stress conditions must always be validated. The physics is in the reference tool, for example, the Monte Carlo simulator. Improving the model without improving the reference tool or without obtaining better experiments is not possible, except with respect to the interpolation. The settings for the local coordinate system must be specified in the Sentaurus Device parameter file.

## **Intel Stress-Induced Hole Mobility Model (hSixBand)**

This model uses the change of band structure and occupation to calculate stress-dependent mobility.

### **Options**

You can switch on dependency on the doping or carrier concentration.

### **Advantages**

The model is derived from physical assumptions.

### **Disadvantages**

Calibration is not straightforward. Only silicon as a channel material is available. The influence of surface orientation cannot be described. The model has been developed and calibrated for uniaxial stress in the <110> direction. The combination of the component normal to the MIS plane with the in-plane stress components is not validated.

## **eSubband Model for Electrons**

This model uses the change of band structure and occupation to calculate the mobility change.

### **Options**

You can switch on dependency on the doping or carrier concentration. Stress-related change in the scattering can be included. Change of effective mass with stress can be added to the model. For the inversion layer, the `MLDA` option can be used.

### **Advantages**

The `MLDA` option allows you to move from bulk to inversion layer conditions, and to take surface or channel orientation dependency into account. The model is derived from physical assumptions. The model is validated and calibrated for silicon and SiGe for different channel and surface orientations. Mole fraction dependency for SiGe is available.

### **Disadvantages**

Calibration is not straightforward.

## **hSubband Model for Holes**

This model uses the change of band structure and occupation to calculate stress-dependent mobility.

### **Options**

You can switch on dependency on the doping or carrier concentration. Stress-related change in the scattering can be included. Change of effective mass with stress can be added to the model. For the inversion layer, the `MLDA` option can be used.

### **Advantages**

The `MLDA` option allows you to move from bulk to inversion layer conditions, and to take surface or channel orientation dependency into account. The model is derived from physical assumptions. The model is validated and calibrated for silicon and SiGe for different channel and surface orientations. Mole fraction dependency for SiGe is available.

### **Disadvantages**

Calibration is not straightforward.

---

## **Unstrained High-Field Mobility**

The low-field mobility models are valid for small driving forces only. To take into account high-field effects, the additional high-field saturation model is introduced in the drift-diffusion model framework.

### **Note:**

Calibrated mole fraction-dependent parameters are available and extensive experience exists. Numeric problems are known or are already solved.

The high-field saturation model should limit the velocity-field relation to the saturation velocity of the material when there is sufficient scattering, and it must provide a way to calibrate the influence of ballistic and quasiballistic transport on the charge carrier transport. In addition, it should allow you to calibrate the germanium mole fraction dependency of the model parameters. Furthermore, because of deficiencies in the drift-diffusion model to describe the current response close to equilibrium, a model is needed that allows you to compensate or, at least, to calibrate for this deficiency.

## Chapter 4: Descriptions of Models

### CMOS Devices

In summary, a drift-diffusion or QDD high-field mobility model for the simulation of SiON/SiO<sub>2</sub> or high-k gate stack FETs without mechanical stress should have the following features:

- Limiting the drift velocity to the saturation velocity for cases with sufficient scattering
- Possibility to calibrate the model with respect to ballistic and quasiballistic transport
- Germanium mole fraction–dependent model parameters
- Possibility to calibrate the model with respect to current response close to equilibrium
- Orientation-dependent model parameters

Sentaurus Device offers the following high-field mobility models for MISFET simulations:

- Extended Canali model is the main model for drift-diffusion simulation and can also be used with the hydrodynamic model. It has calibrated parameters for silicon and SiGe for situations where ballistic or quasiballistic transport is not present. Calibration to short-channel devices where quasiballistic transport occurs can be done using model parameters:

```
Physics { Mobility (HighfieldSaturation) }
```

- Transferred electron model is specially designed for GaAs and materials with a similar band structure:

```
Physics { Mobility (HighfieldSaturation  
(TransferredElectronEffect)) }
```

- Basic model is a simple model with carrier temperature as the driving force and requires the hydrodynamic model:

```
Physics { Mobility (HighfieldSaturation (CarrierTempDriveBasic)) }
```

- Meinerzhagen–Engl model is a Canali-like high-field saturation model with carrier temperature as the variable and requires the hydrodynamic model:

```
Physics { Mobility (HighfieldSaturation (CarrierTempDriveME)) }
```

The common model for drift-diffusion or QDD simulations is the extended Canali model.

---

## Strained High-Field Mobility

In the QDD model, the dependency of high-field mobility on mechanical stress is determined by the strain dependency of the saturation velocity. The saturation velocity covers both the strain dependency of the physical saturation velocity and the strain dependency of the quasiballistic transport. The model is again the Canali model where the parameter `SaturationFactor` controls the stress dependency.

## Gallium Nitride HEMTs

GaN HEMTs have unique qualities that require special attention. First, there is the large band gap that results in very low charge-carrier densities and numeric problems. Second, in the on-state, the current conduction is performed using a 2D electron gas channel in the GaN layer. This has implications for the modeling of mobility. Third, most of these structures use material combinations in addition to pure GaN and AlN, such as AlGaN. The mole fraction of these alloys determines the thermal conductivity, the mobility, and the band gap. For that reason, you need mole fraction-dependent parameters that make the transition from GaN to AlN. In general, linear or parabolic interpolation between GaN and AlN is not sufficient because of the alloy influence. Furthermore, there is the influence of strain causing polarization in the device. In addition, traps strongly influence the device operation, and the saturation velocity behavior differs from silicon.

---

## Silicon Carbide Devices

As another wide-bandgap material, SiC shows some differences to silicon as well. There are numeric problems connected with the small densities caused by the large band gap. The anisotropy of the mobility and of the avalanche coefficients is difficult to handle numerically. Traps, contact behavior, incomplete ionization, and tunneling play more critical roles in SiC devices than in silicon devices. You must include the incomplete ionization ([IncompleteIonization](#)) model in the simulation because of the wide band gap of SiC. Anisotropic behavior can be considered for thermal conductivity, mobility, and impact ionization.

---

## Silicon Smart-Power Devices

Model requirements are similar to those for silicon deep-submicron devices (see [Path A: Basic CMOS Simulation Command File Sections on page 22](#)) fabricated by gate-first processes, but with a greater variety of process and doping conditions and layout specifications. In addition, there is a need for:

- High accuracy over a wide temperature range up to very high temperatures
- Good modeling capabilities for avalanche and breakdown
- Good modeling capabilities for electrostatic discharge (ESD)

For avalanche generation, the `UniBo2` model is calibrated for a temperature range from 300 K to 773 K and is best suited for ESD and high-temperature simulations. It also is recommended for room-temperature breakdown simulations.

# 5

## Quality of Fitting and Extraction

---

*This chapter discusses fitting quality and extraction issues.*

---

### Low-Field Mobility of Planar CMOS Devices With Silicon Channel

This section discusses the requirements and the quality of the extraction of the parameters for the low-field mobility of planar CMOS devices.

---

#### Oxide–Silicon Interface

This section briefly explains how the low-field mobility parameter sets have been calibrated.

Data from Takagi *et al.* [1][2], Nakamura *et al.* [3], and Nayfeh *et al.* [4] has been used to calibrate mobility in the transistor channel. All data is from pure polysilicon/SiO<sub>2</sub> gate stacks with oxide thicknesses of 25 nm for Takagi, 2 nm for Nakamura, and 5 nm for Nayfeh.

This data does not have high-k gate stacks and, therefore, allows you to extract the model parameters of surface phonon, surface roughness, and Coulomb scattering at ionized impurities. On the other hand, process-induced variations in surface roughness and the material composition of the first atomic layers at the isolator–silicon interface can influence mobility and result in different mobilities for different gate-formation process steps. These differences cannot be reflected by a single parameter set. Therefore, the parameter set presented here is a starting point for calibration.

Usually, the extraction of low-field mobility as a function of the effective electric field  $E_{\text{eff}}$  begins with measuring the drain current in the linear regime and, from that, the mobility is calculated for each gate voltage. At the same time, the inversion charge per area  $N_{\text{inv}}$  is calculated from C–V characteristics. Because  $E_{\text{eff}}$  is not measured, it must be calculated from  $N_{\text{inv}}$  using  $E_{\text{eff}} = E_{\text{eff}}(N_{\text{depl}}, N_{\text{inv}}, \eta)$ . Mostly, the depletion approximation with  $N_{\text{depl}}$  as the depletion charge is used for this, where the doping is extracted from other experiments and is assumed to be constant. The result is the dependency  $\mu = \mu(E_{\text{eff}})$ . To obtain the universal behavior, that is, the doping-independent behavior of the mobility for strong inversion, the fitting parameter  $\eta$  is introduced in the equation used to determine the effective field. You must use different values for  $\eta$  to obtain the universal behavior for

## Chapter 5: Quality of Fitting and Extraction

### Low-Field Mobility of Planar CMOS Devices With Silicon Channel

different charge carriers and surface orientations (electrons: 1/2 for (100) and 1/3 for (110), holes: 1/3).

These standard parameters provide mostly good universal behavior for a (100) surface orientation and low-to-moderate doping. For a (110) surface orientation, high doping, or nonplanar and double-gate devices, the universal behavior is mostly not fully achieved. In general, it remains a question of whether the use of this extraction method, and especially the use of the same  $\eta$  in the extraction from measurement and simulation, is correct.

If  $\eta = 1$ , then  $E_{\text{eff}}$  corresponds exactly to the electric field at the interface in the depletion approximation. However,  $\eta < 1$  lowers the field strength, thereby taking into account that the current flow not only is at the surface but also is distributed a few nanometers into the depth of the silicon. Because it is unclear whether the field and current density distribution and the local dependency of mobility on the electric field are described sufficiently in the simulation, it might be difficult to achieve universal behavior in simulations with the same  $\eta$  parameter as in measurement.

Often, this universality is achieved only by introducing an artificial doping dependency for surface phonon scattering (SPS) and surface roughness scattering (SRS) in the Lombardi terms for the mobility models. However, it is unclear whether this doping dependency exists at all, or whether it is only a result of this forced parameter fitting. It can result in an unusual situation where the mobility degradation in intrinsic or very low-doped regions is actually stronger than in high-doped regions and drops to completely unrealistic values.

Because of this, another extraction methodology is used for the mobility parameters. The mobility model is calibrated to the measured  $\mu = \mu(N_{\text{inv}})$  curves. For this, no calibration of  $\eta$  is necessary, and universal behavior is not requested. After this, a check is performed with  $\mu = \mu(E_{\text{eff}})$  but additional calibration is performed only if there are strong disagreements. [Figure 8 to Figure 16](#) show the agreement between measurement and simulation.

When simulating CMOS devices with precalibrated parameter sets, you must always take into account that these parameter sets are *initial* parameter sets that can undergo additional fine-tuning and major changes. The reasons are mainly connected to the dependency of mobility degradation on the processing.

For example, the interface or surface roughness depends on the process conditions and the materials involved. Applying the parameters already extracted to modern FinFET devices with a <110> channel direction often underestimates the inversion mobility, because the surface roughness-related mobility degradation is smaller on the (110) fin sidewalls than in the planar (110) case [5].

Similarly, for surface phonon-related interface mobility, the process conditions and the materials involved introduce some uncertainties that do not allow you to derive a parameter set that is valid for several device types or technology generations. Recalibration is usually required.

The strength of remote Coulomb scattering (RCS) or remote dipole scattering (RDS) depends on the number of charges in the high-k gate stack and their position. The model

## Chapter 5: Quality of Fitting and Extraction

### Low-Field Mobility of Planar CMOS Devices With Silicon Channel

must be calibrated to measurements when switching it on. RCS and RDS have the same origin: the mobility degradation by charges in the high-k gate stack. The difference is in the presence of both negative and positive charges in the case of RDS. For remote phonon scattering (RPS), the parameters are extracted from Monte Carlo simulation. Depending on the properties of the high-k gate stack, fine-tuning might be necessary. However, because it is difficult to extract the correct parameters without having mobility measurements for different interfacial layer thicknesses and different temperatures, you should keep the parameters for RPS and focus on the calibration of RCS and RDS.

The Philips unified mobility (`PhuMob`) model is calibrated to bulk mobility measurements. Usually, fine-tuning is necessary only when performing a custom calibration with high-accuracy requirements. In addition, mobility fine-tuning cannot be separated from the calibration of the doping concentration or dopant activation. Therefore, you should keep the default parameters.

In the framework of the inversion and accumulation layer mobility (`IALMob`) model, when going to inversion layer conditions, 3D Coulomb scattering turns to 2D Coulomb scattering, the `PhuMob` model is switched off, and the 2D Coulomb scattering model takes over. The 2D Coulomb scattering model is a very simple description of reality with many fitting parameters. This model mainly influences the onset of the I–V curves. The default parameters are not very good, and additional calibration is necessary.

The stress dependency of mobility resulting from `hSubband` (holes), `eSubband` (electrons), `MCmob`, and `SBmob` simulations has been compared to the literature and in-house Monte Carlo (Sentaurus Device Monte Carlo) and Kubo–Greenwood (Sentaurus Band Structure) simulations [6][7][8].

## Chapter 5: Quality of Fitting and Extraction

### Low-Field Mobility of Planar CMOS Devices With Silicon Channel

Figure 8 Electron mobility versus areal inversion density for (100) surface in linear scale, with (top to bottom) channel doping of  $3.9e15$ ,  $2e16$ ,  $7.2e16$ ,  $3e17$ ,  $7.7e17$ , and  $2.4e18$

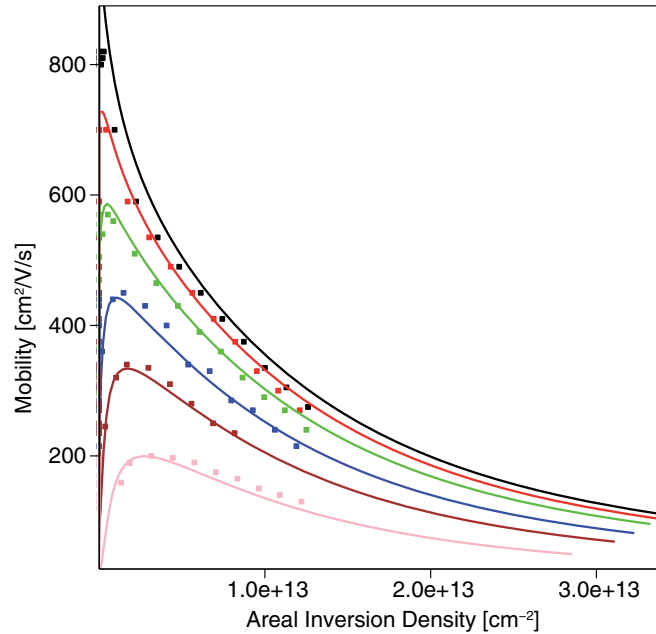
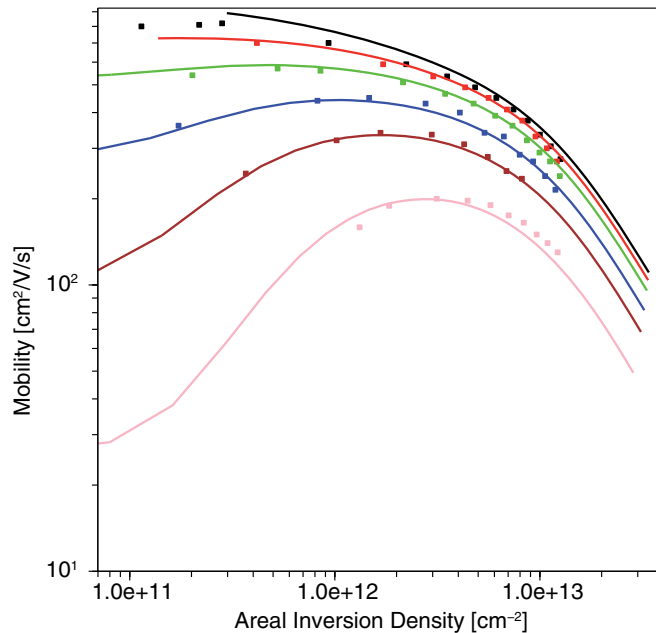


Figure 9 Electron mobility versus areal inversion density for (100) surface in logarithmic scale with (top to bottom) channel doping of  $3.9e15$ ,  $2e16$ ,  $7.2e16$ ,  $3e17$ ,  $7.7e17$ , and  $2.4e18$



## Chapter 5: Quality of Fitting and Extraction

### Low-Field Mobility of Planar CMOS Devices With Silicon Channel

Figure 10 Hole mobility versus areal inversion density for (100) surface in linear scale with (top to bottom) channel doping of  $7.8e15$ ,  $1.6e16$ ,  $5.1e16$ ,  $2.7e17$ , and  $6.6e17$

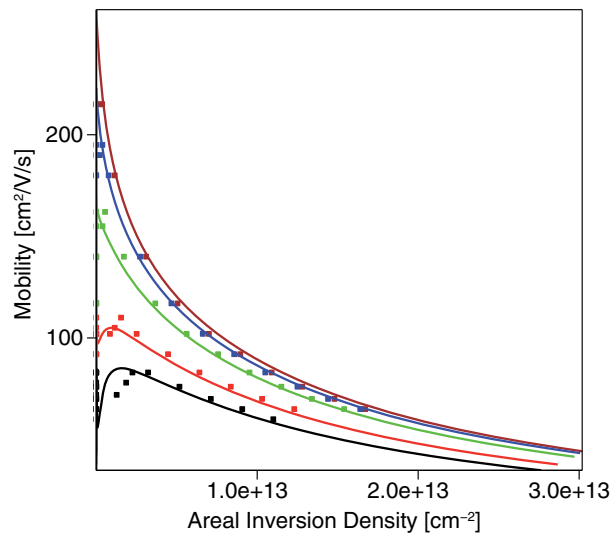
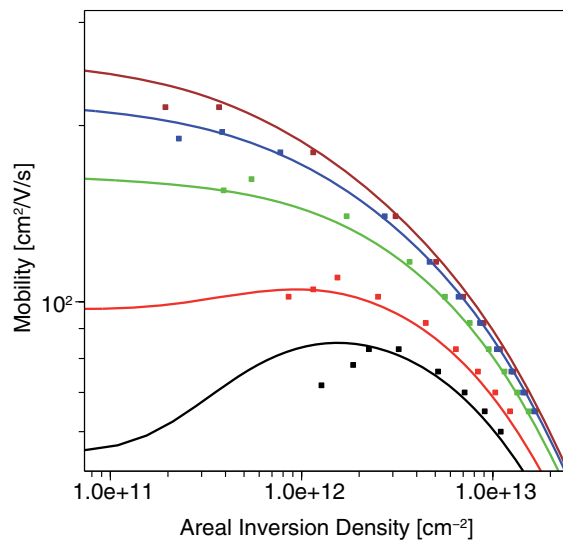


Figure 11 Hole mobility versus areal inversion density for (100) surface in logarithmic scale with (top to bottom) channel doping of  $7.8e15$ ,  $1.6e16$ ,  $5.1e16$ ,  $2.7e17$ , and  $6.6e17$



## Chapter 5: Quality of Fitting and Extraction

### Low-Field Mobility of Planar CMOS Devices With Silicon Channel

Figure 12 Electron mobility versus effective field for (100) surface in linear scale with (top to bottom) channel doping of  $3.9e15$ ,  $2e16$ ,  $7.2e16$ ,  $3e17$ ,  $7.7e17$ , and  $2.4e18$

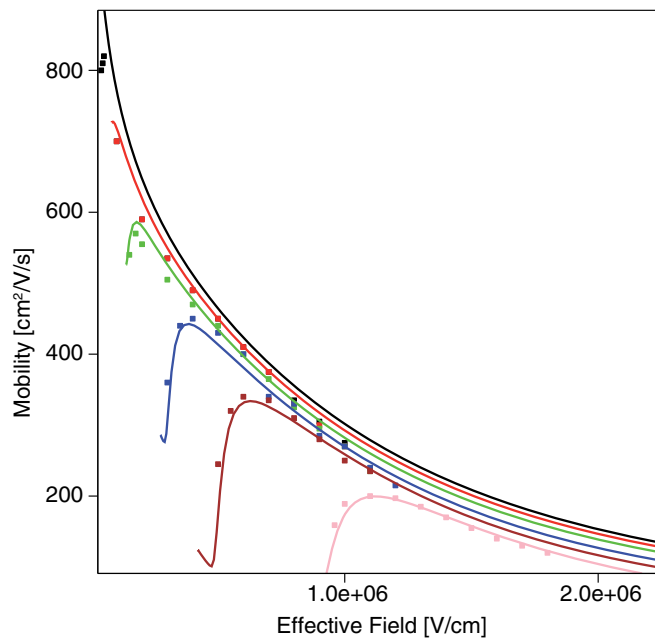
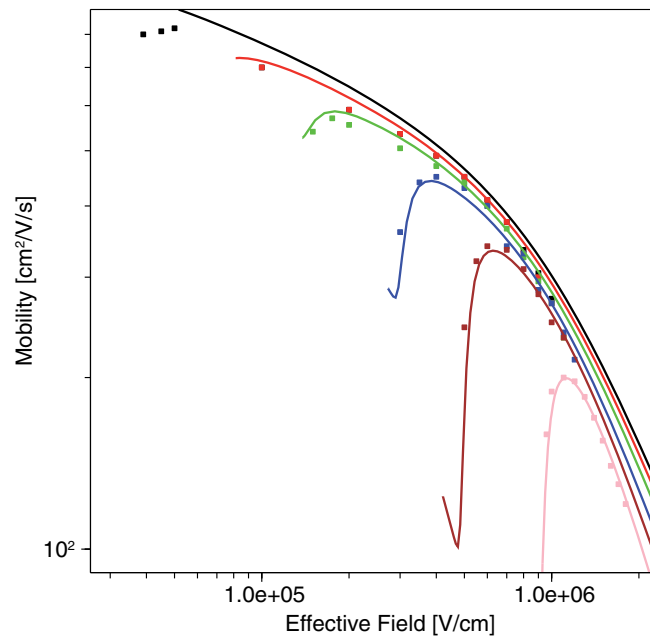


Figure 13 Electron mobility versus effective field for (100) surface in logarithmic scale with (top to bottom) channel doping of  $3.9e15$ ,  $2e16$ ,  $7.2e16$ ,  $3e17$ ,  $7.7e17$ , and  $2.4e18$



## Chapter 5: Quality of Fitting and Extraction

### Low-Field Mobility of Planar CMOS Devices With Silicon Channel

Figure 14 Electron mobility versus areal inversion density for (100) surface as a reference and for (110)/<100> and (110)/<110> in linear scale, with channel doping between 5e17 and 9e17

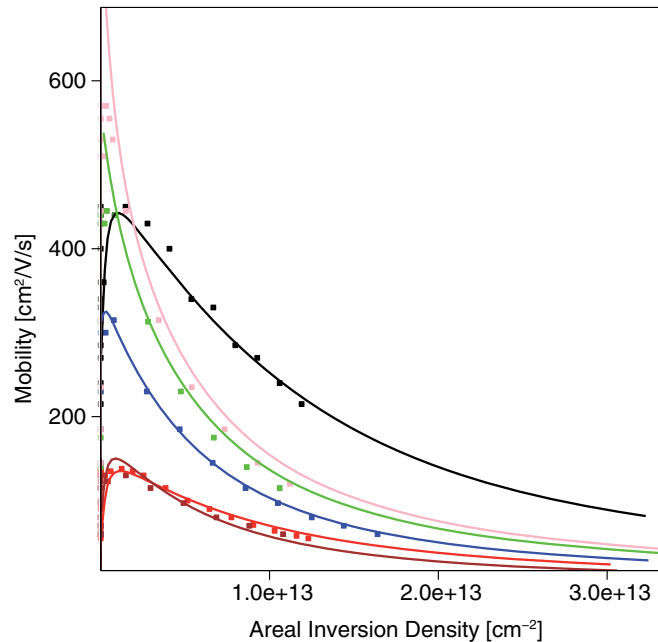
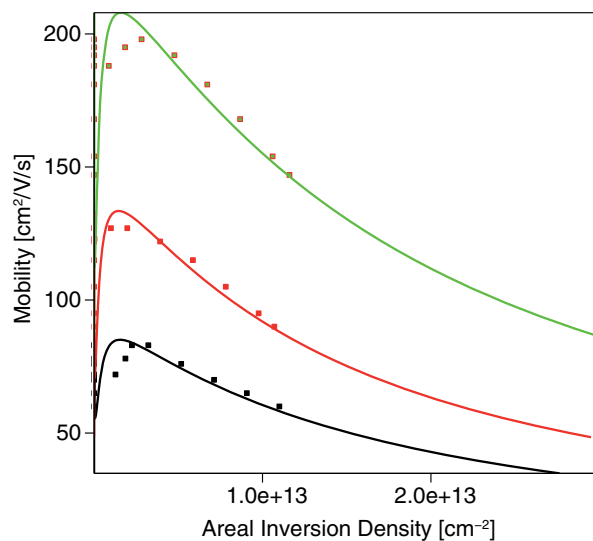


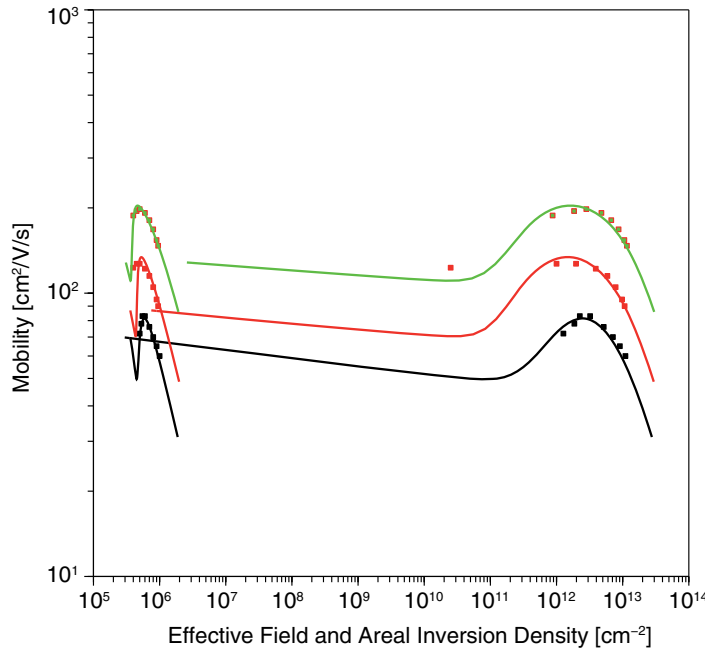
Figure 15 Hole mobility versus areal inversion density for (100) surface as a reference and for (110)/<100> and (110)/<110> in linear scale, with channel doping between 4.5e17 and 6.6e17



## Chapter 5: Quality of Fitting and Extraction

### Low-Field Mobility of Planar CMOS Devices With Silicon Channel

**Figure 16** Hole mobility versus effective field and areal inversion density for (100) surface as a reference and for (110)/<100> and (110)/<110> in double logarithmic scale, with channel doping between 4.5e17 and 6.6e17




---

## Influence of Metal Gate on Inversion Layer Mobility

The parameter set used to produce the results shown in [Figure 8](#) to [Figure 16](#) is derived from measurements on devices with a polysilicon/oxide gate stack. In devices with a metal/oxide gate stack, the channel mobility can differ because of the influence of the metal gate. The same applies to the comparison between polysilicon/HfO<sub>2</sub> and metal/HfO<sub>2</sub> gate stacks.

Usually, the transition from the polysilicon gate to the metal gate results in improved mobility. One reason for this could be the better screening of surface phonons and charges in the gate stack by the charge carriers in the metal gate [\[9\]](#).

**Table 11** Influence of different gate materials on the inversion layer mobility for electrons [\[9\]](#)

Gate stack	Maximum mobility [cm <sup>2</sup> /V/s]	Mobility at E <sub>eff</sub> = 1 MV/cm [cm <sup>2</sup> /V/s]
HfO <sub>2</sub> /Polysilicon	175	145
HfO <sub>2</sub> /TiN	245	200

## Chapter 5: Quality of Fitting and Extraction

### Low-Field Mobility of Planar CMOS Devices With Silicon Channel

The increasing mobility caused by the metal gate can be reflected by an increase of the `IALMob` parameters `B`, `C`, and `delta` by a factor of 1.4.

---

## Influence of High-k Gate Stack on Inversion Layer Mobility

The parameter set used to produce the results shown in [Figure 8](#) to [Figure 16](#) is derived from measurements on devices with a polysilicon/oxide gate stack. In devices with a high-k isolation (for example, with  $\text{HfO}_2$ ), the channel mobility can degrade because of the influence of charges in the gate isolator (RCS or RDS) and RPS.

Often, the charges are arranged in dipole-like configurations. The RCS-related mobility degradation depends on the number and the arrangement of charges in the gate isolator, especially on their distance to the inversion layer. RCS depends greatly on the process conditions and the materials used in the gate stack, and so the variation between technologies and process splits and even over the wafer and between wafers can be large. Therefore, it is not possible to provide well-calibrated default parameters, and custom calibration to the process and device under consideration is usually required. However, the model should describe the major tendencies such as dependency on the thickness of the interfacial oxide or on the concentration of charges in the gate stack.

[Table 12](#) and [Table 13](#) list model parameters for the `RPS` model and for the `InterfaceCharge` models that fulfill these requirements.

*Table 12 Recommended parameters and values for RPS model*

Parameter	Value for electrons	Value for holes	Comments
<code>d_crit</code>	1.0e-7 cm	1.0e-7 cm	Distance between high-k interface and silicon interface
<code>l_crit</code>	7.7e-8 cm	7.7e-8 cm	[10]
<code>murps0</code>	$124 \text{ cm}^2/(\text{Vs})$	$124 \text{ cm}^2/(\text{Vs})$	Extracted from Sentaurus Device Monte Carlo simulation

*Table 13 Recommended parameters and values for InterfaceCharge models (RCS and RDS, NegInterfaceCharge and PosInterfaceCharge models use the same parameters)*

Parameter	Value for electrons	Value for holes	Comments
<code>c_exp</code>	0.5	0.5	
<code>E0</code>	1.0e-6	1.0e-6	

## Chapter 5: Quality of Fitting and Extraction

Low-Field Mobility of Planar CMOS Devices With Silicon Channel

Table 13 Recommended parameters and values for InterfaceCharge models (RCS and RDS, NegInterfaceCharge and PosInterfaceCharge models use the same parameters) (Continued)

Parameter	Value for electrons	Value for holes	Comments
l_crit	7.7e-8	7.7e-8	[10]
mul	250	250	

## Extraction of Contact Resistance Parameters

Stavitski *et al.* [11] measured the contact resistance between PtSi and NiSi, and silicon. Based on this data, the parameters for the Schottky resistance (`SchottkyResist`) model in Sentaurus Device have been extracted (see Table 14).

### Note:

No additional tests or validations have been performed with this parameter set. In addition, the parameters are not included in the parameter files in the `MaterialDB` folder.

Table 14 Parameters for the SchottkyResist model for PtSi and NiSi

Parameter	Value for electrons	Value for holes
<b>PtSi</b>		
barrier	0.8 eV	0.4 eV
mt	0.08	0.08
Rinf	3.0e-10 $\Omega\text{cm}^2$	3.0e-10 $\Omega\text{cm}^2$
<b>NiSi</b>		
barrier	0.6 eV	0.6 eV
mt	0.08	0.08
Rinf	1.0e-9 $\Omega\text{cm}^2$	5.0e-10 $\Omega\text{cm}^2$

---

## Extraction of Parameters for Mobility Models in Accumulation Regime

In the accumulation regime, mobility is influenced by the same mobility degradation mechanisms as in the inversion regime. However, model parameters and the importance of single mobility degradation mechanisms can vary. Especially at higher background doping concentrations, the screening of Coulomb scattering differs between accumulation and inversion.

Because of the importance of the on-state and the measurement data available, the focus is on high accumulation areal densities. Reference [12] provides some specific and well explained measurements of mobilities in accumulation layers in planar bulk devices for different background doping concentrations at room temperature. These measurements have been used as a reference for the simulations with Sentaurus Device using the inversion and accumulation layer mobility (`IALMob`) model.

Despite small differences between accumulation and inversion layer mobility in the on-state claimed in [12], a calibrated parameter set is presented that improves the agreement for electrons. The parameter set also shows how to adjust the accumulation layer model parameters without changing much in the inversion regime. [Table 15](#) shows the parameters used for calibration.

*Table 15 Parameters of IALMob model used for calibration (electrons)*

Parameter	Recommended value	Parameter	Recommended value
<code>lambda</code>	0.02	<code>alpha_sr_D</code>	2.0e-14
<code>alpha_ph2d_A</code>	0.0	<code>lambda_sr</code>	0.02
<code>alpha_ph2d_D</code>	2.0e-14	<code>lambda_sr_A</code>	0.0
<code>lambda_ph2d_A</code>	0.0	<code>lambda_sr_D</code>	1.0
<code>lambda_ph2d_D</code>	1.0	<code>D1_acc</code>	1200
<code>alpha_sr_A</code>	0.0	<code>D2_acc</code>	1200

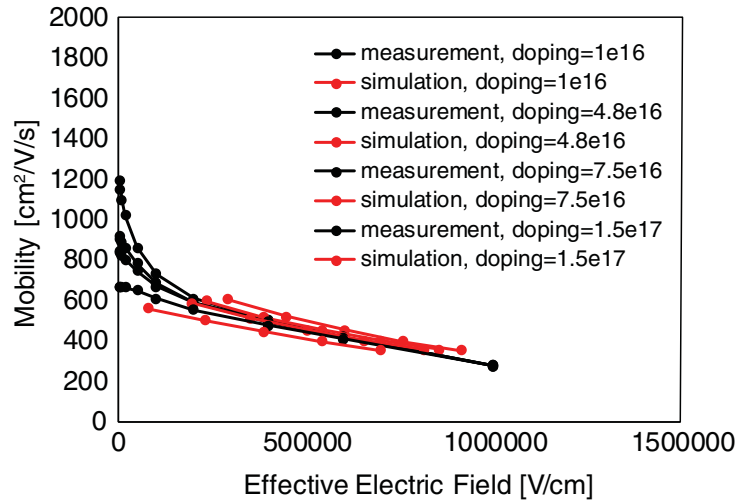
Essentially with these parameter settings, the doping dependence for the inversion case remains switched off and, when there is no accumulation doping, there is no change in the results. However, with `alpha_ph2d_D` or `alpha_sr_D`, and `lambda` or `lambda_sr` larger than zero, the doping dependence for the accumulation regime is switched on. In this way, you can separate the accumulation and inversion regimes.

The parameter set in [Table 15](#) gives reasonable agreement to the measurements in [12] (see [Figure 17](#)).

## Chapter 5: Quality of Fitting and Extraction

### Basic Properties of Silicon Carbide Devices

Figure 17 Mobility versus effective electric field for electrons and different donor doping concentrations; red lines: simulation and black lines: measurements from [12]



---

## Basic Properties of Silicon Carbide Devices

Parameter values and corresponding references can be found in the `4H-SiC.par` and `6H-SiC.par` files and in [13].

All silicon carbide (SiC) polytypes are indirect semiconductors, and the maximum of the upper valence bands is located at the center ( $\Gamma$ -point) of the Brillouin zone. Conduction band minima of 3C-SiC, 6H-SiC, and 4H-SiC are located at point X, point U on the (L-M) line, and point M, respectively.

Photoluminescence or absorption measurements give an exciton band gap  $E_{gx}$ . There are no reliable measured values for binding energies  $E_x$  of free excitons, which are required to obtain the indirect band gap  $E_g = E_{gx} + E_x$ . Since measured values of  $E_x$  range from 10 mV to 80 mV, a mean direct band gap can be assumed by shifting  $E_{gx}$  by 40 mV. In the parameter file, a value of  $Eg0=3.285$  eV is used.

Temperature dependency of the band gap is measured for 6H-SiC in the temperature ranges from 6 K to 200 K and from 300 K to 700 K. The dependency of 3C-SiC is measured in the temperature range from 295 K to 700 K. The dependency of 4H-SiC is assumed to be similar because no experimental data is available.

The effective mass of electrons and holes has been measured by optically detected by either cyclotron resonance or Raman scattering and has been compared to theoretical calculation. The theoretical calculation reproduced well the experimental results.

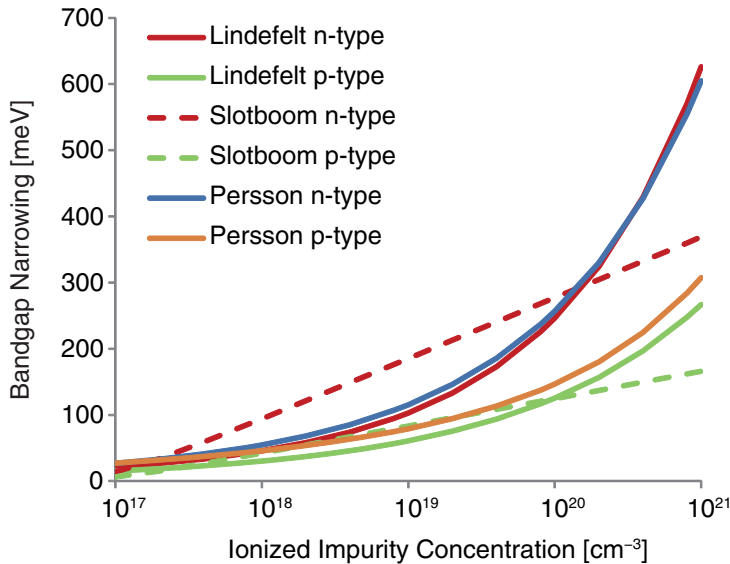
There is no published measured data of bandgap narrowing. The theoretical calculation was first performed by Lindefelt [14] and followed by Persson *et al.* [15]. The former model

## Chapter 5: Quality of Fitting and Extraction

### Basic Properties of Silicon Carbide Devices

constitutes an extension of a semiempirical method originally developed by Jain and Roulston [16]. The latter is based on random phase approximation. Both calculations give the analytic form of band-edge displacement depending on the doping density. The analytic form corresponds to the JainRoulston model implemented in Sentaurus Device.

Figure 18 Results of bandgap narrowing of 4H-SiC from [14] and [15] with the Slotboom model implemented in Sentaurus Device with calibrated coefficients



Electron affinity is calculated assuming the linear dependency of hexagonality together with the measured band offset of the conduction band for 3C-SiC or 6H-SiC, and the calculated result of the band offset of the valence band.

Parameter sets for the Hatakeyama model [17] and the Okuto–Crowell impact ionization model are implemented in the parameter files (see [Content of Parameter Files on page 9](#)). The parameter set for the Okuto–Crowell impact ionization model along the c-axis corresponds to the one reported by Niwa *et al.* [18].

[Figure 19](#) and [Figure 20](#) show the comparison of the impact ionization coefficients of different references.

## Chapter 5: Quality of Fitting and Extraction

### Basic Properties of Silicon Carbide Devices

Figure 19 Hole impact ionization coefficient along the c-axis of 4H-SiC [17][18][19]

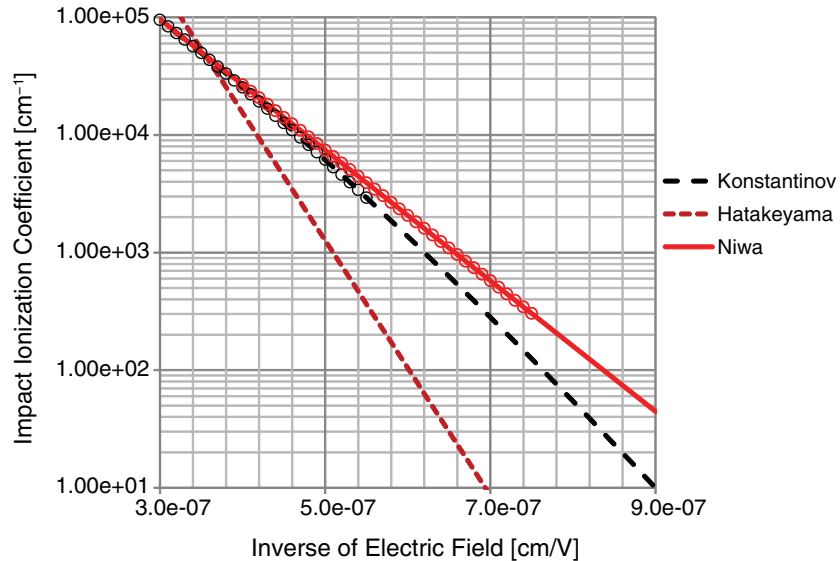
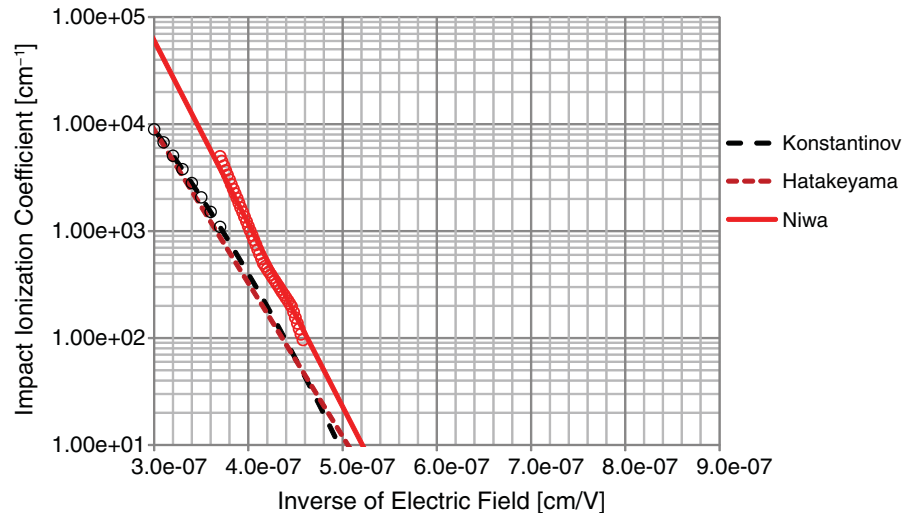


Figure 20 Electron impact ionization coefficient along the c-axis of 4H-SiC [17][18][19]



Temperature dependency of thermal conductivity of 4H-SiC and 6H-SiC perpendicular to the c-axis has been reported. At low temperatures,  $T^3$  dependency and  $T^2$  dependency are observed for 4H-SiC and 6H-SiC, respectively.  $T^2$  dependency is attributed to the scattering of phonons by electrons in the impurity band. Thermal conductivity in 6H-SiC single crystals decreases with increasing electron concentration, and the slope at low temperature can be represented by the  $T^2$  law, which confirms the dominance of electron scattering.

Temperature dependency of thermal conductivity using data from [20], [21], [22], and [23] as

## Chapter 5: Quality of Fitting and Extraction

### Basic Properties of Silicon Carbide Devices

cited in [24] is implemented in the parameter files (see [Content of Parameter Files on page 9](#)). Experimental data is that in the direction perpendicular to the c-axis.

Parameter sets for the Masetti and Arora doping-dependent mobility models are implemented in the parameter files (see [Content of Parameter Files on page 9](#)).

[Figure 21](#) and [Figure 22](#) show a comparison with different literature data.

*Figure 21 Doping-dependent electron mobility at 500 K for n-doped 4H-SiC [25][26][27]*

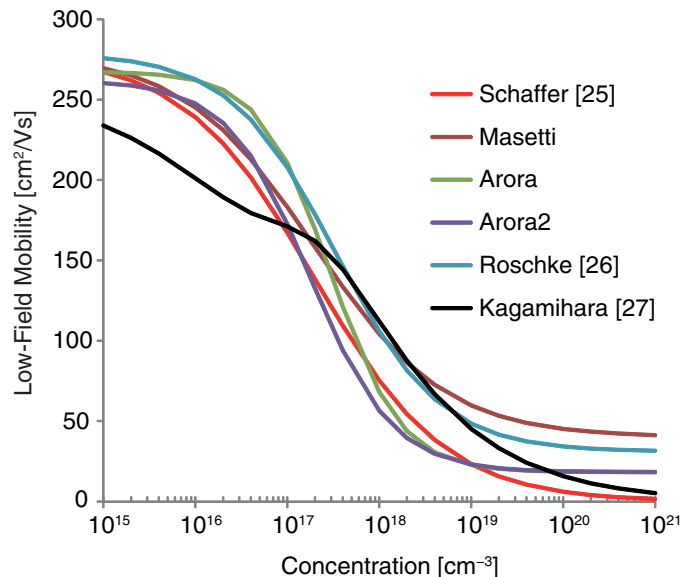
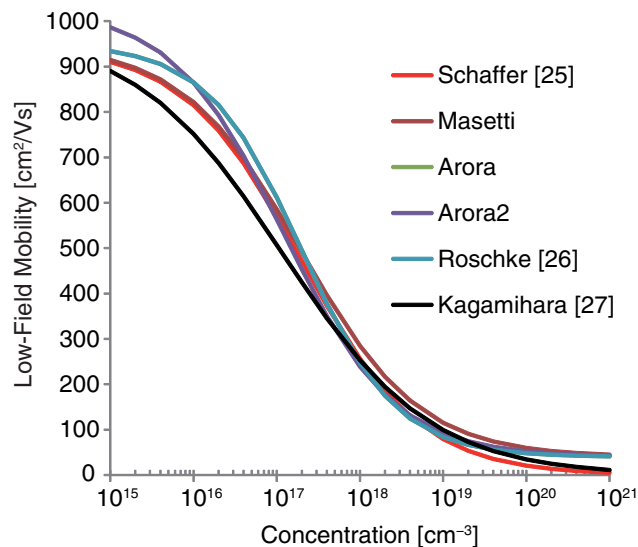


*Figure 22 Doping-dependent electron mobility at 300 K for n-doped 4H-SiC [25][26][27]*

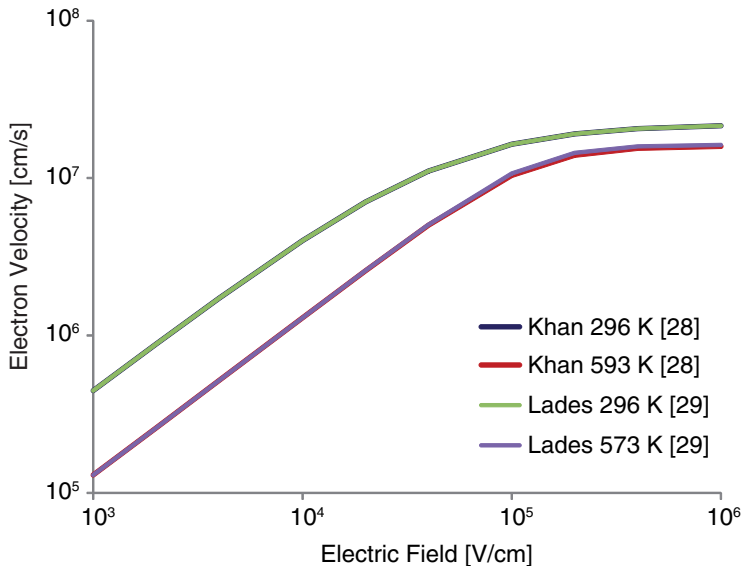


## Chapter 5: Quality of Fitting and Extraction

### Basic Properties of Silicon Carbide Devices

For high-field saturation, all measured data refers to the current flow perpendicular to the c-axis. Parameters for the Canali model are extracted and implemented in the parameter file.

Figure 23 Drift velocity of electrons in 4H-SiC, parallel to basal plane (0001) [28][29]



A nitrogen atom residing on the C lattice site becomes the shallow donor in SiC. A phosphorus atom also is used as a shallow donor (like nitrogen) and has approximately the same ionization energy  $E_c$  – 93 meV at the cubic site and  $E_c$  – 53 meV at the hexagonal site. However, unlike nitrogen, P mainly substitutes at a silicon site, and less than 10% of substitutional P is located at C sites.

Phosphorus has a slightly larger ionization energy at C sites than at Si sites. The ionization energy of N and P donors decreases with increasing donor concentration. Experimental data for cubic and hexagonal N donors in 6H-SiC is available. For N donors in 4H-SiC, experimental data of donor concentration dependency and fitting with empirically formula has been reported.

Aluminum and boron residing on Si lattice sites become acceptors in SiC. For Al acceptors in 4H-SiC, experimental data of acceptor doping concentration dependency and fitting with empirical formulas have been reported [30][31][32].

Figure 24 to Figure 28 show the experimental data and the fit implemented in the `SiC.par` parameter file.

## Chapter 5: Quality of Fitting and Extraction

### Basic Properties of Silicon Carbide Devices

Figure 24 Ionization energy for aluminum-doped 4H-SiC with extracted fit function [30][31][32]

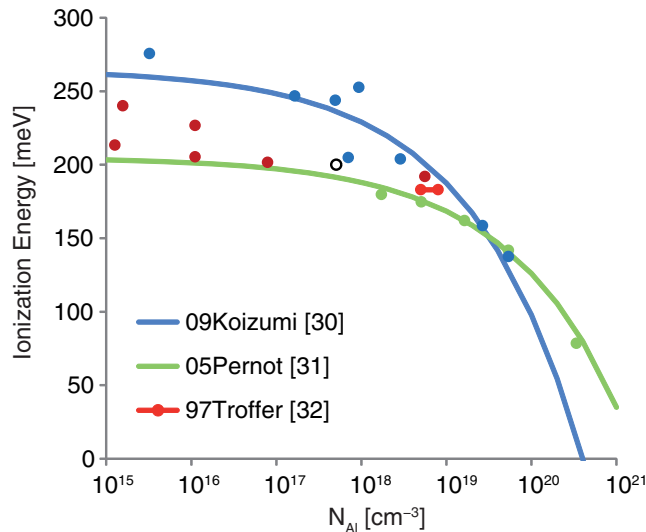
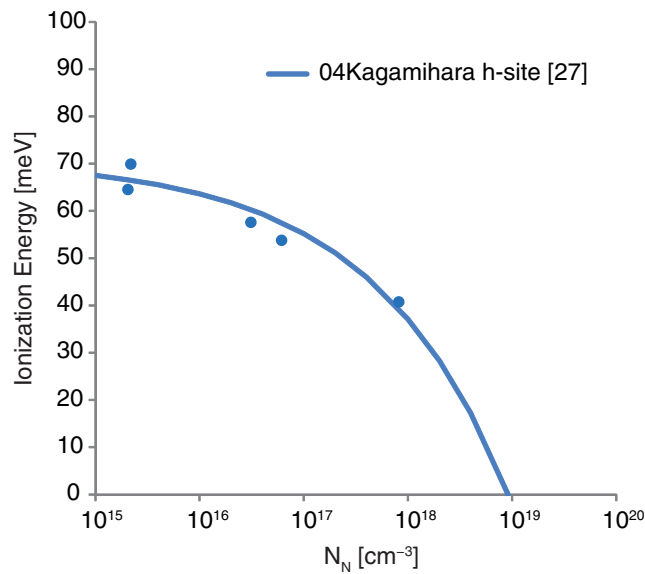


Figure 25 Ionization energy for nitrogen-doped 4H-SiC (hexagonal site) with extracted fit function [27]



## Chapter 5: Quality of Fitting and Extraction

### Basic Properties of Silicon Carbide Devices

Figure 26 Ionization energy for nitrogen-doped 4H-SiC (cubic site) with extracted fit function [27]

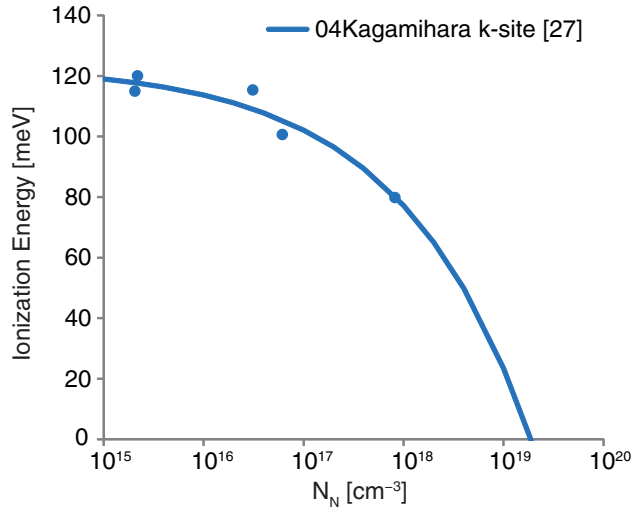
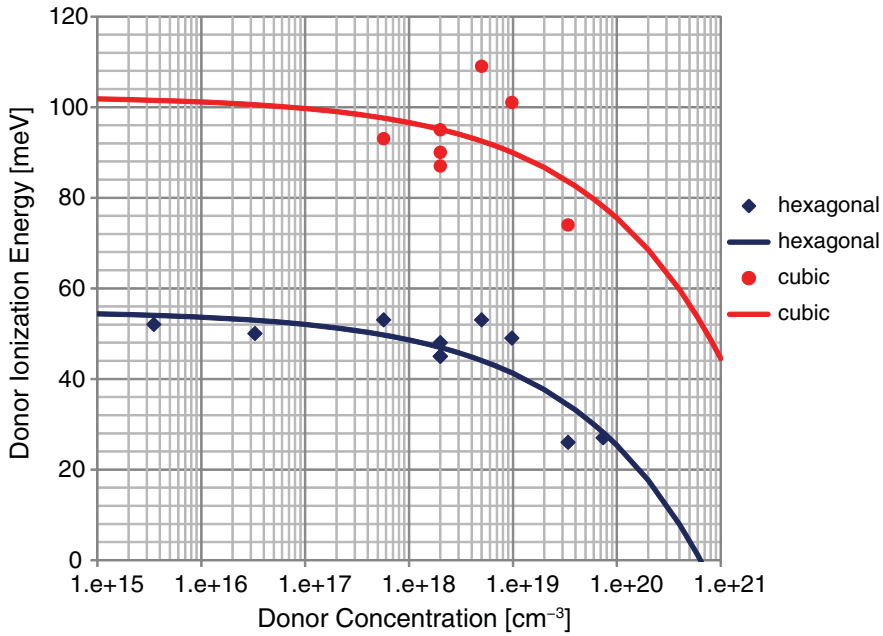


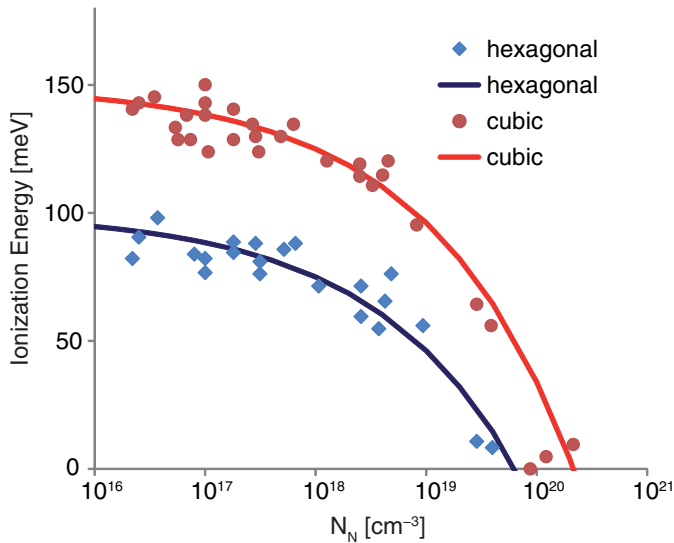
Figure 27 Ionization energy for phosphorus-doped 4H-SiC with extracted fit function



## Chapter 5: Quality of Fitting and Extraction

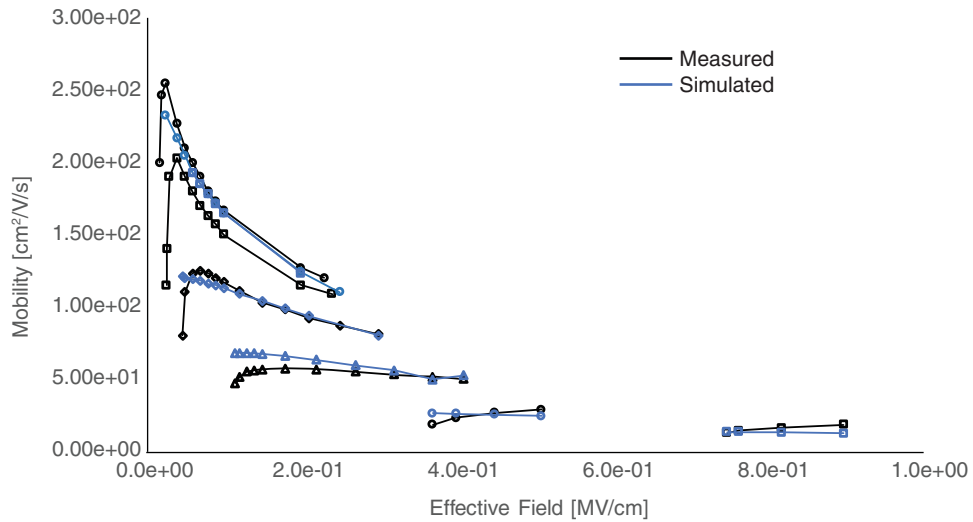
### Basic Properties of Silicon Carbide Devices

Figure 28 Ionization energy for nitrogen-doped 6H-SiC with extracted fit function



The inversion layer mobility parameters have been calibrated for 4H-SiC interfaces to oxide for different doping and trap concentrations as well as gate oxide formation processes. Experimental data is taken from [33], [34], and [35]. Surface phonon, surface roughness, and 2D Coulomb scattering parameters have been adjusted. The parameter files 4H-SiC.par, 4HSiC.par, SiC\_4H.par, and SiliconCarbide.par include the calibrated parameters. Figure 29 shows the comparison between experimental data and simulation results.

Figure 29 Simulated and measured [33] inversion layer mobility



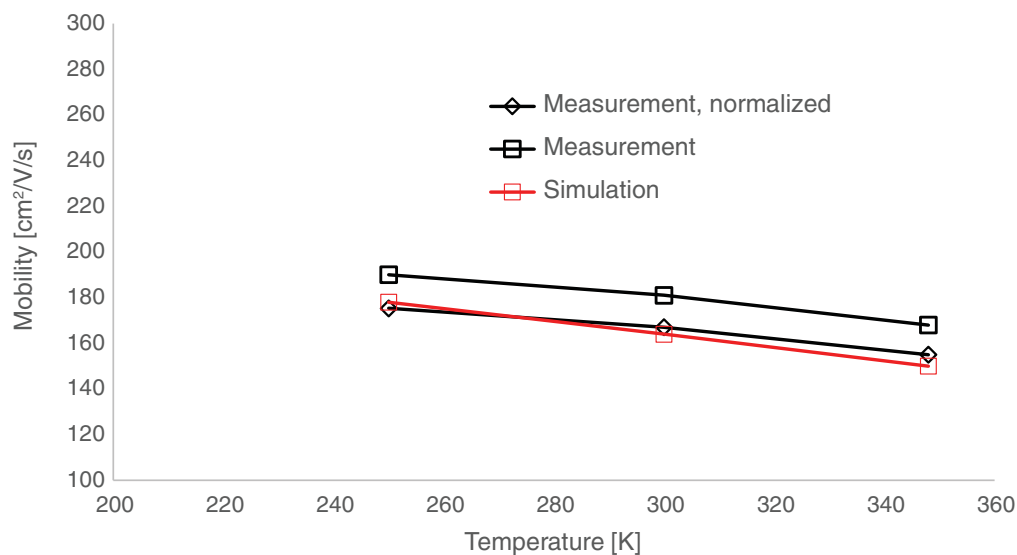
## Chapter 5: Quality of Fitting and Extraction

### Basic Properties of Gallium Nitride Devices

In the calibration of the inversion layer mobility, the incomplete ionization model [36] has been included to achieve better results, especially at lower temperatures, where a large part of the dopants is not activated. To describe the temperature dependence of the mobility, the  $\kappa$  parameter in the phonon scattering term, in the IALMob model, has been adjusted.

Figure 30 shows the comparison between experimental data [37] and simulation results. The measured mobility values over temperature have been normalized to the measured values at 300 K in the set of parameter files used in Figure 29 to compensate for fluctuations between different sets of measurements due to different trap distributions.

Figure 30    Simulated and measured [37] inversion layer mobility at different temperatures and low doping



---

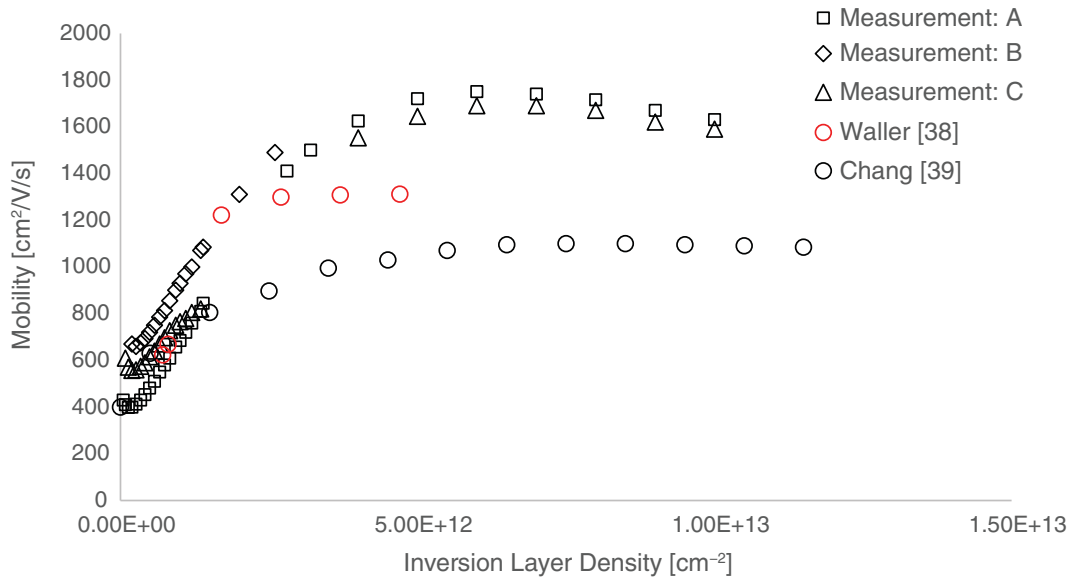
## Basic Properties of Gallium Nitride Devices

The inversion layer mobility parameters have been calibrated for GaN to AlGaN or AlN interfaces.

Experimental data is taken from [38] and [39]. Surface phonon, surface roughness, and 2D Coulomb scattering parameters have been adjusted. The parameter file `GaN.par` includes the calibrated parameters. Figure 31 on page 75 shows the comparison between experimental data and simulation results.

In the IALMob parameter set, the `s` parameter that controls the quantization is set to a higher value, assuming 2D Coulomb scattering dominates in the channel. Therefore, the transition to bulk Coulomb scattering is controlled by `lcrit_c` only.

**Figure 31** Simulated and measured [38][39] inversion layer mobility



## Basic Properties of Indium Gallium Arsenide Devices

Parameter values and references can be found in the `InGaAs.par` file. The following sections briefly show the results of parameter calibration and review various aspects of the calibration.

### Permittivity

The permittivity values for GaAs and InAs materials have been reviewed following the data reported by Adachi [40]. Since there is no experimental data for semiconductor alloys, a linear interpolation scheme has been adopted for indium gallium arsenide ( $\text{In}_{1-x}\text{Ga}_x\text{As}$ ) alloys.

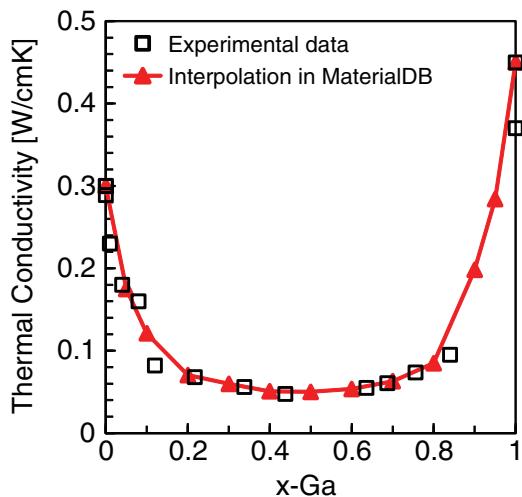
### Lattice Heat Capacity

Similarly, a linear interpolation scheme for heat capacity is used for  $\text{In}_{1-x}\text{Ga}_x\text{As}$  alloys, in which the heat capacity values for GaAs and InAs at 300 K are updated with the ones reported by Adachi [41].

## Thermal Conductivity

The mole fraction dependency of thermal conductivity for  $\text{In}_{1-x}\text{Ga}_x\text{As}$  alloys has been measured by Abrahams *et al.* [42] and Arasly *et al.* [43] at 300 K. Due to a random distribution of Ga and In atoms in the sub-lattice sites, the thermal conductivity values for  $\text{In}_{1-x}\text{Ga}_x\text{As}$  alloys tend to be smaller than for the corresponding binary materials. Figure 32 shows the thermal conductivity model and comparison to experimental data.

Figure 32 Thermal conductivity versus Ga mole fraction for  $\text{In}_{1-x}\text{Ga}_x\text{As}$  alloys at 300 K; experimental data is taken from [42] and [43], and binary data is taken from [44]

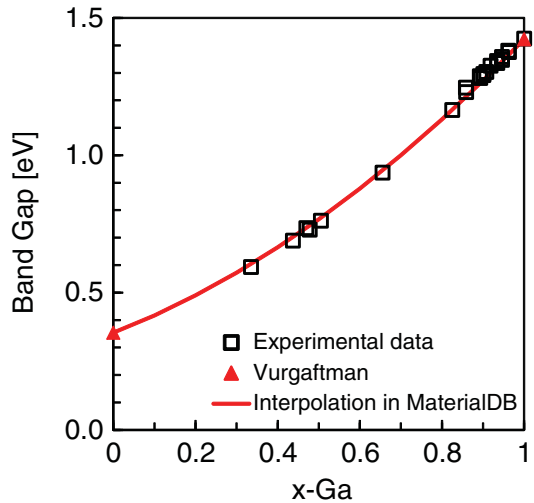


## Band Gap and Electron Affinity

InGaAs ternary materials are direct bandgap materials over the entire composition range, and both the maxima of the upper valence bands and the minima of the conduction band are located at the  $\Gamma$ -point of the Brillouin zone. Photoluminescence and photoreflectance measurements are often used to determine the bandgap energies of  $\text{In}_{1-x}\text{Ga}_x\text{As}$  [45][46] [47]. In the case of the lattice-matched alloy to InP,  $\text{In}_{0.53}\text{Ga}_{0.47}\text{As}$ , which has been investigated extensively, the bandgap energy is generally recognized to be 0.816 eV at 0 K. Therefore, a temperature-independent bowing parameter of 0.477 eV is suggested [48]. As for the Varshni parameters, the values for  $\text{In}_{1-x}\text{Ga}_x\text{As}$  alloys are determined through a linear interpolation based on the ones from GaAs and InAs. Figure 33 shows the composition dependency of bandgap energy at 300 K, plotted with the new set of the bowing parameter and Varshni parameters. The revised bandgap model fits well to the experimental data.

The electron affinity values for the GaAs and InAs binary materials are taken from Adachi [40] and are further derived to obtain the values at 0 K using the revised Varshni parameters. Since little experimental data is available, linearly interpolated electron affinity values are assumed for  $\text{In}_{1-x}\text{Ga}_x\text{As}$  alloys in the parameter file.

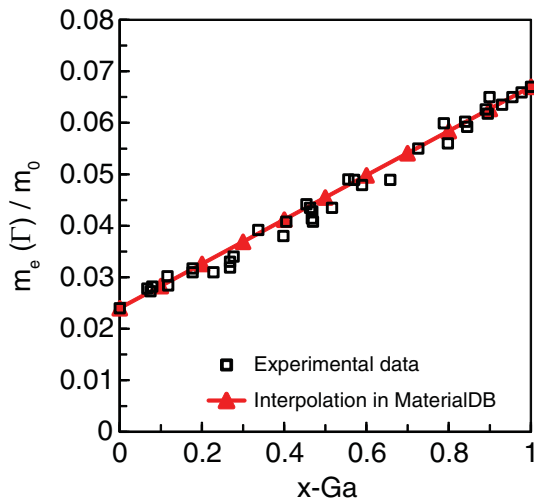
**Figure 33** Band gap versus Ga mole fraction for  $\text{In}_{1-x}\text{Ga}_x\text{As}$  alloys at 300 K; experimental data is taken from [45], [46], and [47]; binary data is taken from [48]



## Density-of-States

The electron effective masses of the  $\Gamma$ -valley of the  $\text{In}_{1-x}\text{Ga}_x\text{As}$  alloys have been measured extensively [41], and the results are shown in Figure 34.

**Figure 34** Electron effective mass of the  $\Gamma$ -valley versus Ga mole fraction for  $\text{In}_{1-x}\text{Ga}_x\text{As}$  alloys at 300 K; experimental data is reprinted from Adachi [41]



A simple linear interpolation scheme using the corresponding GaAs and InAs binary data yields a good fit to the experimental data. In the `InGaAs.par` file, the composition

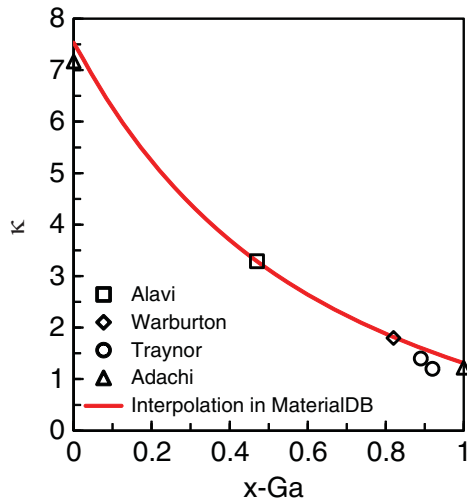
dependency of density-of-states for electrons is a set of tabulated values that are computed from the electron effective masses at 300 K using:

$$N_C(300\text{ K}) = 2.5094 \times 10^{19} \left(\frac{m_e}{m_0}\right)^{\frac{3}{2}} \quad (2)$$

Regarding the hole effective masses for  $\text{In}_{1-x}\text{Ga}_x\text{As}$  alloys, Vurgaftman *et al.* proposed a bowing parameter for each Luttinger valence band parameter:  $\gamma_1$ ,  $\gamma_2$ , and  $\gamma_3$  [48]. In measurement,  $\kappa(x)$ , defined as  $\kappa = -1/3\gamma_1 + 2/3\gamma_2 + \gamma_3 - 2/3$ , has been reported for  $x = 0.47$  and  $x = 0.82-0.92$  [49][50][51].

Figure 35 shows that the interpolation scheme from Vurgaftman *et al.* agrees well with the experimental data to some extent and is used to calculate the composition dependency of the overall hole effective masses,  $m_p$ .

Figure 35  *$\kappa$ -values versus Ga mole fraction for  $\text{In}_{1-x}\text{Ga}_x\text{As}$  alloys; experimental data is taken from [40], [49], [50], and [51]; red line represents the interpolation function suggested by [48]*

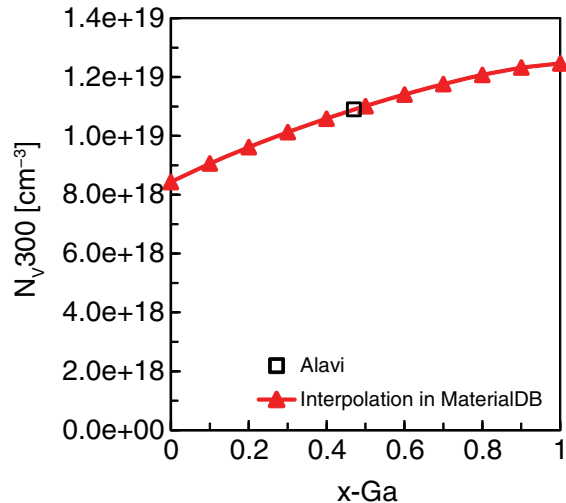


Similarly, a set of tabulated values of density-of-states for holes at 300 K is computed using:

$$N_V(300\text{ K}) = 2.5094 \times 10^{19} \left(\frac{m_p}{m_0}\right)^{\frac{3}{2}} \quad (3)$$

Advanced Calibration Device includes these tabulated values (see Figure 36).

**Figure 36** Valence band density-of-states at 300 K versus Ga mole fraction for  $In_{1-x}Ga_xAs$  alloys; experimental data is computed based on Luttinger parameters taken from [49]; red line is computed following the interpolation scheme suggested by [48]



## Bandgap Narrowing

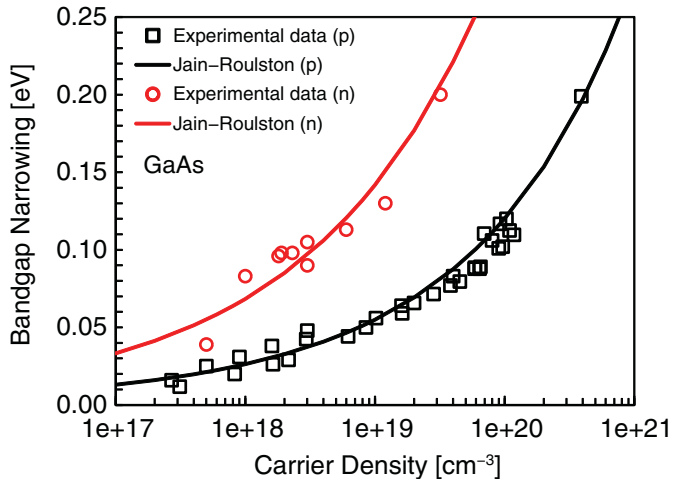
Doping-dependent bandgap narrowing for GaAs, InAs, and  $In_{1-x}Ga_xAs$  materials is accessed using the Jain–Roulston model [52]. The coefficients for p-type doping ( $A_p$ ,  $B_p$ ,  $C_p$ , and  $D_p$ ) in GaAs material are derived from [52], in which the quantities are refined with available up-to-date basic material parameters of GaAs.

Figure 37 on page 80 shows the extent of bandgap narrowing for p-GaAs obtained with the Jain–Roulston model, and it agrees well with the experimental data measured using photoluminescence in the carrier density range from  $2.7e17$  to  $3.9e20\text{ cm}^{-3}$  [53]–[57]. For p-InAs, the coefficients are retrieved in the same way, but the model validation cannot be qualified due to a lack of experimental data (see Figure 38 on page 80).

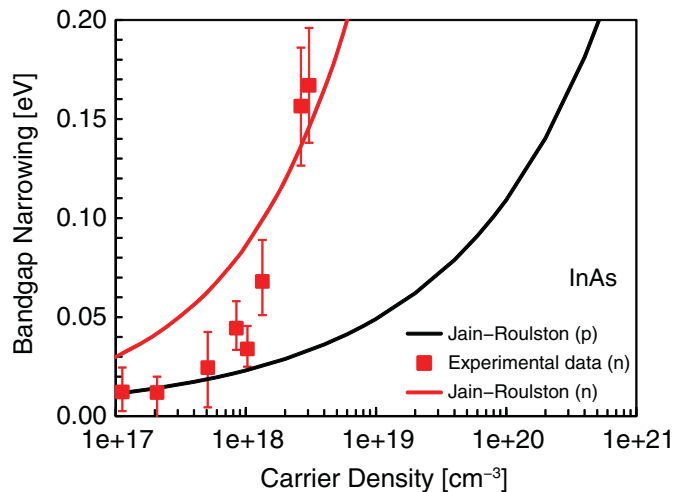
Regarding n-type GaAs and InAs, the formulas in the Jain–Roulston model cannot describe the doping dependencies of bandgap narrowing. Therefore, the corresponding coefficients ( $A_n$ ,  $B_n$ ,  $C_n$ , and  $D_n$ ) are determined preferably through curve fitting based on experimental data. As shown in Figure 37, the bandgap narrowing for n-GaAs with fitted Jain–Roulston coefficients agrees well with experimental data [53][58]. It should be noted that, for n-InAs, the bandgap narrowing value reaches nearly 0.2 eV at the carrier density of  $3e18\text{ cm}^{-3}$  [59], and a higher density is probable, which would alter the band structure drastically. Therefore, a minimum band gap ( $E_{gMin}$ ) value of 0.15 eV is set in the Bandgap model to avoid the occurrence of an unusually low (or negative) band gap.

Since there is little experimental data reported in the literature to resolve the mole fraction dependency of bandgap narrowing for  $In_{1-x}Ga_xAs$ , a simple linear interpolation scheme is adopted for each coefficient in the Jain–Roulston model.

**Figure 37** Doping-dependent bandgap narrowing for  $p$ -GaAs and  $n$ -GaAs at 300 K; experiment data is taken from [53]–[58]; black line is computed following Jain–Roulston model with up-to-date GaAs basic material parameters, and red line is fitted curve based on experimental data from [53] and [58]



**Figure 38** Doping-dependent bandgap narrowing for  $p$ -InAs and  $n$ -InAs at 300 K; black line is computed following Jain–Roulston model with up-to-date InAs basic material parameters, and red line is fitted curve based on experimental data from [59]



## Quantization Effects

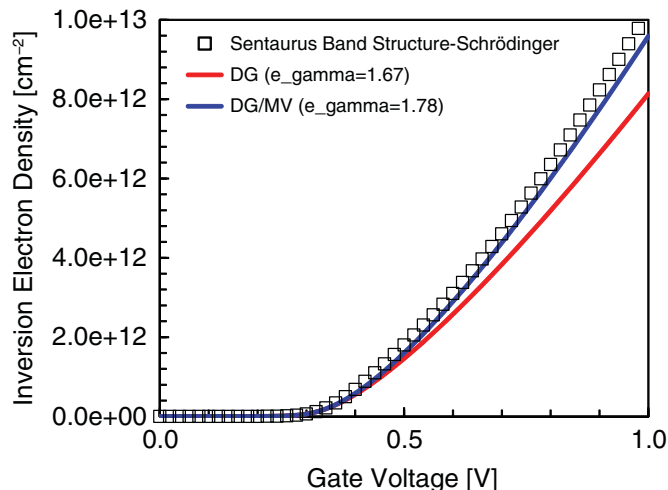
The quantization model is considered in MOS devices to obtain the correct densities and field distributions in channels. The density gradient model in Sentaurus Device would be the first choice for planar and nonplanar  $\text{In}_{1-x}\text{Ga}_x\text{As}$  device simulations, and then a calibration

to the solutions from the Schrödinger equations is required to extract the corresponding quantization parameters.

The 1D Schrödinger solver in Sentaurus Band Structure provides a reference in terms of carrier density distribution in the inversion layer, and the fitting factor ( $\gamma$ ) in the density gradient model then is fitted by minimizing the root-mean-square error of the charge integral over a range of applied gate voltages between these two approaches. The quantization parameter depends on the carrier polarity, the lattice orientation, the material composition, the layer thickness, the channel geometry, and the strain. The `QuantumPotentialParameters` parameter set provides the fitted  $\gamma$  values for simulations of unstrained  $\text{In}_{1-x}\text{Ga}_x\text{As}$  alloys, for both the bulk configuration and the double-gate configuration with channel thicknesses of 10 nm and 20 nm.

For  $\text{In}_{1-x}\text{Ga}_x\text{As}$  materials, you cannot neglect the electron occupancy in the L-valley at a higher gate voltage. Therefore, including the multivalley band structure model in the simulation allows you to determine the electron density-of-states more accurately.

**Figure 39** Inversion electron densities for a 10 nm thick double-gate (110) MOS structure with  $\text{In}_{0.53}\text{Ga}_{0.47}\text{As}$  channel: red line is simulated with the density gradient model and blue line is simulated with the multivalley and density gradient models; in both cases, `e_gamma` parameters have been optimized



The parameters for the `Multivalley` model in the `InGaAs.par` file with mole fraction dependency have been reviewed following the literature [41][48] and the band-structure calculation using the empirical pseudopotential method.

As shown in Figure 39, the electron charge integral in a 10 nm thick  $\text{In}_{0.53}\text{Ga}_{0.47}\text{As}$  double-gate structure simulated with the multivalley and density gradient models fits better to the result obtained with the Schrödinger solver of Sentaurus Band Structure, compared to the one with the density gradient model only. A similar conclusion can be drawn when

observing the carrier distributions at a 1 V gate voltage along the 10 nm channel, as shown in [Figure 40](#).

**Figure 40** Carrier distributions at gate voltage of 1 V for a 10 nm thick double-gate (110) MOS structure with  $\text{In}_{0.53}\text{Ga}_{0.47}\text{As}$  channel: red line is simulated with the density gradient model and blue line is simulated with the multivalley and density gradient models; in both cases,  $e_{\text{gamma}}$  parameters have been optimized

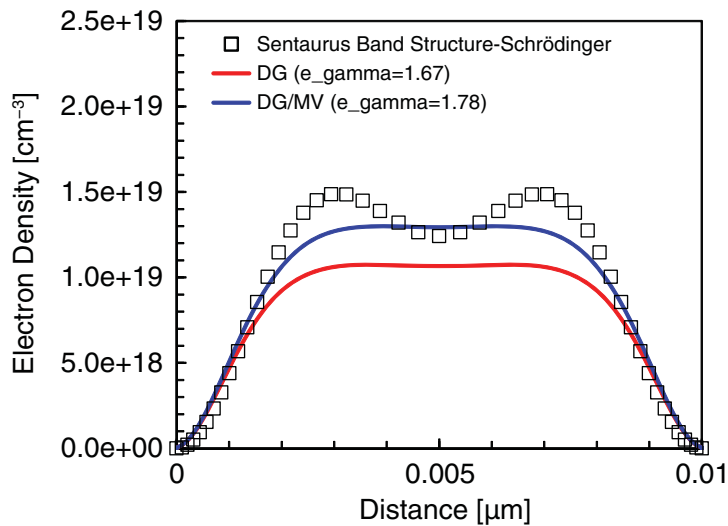


[Figure 41 on page 83](#) shows the tabulated values of fitted  $e_{\text{gamma}}$  and  $h_{\text{gamma}}$  parameters using the density gradient and multivalley models, which are provided in the `InGaAs.par` file for bulk (100) and (110) orientations. It is evident that there is no orientation dependency for the electron quantization parameter, and the compositional variation is also less distinct compared to the hole quantization parameter. The quantization parameter is also a function of layer thickness, as shown in [Figure 42 on page 83](#).

It is important to implement the corresponding quantization parameters designated for a specific layer thickness during simulations, since the discrepancy on the charge distribution is very susceptible to thin layers. For example, the  $e_{\text{gamma}}$  value optimized for a 10 nm channel width could still be used for quantum correction on a 20 nm thick channel, but with a slightly larger error. However, the same value might be only appropriate to use for thin layers down to 8 nm. If the layer thickness is less than 8 nm, you should perform a quantization calibration again to extract the correct quantization parameter.

**Figure 41** Fitted gamma values versus Ga mole fraction for bulk MOS structures with  $In_{1-x}Ga_xAs$  alloys using density gradient and multivalley models

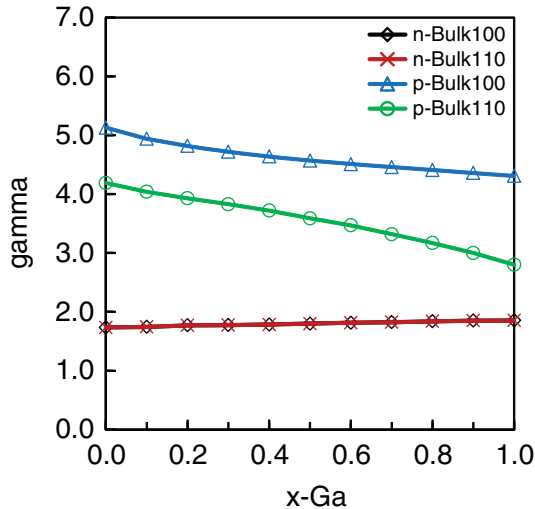
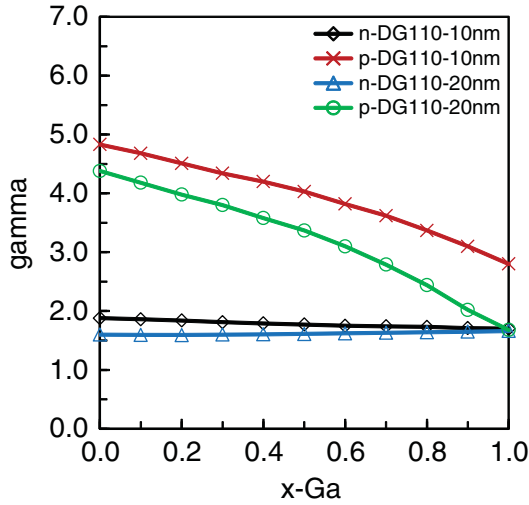


**Figure 42** Fitted gamma values versus Ga mole fraction for 10 nm and 20 nm double-gate MOS structures with  $In_{1-x}Ga_xAs$  alloys using density gradient and multivalley models



## Low-Field Bulk Mobility and Its Doping Dependency

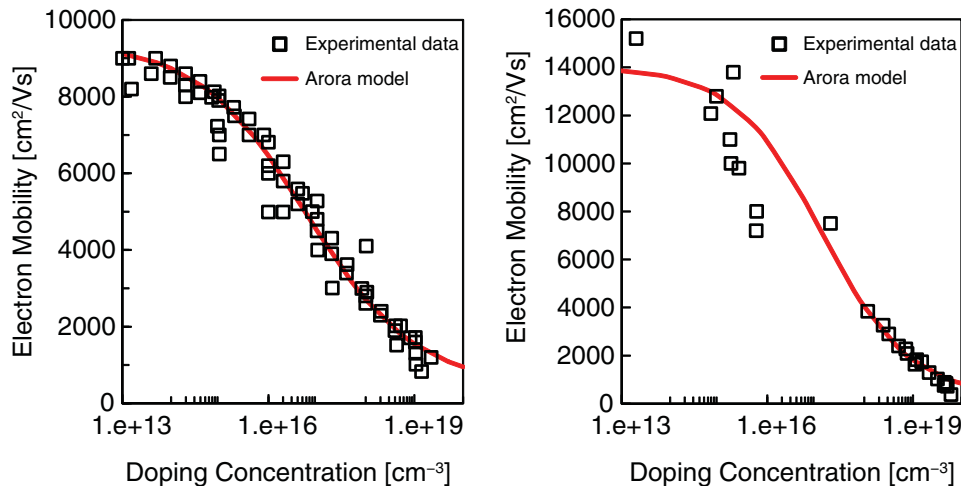
Low-field bulk mobility is a critical parameter to determine the current–voltage characteristics of InGaAs metal–insulator–semiconductor (MIS) devices, and it is dependent on mole fraction, temperature, doping, inversion charge, and channel direction for unstrained InGaAs materials.

Accurate theoretical models accounting for diverse scattering mechanisms can be complex and might apply only to limited conditions. Therefore, empirical fitting based on available experimental data can be an alternative.

The coefficients in the ConstantMobility and DopingDependence parameter sets of the `InGaAs.par` file have been reviewed and implemented following the empirical mobility model suggested in [60].

Reference [60] provides calibrated parameters in the empirical Caughey–Thomas mobility model for temperature and doping dependency, for unstrained GaAs, InAs, and  $\text{In}_{0.53}\text{Ga}_{0.47}\text{As}$  materials. These parameters are transformed to the parameters of the Arora model for use in Sentaurus Device. Figure 43 demonstrates the doping dependency of electron mobility for unstrained GaAs and  $\text{In}_{0.53}\text{Ga}_{0.47}\text{As}$  using the Arora model.

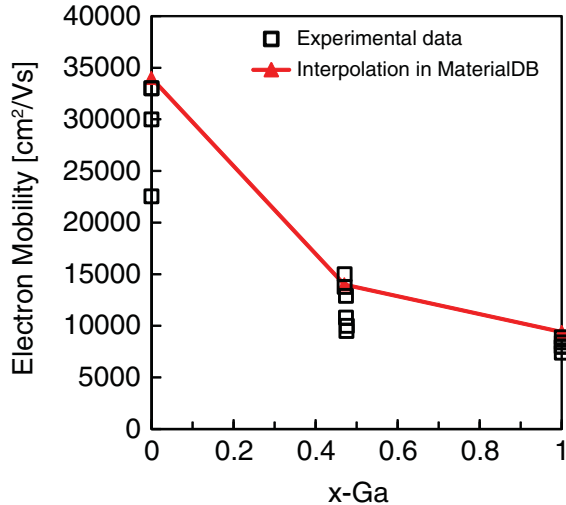
**Figure 43** Doping-dependent low-field electron mobility for (left) GaAs and (right)  $\text{In}_{0.53}\text{Ga}_{0.47}\text{As}$  at 300 K; red lines are computed using the Arora model with fitted parameters from [60]



The doping dependency of low-field mobility for  $\text{In}_{1-x}\text{Ga}_x\text{As}$  alloys, apart from  $\text{In}_{0.53}\text{Ga}_{0.47}\text{As}$  material, is usually less investigated. Therefore, a two-sectional linear interpolation scheme is used, based on InAs,  $\text{In}_{0.53}\text{Ga}_{0.47}\text{As}$ , and GaAs for each parameter in the Arora model.

Figure 44 on page 85 shows the compositional dependency of the low-field electron mobility for  $\text{In}_{1-x}\text{Ga}_x\text{As}$  alloys suggested in the `InGaAs.par` file with some experimental data.

**Figure 44** Low-field electron mobility at 300 K versus Ga mole fraction for  $\text{In}_{1-x}\text{Ga}_x\text{As}$  alloys; experimental data is reprinted from [61]; red line is the interpolation curve suggested in the InGaAs.par file



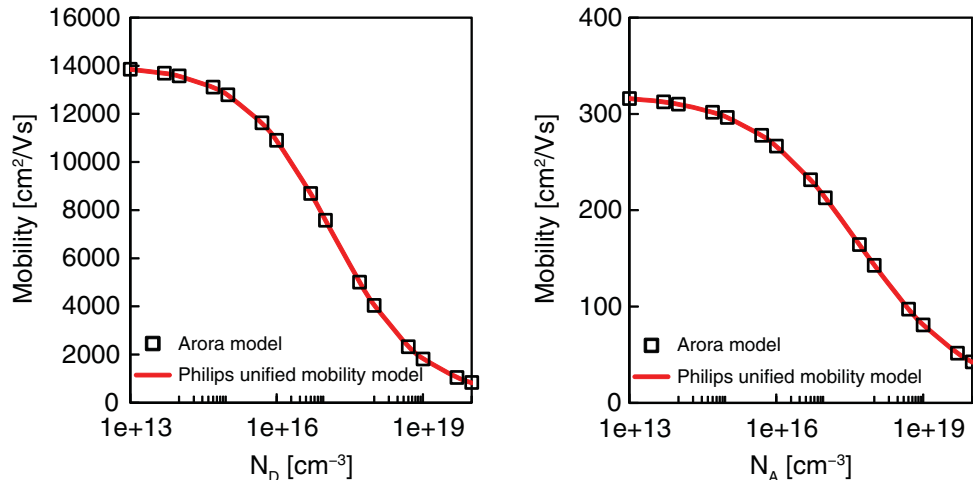
## Philips Unified Mobility Model

This model describes both majority and minority carrier mobility in bulk, taking into account phonon scattering, impurity scattering, carrier–carrier scattering, and screening of scattering processes. In the MaterialDB folder, the parameters for majority carrier mobility in InAs,  $\text{In}_{0.53}\text{Ga}_{0.47}\text{As}$ , and GaAs materials have been calibrated without considering the minority impurity scattering where other coefficients, such as the clustering functions and the screening parameters, are preserved as the default ones from silicon material.

The maximum carrier mobility ( $\mu_{\max}$ ), the minimum carrier mobility ( $\mu_{\min}$ ), and the exponent ( $\theta$ ) for  $\text{In}_{1-x}\text{Ga}_x\text{As}$  alloys are transformed from the corresponding ConstantMobility and Arora models. Then, the reference density ( $N_{\text{ref}}$ ) and the exponent ( $\alpha$ ) coefficients can be fitted to the doping-dependent mobility given by the Arora model within a doping range between  $1.0\text{e}13 \text{ cm}^{-3}$  and  $1.0\text{e}20 \text{ cm}^{-3}$  for GaAs and  $\text{In}_{0.53}\text{Ga}_{0.47}\text{As}$ . Since the intrinsic density of InAs is relatively larger compared to GaAs and  $\text{In}_{0.53}\text{Ga}_{0.47}\text{As}$ , the fitting range for InAs is limited to the range from  $1\text{e}15 \text{ cm}^{-3}$  to  $1\text{e}20 \text{ cm}^{-3}$ .

Figure 45 on page 86 presents the electron and hole mobility in  $\text{In}_{0.53}\text{Ga}_{0.47}\text{As}$  material at various doping levels for the Philips unified mobility model with fitted coefficients.

**Figure 45** Doping-dependent low field mobility for (left) electron and (right) hole majority carriers in  $\text{In}_{0.53}\text{Ga}_{0.47}\text{As}$  alloy at 300 K; red lines are computed with the Philips unified mobility model with fitted parameters suggested in the *InGaAs.par* file



## Inversion Layer Mobility

This section discusses inversion layer mobility.

## Inversion and Accumulation Layer Mobility Model

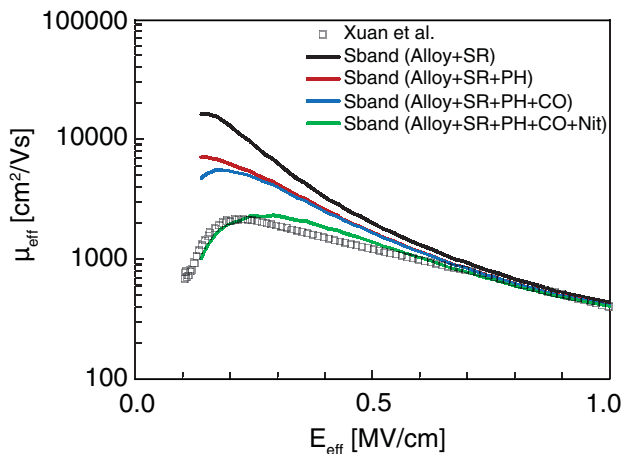
In a MOSFET device, the surface roughness and the surface phonon scattering can degrade carrier mobility at the proximity of a semiconductor–insulator interface due to a high electric field, normal to the channel interface imposed across the channel region. Since  $\text{In}_{1-x}\text{Ga}_x\text{As}$  alloys have the potential to realize n-MOSFET devices, parameter calibration with respect to available experimental data is required to establish a more accurate mobility degradation model.

This section describes how the parameters in the `MaterialDB` folder have been calibrated for the inversion and accumulation layer mobility (`IALMob`) model.

The calibration methodology involves two main steps and concerns mainly the electron mobility in the inversion layer. First, with some initial calibrations with respect to the experimental data to account for the process variations, the 1D mobility calculator of Sentaurus Band Structure provides a reference in terms of mobility in the inversion layer for the entire mole fraction range. The experimental data used in this step was reported by Xuan et al. [62] on an inversion-type n-channel  $\text{In}_{0.53}\text{Ga}_{0.47}\text{As}$  MOSFET with 8 nm thick atomic layer deposition (ALD)  $\text{Al}_2\text{O}_3$  as the gate dielectric. Second, the coefficients of each scattering mechanism of the `IALMob` model are extracted by comparing the mobility values between these two simulation approaches.

Figure 46 shows the dispersion curves of the mobility field in the  $\text{In}_{0.53}\text{Ga}_{0.47}\text{As}$  inversion layer simulated using the 1D mobility calculator of Sentaurus Band Structure with various combinations of the alloy, surface roughness (SR), phonon (PH), and Coulomb (CO) scattering models, in which parameters  $\Delta$  and  $\Lambda$  of the surface-roughness power-spectrum model with exponential density function have been optimized for the effective electric field in the range 0.6–1.0 MV/cm. Afterwards, the mobility offset with respect to experimental data, after considering all the available scattering models such as alloy, surface roughness, phonon, and Coulomb scattering, as well as the fixed charge trap model, can be reduced further in the range 0.1–0.4 MV/cm by adjusting the interface charge density.

**Figure 46** Effective electron mobility versus effective electric field for  $\text{In}_{0.53}\text{Ga}_{0.47}\text{As}$  ( $p$ -doping=1e17 cm<sup>-3</sup> in channel) MOSFET with ALD  $\text{Al}_2\text{O}_3$ ; simulation results are obtained using 1D mobility calculator of Sentaurus Band Structure with various combinations of scattering models, in which the surface roughness parameters ( $\Delta=2.2\text{e-}7\text{ cm}$ ;  $\Lambda=4.6\text{e-}8\text{ cm}$ ) and the interface charge density ( $N_{it}=4.3\text{e}12\text{ cm}^{-2}$ ) have been calibrated; experimental data is taken from [62]



For the `IALMob` model, the calibration has been performed with the parameters of 3D phonon scattering and 3D Coulomb scattering taken from the constant mobility model and the Philips unified mobility model, respectively, and the 2D and 3D parts of phonon scattering are combined with `PhononCombination=1`. Since it is necessary to distinguish the contribution of various scattering mechanisms in the `IALMob` model, first 2D Coulomb scattering is disregarded by designating a large value in factors such as  $D_{1,\text{inv}}$  and  $D_{2,\text{inv}}$ . Then, the resulting effective mobility values are compared to Sentaurus Band Structure results, for which only surface roughness scattering and phonon scattering are activated, for  $p$ -doping between 1e15 and 1e18 cm<sup>-3</sup>.

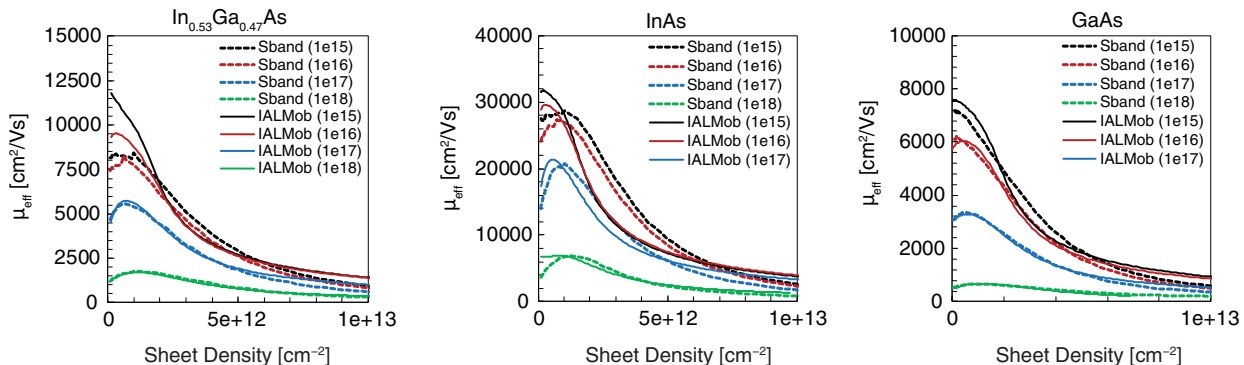
At this step, the reviewed parameters principally include coefficients accounting for 2D phonon scattering ( $B$ ,  $C$ , and  $\lambda$ ) and those representing surface roughness scattering ( $\delta$ ,  $A^*$ , and  $\lambda_{sr}$ ), where the  $\lambda$  and  $\lambda_{sr}$  coefficients describe the doping dependencies of phonon and

surface roughness scattering, respectively. Other parameters are kept as the ones for silicon material.

After the coefficients for surface roughness scattering and 2D phonon scattering are determined, the parameters for 2D Coulomb scattering ( $D_{1,\text{inv}}$ ,  $D_{2,\text{inv}}$ , and  $v_{1,\text{inv}}$ ) can be fitted with respect to Sentaurus Band Structure results when Coulomb scattering is implemented.

**Figure 47** compares the effective electron mobility versus sheet density at various p-doping levels in the channel region between the `IALMob` model with calibrated parameters and Sentaurus Band Structure results for  $\text{In}_{0.53}\text{Ga}_{0.47}\text{As}$ , InAs, and GaAs. Regarding the interpolation scheme for the `IALMob` model in  $\text{In}_{1-x}\text{Ga}_x\text{As}$  alloys, a two-sectional linear curve is used, based on  $\text{In}_{0.53}\text{Ga}_{0.47}\text{As}$ , InAs, and GaAs for each parameter previously mentioned.

**Figure 47** Effective electron mobility versus sheet density for (left)  $\text{In}_{0.53}\text{Ga}_{0.47}\text{As}$ , (middle) InAs, and (right) GaAs MOSFET with ALD  $\text{Al}_2\text{O}_3$  at various p-doping levels in the channel region; dotted lines are obtained using 1D mobility calculator of Sentaurus Band Structure in combination with surface roughness, phonon, and Coulomb scattering models, and the alloy scattering model is further considered for  $\text{In}_{0.53}\text{Ga}_{0.47}\text{As}$ ; solid lines are obtained using the `IALMob` model with calibrated parameters suggested in the `InGaAs.par` file



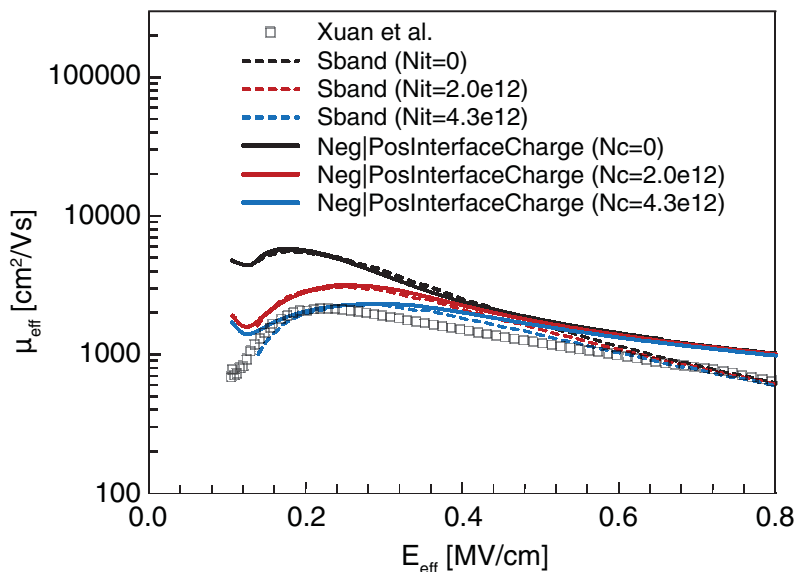
## Interface Charge Mobility Model

Following the results of the mobility calibration for the `IALMob` model, the mobility degradation model due to interface charges has been fine-tuned, including the `NegInterfaceCharge` and `PosInterfaceCharge` models in Sentaurus Device. As shown in [Figure 46 on page 87](#), the Sentaurus Band Structure mobility calculator can fit well to the experimental data from Xuan *et al.* [62] when interface charge density ( $N_{\text{it}}$ ) is fitted to be  $4.3 \times 10^{12} \text{ cm}^{-2}$ .

To calibrate parameters such as  $\mu_1$ ,  $C_{\text{trans}}$ ,  $l_{\text{crit}}$ , and  $E_0$  for the `NegInterfaceCharge` and `PosInterfaceCharge` models, the mobility values for two more  $N_{\text{it}}$  levels, 0 and  $2.0 \times 10^{12}$ , are also computed using Sentaurus Band Structure.

Figure 48 presents the curves of mobility versus field for  $\text{In}_{0.53}\text{Ga}_{0.47}\text{As}$  material when implementing the `IALMob` model and the negative and positive interface charge mobility models with calibrated parameters with respect to Sentaurus Band Structure results. Similar to other mobility models, the interpolation scheme for the `NegInterfaceCharge` and `PosInterfaceCharge` models in  $\text{In}_{1-x}\text{Ga}_x\text{As}$  alloys uses a two-sectional linear curve based on InAs,  $\text{In}_{0.53}\text{Ga}_{0.47}\text{As}$ , and GaAs.

*Figure 48 Effective electron mobility versus effective electric field for  $\text{In}_{0.53}\text{Ga}_{0.47}\text{As}$  ( $p$ -doping= $1\text{e}17 \text{ cm}^{-3}$  in channel) MOSFET with ALD  $\text{Al}_2\text{O}_3$ ; dotted lines are obtained using 1D mobility calculator of Sentaurus Band Structure with alloy, surface roughness, phonon, and Coulomb scattering models, as well as interface trap model with charge density of 0,  $2.0\text{e}12$ , and  $4.3\text{e}12 \text{ cm}^{-2}$ ; solid lines are obtained using the `NegInterfaceCharge` and `PosInterfaceCharge` models with calibrated parameters suggested in the `InGaAs.par` file*



## Strained Low-Field Mobility

This section discusses strained low-field mobility.

## Multivalley Electron Mobility Model

Mechanical stress in devices can change the band structure and carrier mobility, and is considered an approach to enhance mobility. The multivalley electron mobility (`eSubband`) model with default parameters has been tested on several  $\text{In}_{1-x}\text{Ga}_x\text{As}$ -based FETs on which either uniaxial or biaxial stress is applied [63][64][65][66]. The simulations reproduce the trend of electron mobility enhancement for tensile stress. However, the enhancement generally tends to be lower than for experimental data.

Since the investigated device structures and conditions are very diverse and incomplete, a more unified and better set of model parameters has not been established (for example, to consider the dependencies on mole fraction and geometry for  $\text{In}_{1-x}\text{Ga}_x\text{As}$  materials) and default parameters have been kept.

## Piezoresistance Mobility Model

Due to a lack of published experimental results for  $\text{In}_{1-x}\text{Ga}_x\text{As}$  alloys, the related piezoresistive coefficients are difficult to determine. Nainani *et al.* [67] demonstrated the conductivity extraction for n- $\text{In}_{0.2}\text{Ga}_{0.8}\text{As}$  material using the transfer length method and suggested a similar value for the longitudinal piezoresistive coefficient for n- $\text{In}_{0.2}\text{Ga}_{0.8}\text{As}$  as for n-Si.

---

## Basic Properties of Silicon Germanium Devices

The `SiliconGermaniumc100.par` and `SiliconGermaniumc110.par` files contain the parameters for silicon germanium (SiGe) MOS devices. See [Content of Parameter Files on page 9](#).

---

## Permittivity

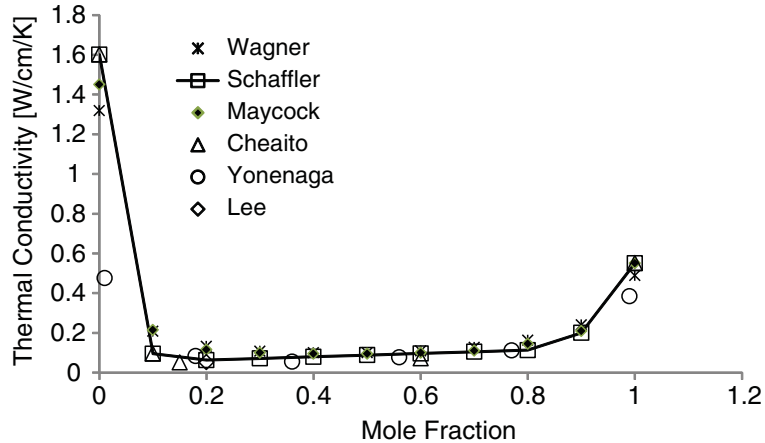
The low-frequency relative dielectric constant values are interpolated linearly between the corner values of 11.7 (silicon) and 16.2 (germanium) for each Ge mole fraction (see [68]).

---

## Thermal Conductivity

The mole fraction dependency of the thermal conductivity is extracted from data from Schaffler [68] (see [Figure 49](#)). Data is implemented piecewise linearly in the parameter file.

**Figure 49** Thermal conductivity versus mole fraction [68][69][70][71][72][73]; solid line is the implementation in the parameter file



---

## Band Structure

Band structure data (band gap and affinity) is extracted from [74] (see [Figure 50](#) and [Figure 51 on page 92](#)). The bandgap narrowing is extracted from Jain and Roulston [16] (see [Figure 52 on page 93](#)) where the `oldSlotboom` model is used for fitting (see the *Sentaurus™ Device User Guide*).

Linear interpolation between silicon and germanium values is performed for the prefactor of the `oldSlotboom` model to describe the mole fraction dependency. All data is implemented piecewise linearly in the parameter file.

**Chapter 5: Quality of Fitting and Extraction**  
Basic Properties of Silicon Germanium Devices

Figure 50 Band gap as a function of mole fraction

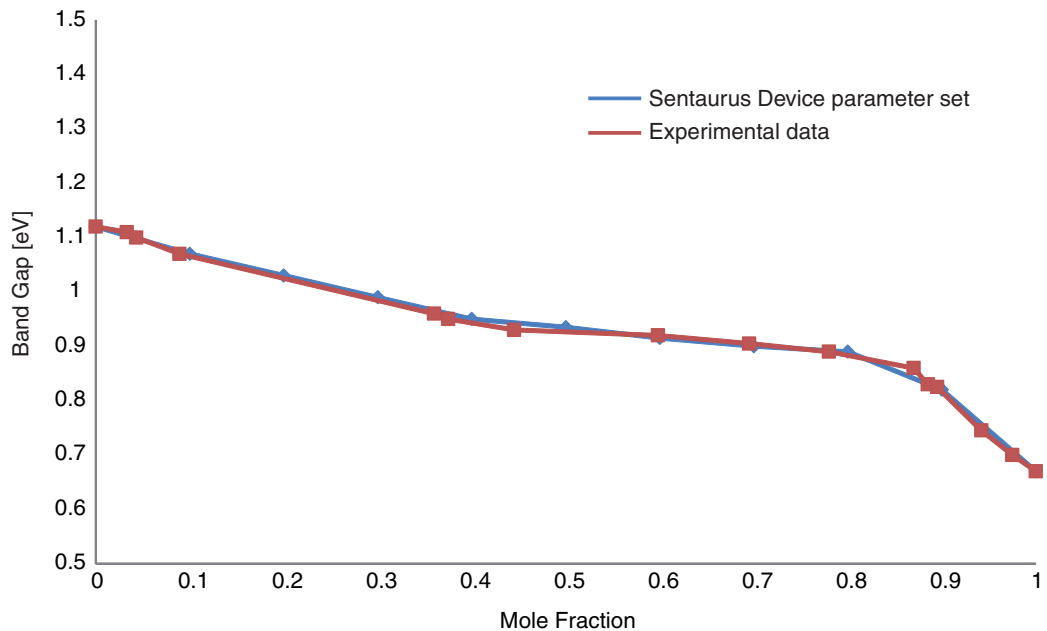
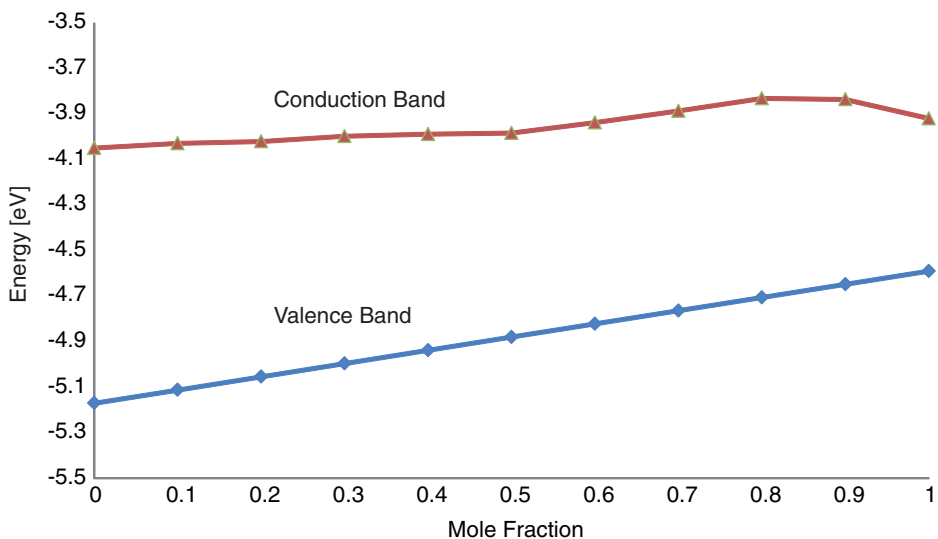
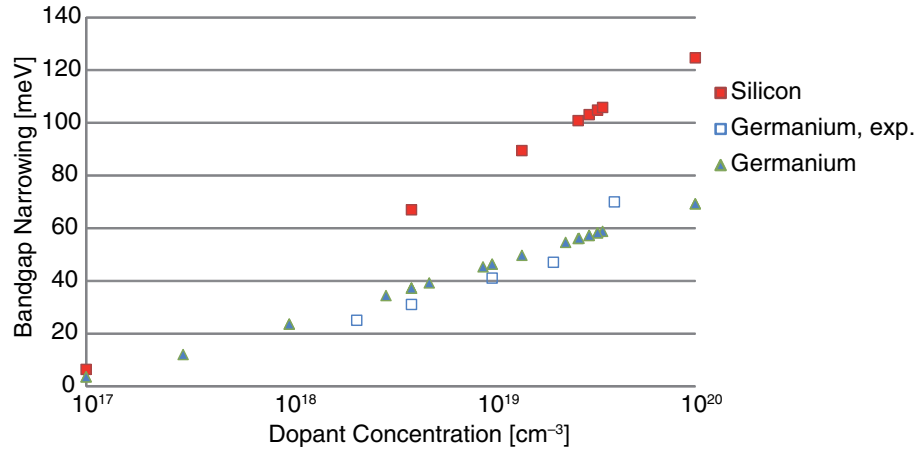


Figure 51 Conduction and valence bands as a function of mole fraction



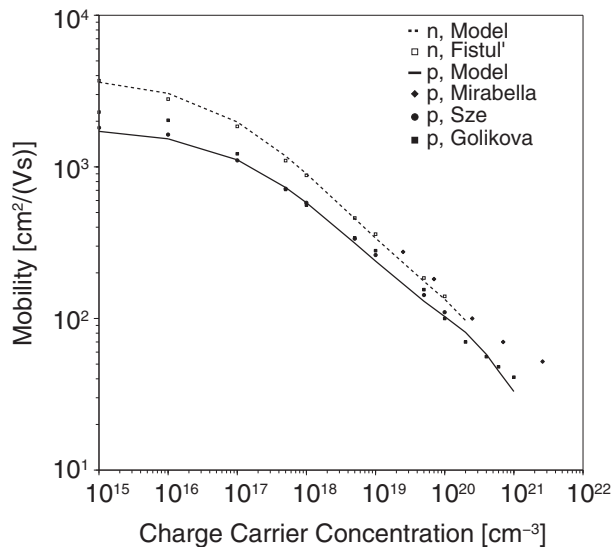
**Figure 52** Bandgap narrowing for silicon and germanium; a prefactor of 5 meV for the OldSlotboom model is used



## Bulk Low-Field Mobility

The bulk low-field mobility PhuMob model parameters for silicon, SiGe, and germanium are extracted from different measurements with the focus on the data from Golikova *et al.* [75] and Fistul' *et al.* [76]. Figure 53 shows the results of this calibration for germanium. The model parameters are implemented piecewise linearly.

**Figure 53** Measurements from different sources [75][76][77][78], with [79] used as the reference measurement, for the doping dependency of electron and hole mobility in Ge and the implementation in the Sentaurus Device parameter files (lines)



---

## Ballistic Mobility

Quasiballistic transport is important and should be considered when scaling devices towards short channels. For this, it is required to extend the drift-diffusion (DD) model by combining an additional ballistic mobility with the standard drift-diffusion mobility. In Sentaurus Device, the ballistic mobility can be described by either the channel length-dependent model or the kinetic velocity model (KVM) [80]. The latter has the advantage of avoiding explicit channel length dependence and is used to extract the corresponding ballistic mobility parameters.

The ballistic mobility model parameters are calibrated with the solution of the subband-based Boltzmann transport equation (subband-BTE) as reference. The fitting parameter ( $k$ ) in the KVM is mostly determined by fitting the on-state current at low field over a range of channel lengths between these two approaches. Moreover, the parameters  $\beta_0$  and the saturation velocity  $v_{sat0}$  in the high-field saturation model are adjusted as well by fitting the on-state current at high field. In this way, ballistic mobility can be separated from high-field drift-diffusion mobility. Note that, the ballistic mobility model parameters and the high-field saturation model parameters can depend on the carrier polarity, the channel geometry, the layer thickness, the material composition, and the strain.

The devices used for parameter extraction are 3D square SiGe n-type and p-type MOSFET nanowires with a cross-sectional area of  $5\text{ nm} \times 5\text{ nm}$ . The gate length ( $L_{gate}$ ) varies from 200 nm to 7 nm, and the channel direction is along the  $\langle 110 \rangle$  crystal orientation.

To activate the KVM, specify the following command in the `Physics` section of the Sentaurus Device command file:

```
Mobility (
    BalMob ( KVM(Full) Fermi Frensley )
)
```

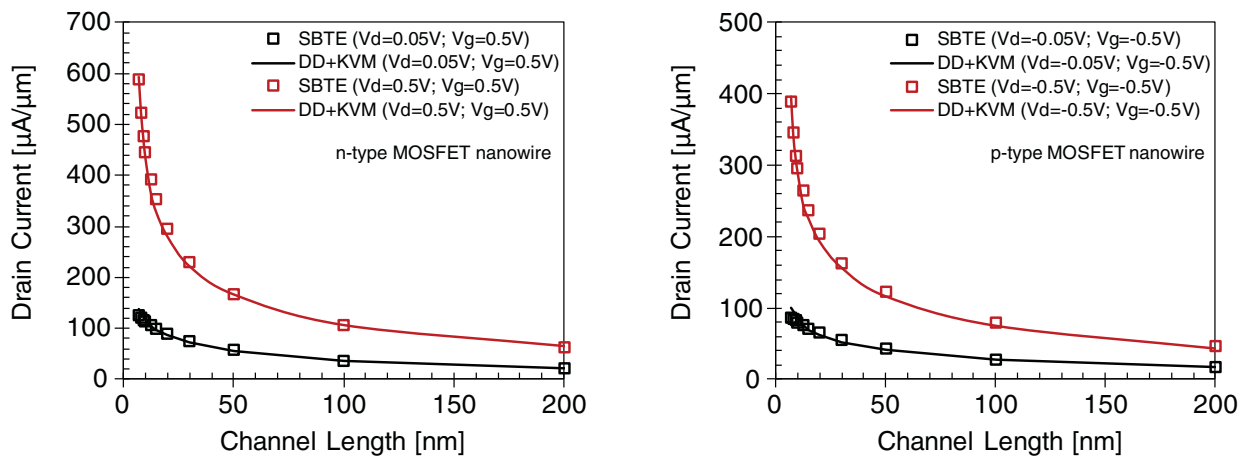
Here, the thermionic emission and free carrier acceleration terms are both considered in the KVM. As the first step, the long-channel mobility is calibrated to the subband-BTE simulation at on-state using the inversion and accumulation layer mobility (`IALMOb`) model in drift-diffusion. Second, the channel access resistance ( $R_0$ ) is extracted from the gate length dependence of the total resistance using the equation  $R = R_0 + R'L_{gate}$ . The difference of  $R_0$  between the subband-BTE and drift-diffusion simulations can be added in the Sentaurus Device simulation either as an additional lumped resistance or by modifying the mobility model parameters in source/drain regions. After that, the parameters of the KVM and the high-field saturation model are optimized to match the on-state current at low-drain and high-drain bias voltages. It is likely that you must iterate the calibration procedures previously mentioned to optimize the parameters. For a detailed description, see [Chapter 4 on page 43](#).

[Figure 54 on page 95](#) shows the on-state drain current obtained using the drift-diffusion simulation with the KVM at low-drain and high-drain bias voltages. The parameters of the KVM and the high-field saturation model have been optimized with respect to the simulation

results of the Subband-BTE solver over a wide range of channel lengths and for germanium mole fractions from 0 to 1, as shown in [Figure 55 on page 96](#).

Note that the slope of resistance as a function of gate length is found to vary nonlinearly at short channels when the KVM is implemented, and it then leads to a slightly lowered fitting accuracy for channels shorter than 10 nm. This behavior is under investigation and might result in a parameter update.

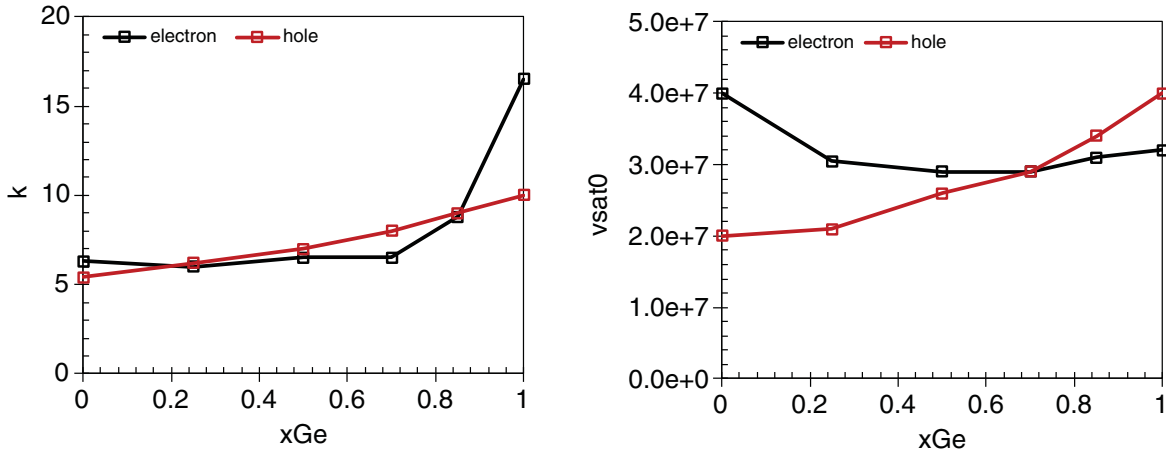
**Figure 54** Drain current versus channel length for  $5\text{ nm} \times 5\text{ nm}$  Si (left) n-type MOSFET nanowire and (right) p-type MOSFET nanowire, at low-drain and high-drain bias voltages; squares obtained using Subband-BTE solver in combination with surface roughness, phonon, and Coulomb scattering models; solid lines obtained using KVM with calibrated parameters for electrons ( $k=6.3$ ,  $T_{\text{factor}}=1.52$ , and  $B_{\text{factor}}=0.3$  in KVM;  $\beta_{\text{alpha}}=0.74$  and  $v_{\text{sat0}}=4\text{e}7$  in high-field saturation model) and for holes ( $k=5.4$ ,  $T_{\text{factor}}=1.52$ , and  $B_{\text{factor}}=0.3$  in KVM;  $\beta_{\text{alpha}}=1.0$  and  $v_{\text{sat0}}=2\text{e}7$  in high-field saturation model)



## Chapter 5: Quality of Fitting and Extraction

### References

Figure 55 Calibrated parameters (left)  $k$  in KVM and (right)  $v_{sat0}$  in high-field saturation model versus Ge mole fraction for  $5\text{ nm} \times 5\text{ nm}$  SiGe n-type and p-type MOSFET nanowires



---

## References

- [1] S. Takagi *et al.*, “On the Universality of Inversion Layer Mobility in Si MOSFET’s: Part I—Effects of Substrate Impurity Concentration,” *IEEE Transactions on Electron Devices*, vol. 41, no. 12, pp. 2357–2362, 1994.
- [2] S. Takagi *et al.*, “On the Universality of Inversion Layer Mobility in Si MOSFET’s: Part II—Effects of Surface Orientation,” *IEEE Transactions on Electron Devices*, vol. 41, no. 12, pp. 2363–2368, 1994.
- [3] H. Nakamura *et al.*, “Effects of Selecting Channel Direction in Improving Performance of Sub-100 nm MOSFETs Fabricated on (110) Surface Si Substrate,” *Japanese Journal of Applied Physics*, vol. 43, no. 4B, pp. 1723–1728, 2004.
- [4] H. M. Nayfeh *et al.*, “Influence of High Channel Doping on the Inversion Layer Electron Mobility in Strained Silicon n-MOSFETs,” *IEEE Electron Device Letters*, vol. 24, no. 4, pp. 248–250, 2003.
- [5] C. D. Young *et al.*, “(110) and (100) Sidewall-oriented FinFETs: A performance and reliability investigation,” *Solid-State Electronics*, vol. 78, pp. 2–10, December 2012.
- [6] A. T. Pham, C. Jungemann, and B. Meinerzhagen, “Modeling and validation of piezoresistive coefficients in Si hole inversion layers,” *Solid-State Electronics*, vol. 53, no. 12, pp. 1325–1333, 2009.
- [7] F. M. Bufler, A. Erlebach, and M. Oulmane, “Hole Mobility Model With Silicon Inversion Layer Symmetry and Stress-Dependent Piezoconductance Coefficients,” *IEEE Electron Device Letters*, vol. 30, no. 9, pp. 996–998, 2009.

## Chapter 5: Quality of Fitting and Extraction

### References

- [8] P. Packan *et al.*, "High Performance Hi-K + Metal Gate Strain Enhanced Transistors on (110) Silicon," in *IEDM Technical Digest*, San Francisco, CA, USA, pp. 1–4, December 2008.
- [9] R. Chau *et al.*, "High- $\kappa$ /Metal-Gate Stack and Its MOSFET Characteristics," *IEEE Electron Device Letters*, vol. 25, no. 6, pp. 408–410, 2004.
- [10] M. Cassé *et al.*, "Carrier Transport in  $\text{HfO}_2$ /Metal Gate MOSFETs: Physical Insight Into Critical Parameters," *IEEE Transactions on Electron Devices*, vol. 53, no. 4, pp. 759–768, 2006.
- [11] N. Stavitski *et al.*, "Evaluation of Transmission Line Model Structures for Silicide-to-Silicon Specific Contact Resistance Extraction," *IEEE Transactions on Electron Devices*, vol. 55, no. 5, pp. 1170–1176, 2008.
- [12] J. B. McKeon *et al.*, "Experimental Determination of Electron and Hole Mobilities in MOS Accumulation Layers," *IEEE Electron Device Letters*, vol. 18, no. 5, pp. 200–202, 1997.
- [13] Y. Asahi, *Physical parameters for 4H-SiC and 6H-SiC*, Internal Report, Mountain View, California: Synopsys, Inc., November 2012.
- [14] U. Lindefelt, "Doping-induced band edge displacements and band gap narrowing in 3C-, 4H-, 6H-SiC, and Si," *Journal of Applied Physics*, vol. 84, no. 5, pp. 2628–2637, 1998.
- [15] C. Persson, U. Lindefelt, and B. E. Sernelius, "Band gap narrowing in n-type and p-type 3C-, 2H-, 4H-, 6H-SiC, and Si," *Journal of Applied Physics*, vol. 86, no. 8, pp. 4419–4427, 1999.
- [16] S. C. Jain and D. J. Roulston, "A Simple Expression for Band Gap Narrowing (BGN) in Heavily Doped Si, Ge, GaAs and  $\text{Ge}_x\text{Si}_{1-x}$  Strained Layers," *Solid-State Electronics*, vol. 34, no. 5, pp. 453–465, 1991.
- [17] T. Hatakeyama *et al.*, "Impact ionization coefficients of 4H silicon carbide," *Applied Physics Letters*, vol. 85, no. 8, pp. 1380–1382, 2004.
- [18] H. Niwa, J. Suda, and T. Kimoto, "Temperature Dependence of Impact Ionization Coefficients in 4H-SiC," *Materials Science Forum*, vol. 778-780, pp. 461–466, 2014.
- [19] A. O. Konstantinov *et al.*, "Ionization rates and critical fields in 4H silicon carbide," *Applied Physics Letters*, vol. 71, no. 1, pp. 90–92, 1997.
- [20] Y. S. Touloukian and E. H. Buyco, *Specific Heat: Nonmetallic Solids*, Thermophysical Properties of Matter, TPRC Data Series, vol. 5, New York: IFI/Plenum, 1970.
- [21] Y. S. Touloukian and C. Y. Ho (eds.), *Thermal Conductivity—Nonmetallic Solids*, Thermophysical Properties of Matter, TPRC Data Series, vol. 2, New York: IFI/Plenum, 1970.
- [22] E. A. Burgemeister, W. von Muench, and E. Pettenpaul, "Thermal conductivity and electrical properties of 6H silicon carbide," *Journal of Applied Physics*, vol. 50, no. 9, pp. 5790–5794, 1979.

## Chapter 5: Quality of Fitting and Extraction

### References

- [23] D. Morelli *et al.*, “Carrier concentration dependence of the thermal conductivity of silicon carbide,” in *5th Silicon Carbide and Related Materials Conference*, Washington, DC, USA, pp. 313–315, November 1993.
- [24] D. T. Morelli *et al.*, “Phonon-electron scattering in single crystal silicon carbide,” *Applied Physics Letters*, vol. 63, no. 23, pp. 3143–3145, 1993.
- [25] W. J. Schaffer *et al.*, “Conductivity Anisotropy in Epitaxial 6H and 4H SiC,” in *MRS Symposium Proceedings, Diamond, SiC and Nitride Wide Bandgap Semiconductors*, vol. 339, San Francisco, CA, USA, pp. 595–600, April 1994.
- [26] M. Roschke and F. Schwierz, “Electron Mobility Models for 4H, 6H, and 3C SiC,” *IEEE Transactions on Electron Devices*, vol. 48, no. 7, pp. 1442–1447, 2001.
- [27] S. Kagamihara *et al.*, “Parameters required to simulate electric characteristics of SiC devices for *n*-type 4H–SiC,” *Journal of Applied Physics*, vol. 96, no. 10, pp. 5601–5606, 2004.
- [28] I. A. Khan and J. A. Cooper, Jr., “Measurement of High Field Electron Transport in Silicon Carbide,” *Materials Science Forum*, vol. 264-268, pp. 509–512, February 1998.
- [29] M. Lades, *Modeling and Simulation of Wide Bandgap Semiconductor Devices: 4H/6H-SiC*, PhD thesis, Technischen Universität, Munich, Germany, 2000.
- [30] A. Koizumi, J. Suda, and T. Kimoto, “Temperature and doping dependencies of electrical properties in Al-doped 4H-SiC epitaxial layers,” *Journal of Applied Physics*, vol. 106, no. 1, p. 013716, 2009.
- [31] J. Pernot, S. Contreras and J. Camassel, “Electrical transport properties of aluminum-implanted 4H–SiC,” *Journal of Applied Physics*, vol. 98, no. 2, p. 023706, 2005.
- [32] T. Troffer *et al.*, “Doping of SiC by Implantation of Boron and Aluminum,” *Physica Status Solidi (a)*, vol. 162, no. 1, pp. 277–298, 1997.
- [33] M. Noguchi *et al.*, “Determination of intrinsic phonon-limited mobility and carrier transport property extraction of 4H-SiC MOSFETs,” in *IEDM Technical Digest*, San Francisco, CA, USA, pp. 219–222, December 2017.
- [34] M. Noguchi *et al.*, “Hall effect mobility for SiC MOSFETs with increasing dose of nitrogen implantation into channel region,” *Japanese Journal of Applied Physics*, vol. 57, no. 4S, p. 04FR13, 2018.
- [35] T. Hatakeyama *et al.*, “Characterization of traps at nitrided SiO<sub>2</sub>/SiC interfaces near the conduction band edge by using Hall effect measurements,” *Applied Physics Express*, vol. 10, no. 4, p. 046601, 2017.
- [36] *Sentaurus™ Device User Guide*, Version T-2022.03, Mountain View, California: Synopsys, Inc., 2022.

## Chapter 5: Quality of Fitting and Extraction

### References

- [37] M. Noguchi *et al.*, "Carrier transport properties in inversion layer of Si-face 4H–SiC MOSFET with nitrided oxide," *Japanese Journal of Applied Physics*, vol. 58, no. 3, p. 031004, 2019.
- [38] W. M. Waller *et al.*, "Subthreshold Mobility in AlGaN/GaN HEMTs," *IEEE Transactions on Electron Devices*, vol. 63, no. 5, pp. 1861–1865, 2016.
- [39] S.-J. Chang *et al.*, "Investigation of channel mobility in AlGaN/GaN high-electron-mobility transistors," *Japanese Journal of Applied Physics*, vol. 55, no. 4, p. 044104, 2016.
- [40] S. Adachi, *Properties of Group-IV, III–V and II–VI Semiconductors*, West Sussex, England: John Wiley & Sons, 2005.
- [41] S. Adachi, *Properties of Semiconductor Alloys: Group-IV, III–V and II–VI Semiconductors*, West Sussex, England: John Wiley & Sons, 2009.
- [42] M. S. Abrahams, R. Braunstein, and F. D. Rosi, "Thermal, Electrical and Optical Properties of (In,Ga)As Alloys," *Journal of Physics and Chemistry of Solids*, vol. 10, no. 2–3, pp. 204–210, 1959.
- [43] D. G. Arasly, R. N. Ragimov, and M. I. Aliev, "Characteristics of phonon scattering in  $\text{Ga}_x\text{In}_{1-x}\text{As}$  solid solutions," *Soviet Physics Semiconductors*, vol. 24, no. 2, pp. 225–226, 1990.
- [44] S. Adachi, "Lattice thermal conductivity of group-IV and III-V semiconductor alloys," *Journal of Applied Physics*, vol. 102, p. 063502, September 2007.
- [45] R. E. Nahory, M. A. Pollack, and J. C. DeWinter, "Growth and characterization of liquid-phase epitaxial  $\text{In}_x\text{Ga}_{1-x}\text{As}$ ," *Journal of Applied Physics*, vol. 46, no. 2, pp. 775–782, 1975.
- [46] T. J. Kim *et al.*, "Dielectric functions of  $\text{In}_x\text{Ga}_{1-x}\text{As}$  alloys," *Physical Review B*, vol. 68, no. 11, p. 115323, 2003.
- [47] D. K. Gaskill *et al.*, "Band-gap determination by photoreflectance of InGaAs and InAlAs lattice matched to InP," *Applied Physics Letters*, vol. 56, no. 13, pp. 1269–1271, 1990.
- [48] I. Vurgaftman, J. R. Meyer, and L. R. Ram-Mohan, "Band parameters for III–V compound semiconductors and their alloys," *Journal of Applied Physics*, vol. 89, no. 11, pp. 5815–5875, 2001.
- [49] K. Alavi, R. L. Aggarwal, and S. H. Groves, "Interband magnetoabsorption of  $\text{In}_{0.53}\text{Ga}_{0.47}\text{As}$ ," *Physical Review B*, vol. 21, no. 3, pp. 1311–1315, 1980.
- [50] R. J. Warburton *et al.*, "Valence band spin splitting in strained  $\text{In}_{0.18}\text{Ga}_{0.82}\text{As}/\text{GaAs}$  quantum wells," *Semiconductor Science and Technology*, vol. 6, no. 5, pp. 359–364, 1991.
- [51] N. J. Traynor *et al.*, "Highly nonlinear Zeeman splitting of excitons in semiconductor quantum wells," *Physical Review B*, vol. 55, no. 23, pp. 15701–15705, 1997.

## Chapter 5: Quality of Fitting and Extraction

### References

- [52] S. C. Jain, J. M. McGregor, and D. J. Roulston, "Band-gap narrowing in novel III-V semiconductors," *Journal of Applied Physics*, vol. 68, no. 7, pp. 3747–3749, 1990.
- [53] G. Borghs *et al.*, "Band-gap narrowing in highly doped *n*- and *p*-type GaAs studied by photoluminescence spectroscopy," *Journal of Applied Physics*, vol. 66, no. 9, pp. 4381–4386, 1989.
- [54] B. J. Aitchison *et al.*, "Enhanced hot-electron photoluminescence from heavily carbon-doped GaAs," *Applied Physics Letters*, vol. 56, no. 12, pp. 1154–1156, 1990.
- [55] D. Olego and M. Cardona, "Photoluminescence in heavily doped GaAs. I. Temperature and hole-concentration dependence," *Physical Review B*, vol. 22, no. 2, pp. 886–893, 1980.
- [56] Z. H. Lu, M. C. Hanna, and A. Majerfeld, "Determination of band gap narrowing and hole density for heavily C-doped GaAs by photoluminescence spectroscopy," *Applied Physics Letters*, vol. 64, no. 1, pp. 88–90, 1994.
- [57] B. P. Yan, J. S. Luo, and Q. L. Zhang, "Study of band-gap narrowing effect and nonradiative recombination centers for heavily C-doped GaAs by photoluminescence spectroscopy," *Journal of Applied Physics*, vol. 77, no. 9, pp. 4822–4824, 1995.
- [58] H. Yao and A. Compaan, "Plasmons, photoluminescence, and band-gap narrowing in very heavily doped *n*-GaAs," *Applied Physics Letters*, vol. 57, no. 2, pp. 147–149, 1990.
- [59] N. A. Semikolenova, I. M. Nesmelova, and E. N. Khabarov, "Investigation of the impurity interaction mechanism in indium arsenide," *Soviet Physics Semiconductors*, vol. 12, no. 10, pp. 1139–1142, 1978.
- [60] M. Sotoodeh, A. H. Khalid, A. A. Rezazadeh, "Empirical low-field mobility model for III–V compounds applicable in device simulation codes," *Journal of Applied Physics*, vol. 87, no. 6, pp. 2890–2900, 2000.
- [61] Ch. Köpf, H. Kosina, and S. Selberherr, "Physical Models for Strained and Relaxed GaInAs Alloys: Band Structure and Low-Field Transport," *Solid-State Electronics*, vol. 41, no. 8, pp. 1139–1152, 1997.
- [62] Y. Xuan *et al.*, "Submicrometer Inversion-Type Enhancement-Mode InGaAs MOSFET With Atomic-Layer-Deposited Al<sub>2</sub>O<sub>3</sub> as Gate Dielectric," *IEEE Electron Device Letters*, vol. 28, no. 11, pp. 935–938, 2007.
- [63] S. Suthram *et al.*, "Strain Additivity in III-V Channels for CMOSFETs beyond 22nm Technology Node," in *Symposium on VLSI Technology*, Honolulu, HI, USA, pp. 182–183, June 2008.
- [64] L. Xia and J. A. del Alamo, "Mobility Enhancement in Indium-rich N-channel In<sub>x</sub>Ga<sub>1-x</sub>As HEMTs by Application of <110> Uniaxial Strain," in *International Conference on Indium Phosphide and Related Materials (IPRM)*, Takamatsu, Japan, pp. 1–4, May 2010.

## Chapter 5: Quality of Fitting and Extraction

### References

- [65] S. H. Kim *et al.*, "Enhancement Technologies and Physical Understanding of Electron Mobility in III-V  $n$ -MOSFETs with Strain and MOS Interface Buffer Engineering," in *IEDM Technical Digest*, Washington, DC, USA, pp. 311–314, December 2011.
- [66] C. Rossel *et al.*, "Strain effects on  $n$ -InGaAs heterostructure-on-insulator made by direct wafer bonding," *Solid-State Electronics*, vol. 98, pp. 88–92, August 2014.
- [67] A. Nainani *et al.*, "Study of piezoresistance under uniaxial stress for technologically relevant III-V semiconductors using wafer bending experiments," *Applied Physics Letters*, vol. 96, no. 24, p. 242110, 2010.
- [68] F. Schäffler, "Silicon-Germanium ( $\text{Si}_{1-x}\text{Ge}_x$ )," *Properties of Advanced Semiconductor Materials: GaN, AlN, InN, BN, SiC, SiGe*, M. E. Levinshtein, S. L. Rumyantsev, and M. S. Shur (eds.), New York: John Wiley & Sons, 2001.
- [69] M. Wagner, *Simulation of Thermoelectric Devices*, PhD thesis, Technischen Universität Wien, Austria, November 2007.
- [70] R. Cheaito *et al.*, "Experimental Investigation of Size Effects on the Thermal Conductivity of Silicon-Germanium Alloy Thin Films," *Physical Review Letters*, vol. 109, no. 19, p. 195901, 2012.
- [71] I. Yonenaga *et al.*, "Thermal and Electrical Properties of Czochralski Grown GeSi Alloys," in *Proceedings of the 17th International Conference on Thermoelectrics (ICT)*, Nagoya, Japan, pp. 402–405, May 1998.
- [72] P. D. Maycock, "Thermal Conductivity of Silicon, Germanium, III–V Compounds and III–V Alloys," *Solid-State Electronics*, vol. 10, no. 3, pp. 161–168, 1967.
- [73] S.-M. Lee, D. G. Cahill, and R. Venkatasubramanian, "Thermal conductivity of Si–Ge superlattices," *Applied Physics Letters*, vol. 70, no. 22, pp. 2957–2959, 1997.
- [74] C. Penn, T. Fromherz, and G. Bauer, "Energy gaps and band structure of SiGe and their temperature dependence," *Properties of Silicon Germanium and SiGe:Carbon*, EMIS Datareviews Series, no. 24, London: INSPEC, 2000.
- [75] O. A. Golikova, B. Ya. Moizhes, and L. S. Stil'bans, "Hole Mobility of Germanium as a Function of Concentration and Temperature," *Soviet Physics - Solid State*, vol. 3, no. 10, pp. 2259–2265, 1962.
- [76] V. I. Fistul', M. I. Iglitsyn, and É. M. Omel'yanovskii, "Mobility of Electrons in Germanium Strongly Doped With Arsenic," *Soviet Physics - Solid State*, vol. 4, no. 4, pp. 784–785, 1962.
- [77] S. M. Sze and J. C. Irvin, "Resistivity, Mobility and Impurity Levels in GaAs, Ge, and Si at 300° K," *Solid-State Electronics*, vol. 11, no. 6, pp. 599–602, 1968.
- [78] S. Mirabella *et al.*, "Activation and carrier mobility in high fluence B implanted germanium," *Applied Physics Letters*, vol. 92, p. 251909, June 2008.

## Chapter 5: Quality of Fitting and Extraction

### References

- [79] L. Hutin *et al.*, "Activation level in boron-doped thin germanium-on-insulator (GeOI): Extraction method and impact of mobility," *Materials Science in Semiconductor Processing*, vol. 11, no. 5–6, pp. 267–270, 2008.
- [80] O. Penzin *et al.*, "Kinetic Velocity Model to Account for Ballistic Effects in the Drift-Diffusion Transport Approach," *IEEE Transactions on Electron Devices*, vol. 64, no. 11, pp. 4599–4606, 2017.

# A

## Physical Model Interface Models

---

*This appendix describes the physical model interface (PMI) models of Advanced Calibration Device.*

---

### Features of the MCmob and SBmob Models

The PMI models `MCmob` and `SBmob` of Sentaurus Device are based on nonlinear relations between the mobility enhancement and the stress components where the coefficients of the equations are extracted from reference tools such as Sentaurus Band Structure (`SBmob`) or Sentaurus Device Monte Carlo (`MCmob`). The corresponding command file sections are explained in [Chapter 2 on page 21](#).

The features of the `MCmob` model are as follows:

- Calculates the hole mobility enhancement by stress for silicon and SiGe for mole fractions from 0% to 100% for the channel direction and wafer orientation combinations  $<110>/(001)$ ,  $<110>/(110)$ , and  $<100>/(001)$
- Calculates the electron mobility enhancement by stress for silicon for the channel direction and wafer orientation combinations  $<110>/(001)$ ,  $<110>/(110)$ , and  $<100>/(001)$
- Determines the crystallographic surface or interface orientation automatically

The features of the `SBmob` model are as follows:

- Calculates the electron and hole mobility enhancement by stress for silicon and SiGe for mole fractions from 0% to 100% for the channel direction and wafer orientation combinations  $<110>/(001)$ ,  $<110>/(110)$ , and  $<100>/(001)$
- Determines the crystallographic surface or interface orientation automatically

These models are designed for semiconductor–isolator interfaces as in a metal–insulator–semiconductor (MIS) structure where the bulk symmetry typical for the standard piezoresistance model is broken. This makes it necessary to determine the direction of the interface normal with respect to the device coordinate system.

## Appendix A: Physical Model Interface Models

### Parameters

#### Note:

This detection is not performed fully and automatically, and you must specify parameters in the Sentaurus Device parameter file (see [Parameters](#)).

---

## Parameters

You use the same parameters and parameter syntax for both the `MCmob` and `SBmob` models.

*Table 16 Parameters of the MCmob and SBmob models*

Parameter	Description
<code>autoorientation</code>	Switches on the detection of the crystallographic surface orientation. Valid options are: <ul style="list-style-type: none"><li>• 0: No detection of crystallographic surface orientation, but crystallographic surface orientation is defined by <code>waferori</code>.</li><li>• 1: Detects crystallographic surface orientation.</li><li>• 2: Detects crystallographic surface orientation and adaptation of local coordinate system (coordinate system used to match the stress components to the MIS plane orientation and channel direction at each mesh node) for FinFET-like structures with &lt;110&gt; channel orientation.</li><li>• 3: Detects crystallographic surface orientation; local coordinate systems are defined using parameters in the Sentaurus Device parameter file.</li></ul> Default: 0
<code>channelori</code>	Sets the channel direction. Valid options are: <ul style="list-style-type: none"><li>• 100: &lt;100&gt; channel direction.</li><li>• 110: &lt;110&gt; channel direction.</li></ul> Default: 110
<code>ConstantMoleFraction</code>	Switches between reading the mole-fraction distribution from a TDR file and setting the constant mole fraction in the parameter file. Valid options are: <ul style="list-style-type: none"><li>• 0: Read from TDR file.</li><li>• 1: User sets mole fraction in Sentaurus Device parameter file.</li></ul>
<code>ConstantStress</code>	Switches between reading the distribution of stress components from a TDR file and setting the constant stress components in the parameter file. Valid options are: <ul style="list-style-type: none"><li>• 0: Read from TDR file.</li><li>• 1: User sets constant stress components in Sentaurus Device parameter file.</li></ul>

## Appendix A: Physical Model Interface Models

### Parameters

*Table 16 Parameters of the MCmob and SBmob models (Continued)*

Parameter	Description
coordinatesystem	Specifies the global coordinate system in Sentaurus Device. Default: 0 See <a href="#">Specifying Device Coordinate Systems on page 108</a> .
corrections	Controls interpolation in the stress space. Valid options are: <ul style="list-style-type: none"><li>• 0: Results in a linear superposition of the mobility response to the uniaxial stress components.</li><li>• 1: Switches on cross-corrections (terms with mixed stress components).</li></ul> You must define the cross-corrections in the parameter file (default: all cross-corrections are set to zero). Default: 0 <b>Note:</b> This parameter is available only for the MCmob model.
DeltaMuPrefactors100c100x	Scales the mobility enhancement caused by stress in the current flow direction for channel direction <100> and surface orientation (100).
DeltaMuPrefactors100c100y	Scales the mobility enhancement caused by stress normal to the MIS interface for channel direction <100> and surface orientation (100).
DeltaMuPrefactors100c100z	Scales the mobility enhancement caused by stress in-plane with the MIS interface and normal to the current flow direction for channel direction <100> and surface orientation (100).
DeltaMuPrefactors100c110x	Scales the mobility enhancement caused by stress in the current flow direction for channel direction <110> and surface orientation (100).
DeltaMuPrefactors100c110y	Scales the mobility enhancement caused by stress normal to the MIS interface for channel direction <110> and surface orientation (100).
DeltaMuPrefactors100c110z	Scales the mobility enhancement caused by stress in-plane with the MIS interface and normal to the current flow direction for channel direction <110> and surface orientation (100).
DeltaMuPrefactors110c100x	Scales the mobility enhancement caused by stress in the current flow direction for channel direction <100> and surface orientation (110).

## Appendix A: Physical Model Interface Models

### Parameters

*Table 16 Parameters of the MCmob and SBmob models (Continued)*

Parameter	Description
DeltaMuPrefactors110c100y	Scales the mobility enhancement caused by stress normal to the MIS interface for channel direction <100> and surface orientation (110).
DeltaMuPrefactors110c100z	Scales the mobility enhancement caused by stress in-plane with the MIS interface and normal to the current flow direction for channel direction <100> and surface orientation (110).
DeltaMuPrefactors110c110x	Scales the mobility enhancement caused by stress in the current flow direction for channel direction <110> and surface orientation (110).
DeltaMuPrefactors110c110y	Scales the mobility enhancement caused by stress normal to the MIS interface for channel direction <110> and surface orientation (110).
DeltaMuPrefactors110c110z	Scales the mobility enhancement caused by stress in-plane with the MIS interface and normal to the current flow direction for channel direction <110> and surface orientation (110).
DeltaMuPrefactors111c110x	Scales the mobility enhancement caused by stress in the current flow direction for channel direction <110> and surface orientation (111).
DeltaMuPrefactors111c110y	Scales the mobility enhancement caused by stress normal to the MIS interface for channel direction <110> and surface orientation (111).
DeltaMuPrefactors111c110z	Scales the mobility enhancement caused by stress in-plane with the MIS interface and normal to the current flow direction for channel direction <110> and surface orientation (111).
MoleFraction	SiGe mole fraction when ConstantMoleFraction=1.
referenceplanecoordinatex1	Coordinate of the first reference plane in the x-direction of the device coordinate system (yz plane, default: 1e6).
referenceplanecoordinatex2	Coordinate of the second reference plane in the x-direction of the device coordinate system (yz plane, default: 1e6).
referenceplanecoordinatey1	Coordinate of the first reference plane in the y-direction of the device coordinate system (xz plane, default: 1e6).
referenceplanecoordinatey2	Coordinate of the second reference plane in the y-direction of the device coordinate system (xz plane, default: 1e6).

## Appendix A: Physical Model Interface Models

### Parameters

*Table 16 Parameters of the MCmob and SBmob models (Continued)*

Parameter	Description
referenceplanecoordinatez1	Coordinate of the first reference plane in the z-direction of the device coordinate system (xy plane, default: 1e6).
referenceplanecoordinatez2	Coordinate of the second reference plane in the z-direction of the device coordinate system (xy plane, default: 1e6).
referenceplanesystemx1	Defines the local coordinate system for the reference plane parallel to the yz plane at the position $x=referenceplanecoordinatez1$ (default: -1).
referenceplanesystemx2	Defines the local coordinate system for the reference plane parallel to the yz plane at the position $x=referenceplanecoordinatez2$ (default: -1).
referenceplanesystemy1	Defines the local coordinate system for the reference plane parallel to the xz plane at the position $y=referenceplanecoordinatez1$ (default: -1).
referenceplanesystemy2	Defines the local coordinate system for the reference plane parallel to the xz plane at the position $y=referenceplanecoordinatez2$ (default: -1).
referenceplanesystemz1	Defines the local coordinate system for the reference plane parallel to the xy plane at the position $y=referenceplanecoordinatez1$ (default: -1).
referenceplanesystemz2	Defines the local coordinate system for the reference plane parallel to the xy plane at the position $y=referenceplanecoordinatez2$ (default: -1).
Stress_xx	$S_{xx}$ stress component in the device coordinate system when ConstantStress=1.
Stress_yy	$S_{yy}$ stress component in the device coordinate system when ConstantStress=1.
Stress_zz	$S_{zz}$ stress component in the device coordinate system when ConstantStress=1.
waferori	Sets the wafer orientation. Valid options are: <ul style="list-style-type: none"><li>• 100: (001) wafer orientation.</li><li>• 110: (110) wafer orientation.</li></ul> Default: 100

## Appendix A: Physical Model Interface Models

### Parameters

---

## Specifying Device Coordinate Systems

For planar devices with one conducting MIS plane, you can use the default parameters and no additional information is necessary when a device coordinate system has the following configuration:

- x: Channel direction
- y: Normal to the MIS interface
- z: In-plane with the MIS interface but normal to the channel direction, and the wafer orientation equals (100)

For other device coordinate systems and one conducting MIS plane, you must set the parameter `coordinatesystem` in the Sentaurus Device parameter file for the following configurations:

- `coordinatesystem=1:`  
x: Channel direction  
z: Direction normal to the MIS interface  
y: In-plane with the MIS interface but normal to the channel direction
- `coordinatesystem=2:`  
y: Channel direction  
x: Direction normal to the MIS interface  
z: In-plane with the MIS interface but normal to the channel direction
- `coordinatesystem=3:`  
y: Channel direction  
z: Direction normal to the MIS interface  
x: In-plane with the MIS interface but normal to the channel direction
- `coordinatesystem=4:`  
z: Channel direction  
x: Direction normal to the MIS interface  
y: In-plane with the MIS interface but normal to the channel direction
- `coordinatesystem=5:`  
z: Channel direction  
y: Direction normal to the MIS interface  
x: In-plane with the MIS interface but normal to the channel direction

---

## Specifying Local Coordinate Systems

For general applications and for FinFETs with <100> channel direction and (100) wafer orientation, you must define the local coordinate system manually in the Sentaurus Device parameter file using the `referenceplanesystem*` parameters.

## Appendix A: Physical Model Interface Models

### Parameters

You can specify the following configurations of the local coordinate system:

- For a MIS interface in the xz plane close to `referenceplanecoordinatey1` or `referenceplanecoordinatey2`:
  - `referenceplanesystemy1=0` or `referenceplanesystemy2=0` specifies:
    - x: Channel direction
    - y: Direction normal to the MIS interface
    - z: In-plane with the MIS interface but normal to the channel direction
  - `referenceplanesystemy1=1` or `referenceplanesystemy2=1` specifies:
    - z: Channel direction
    - y: Direction normal to the MIS interface
    - x: In-plane with the MIS interface but normal to the channel direction
- For a MIS interface in the xy plane close to `referenceplanecoordinatez1` or `referenceplanecoordinatez2`:
  - `referenceplanesystemz1=0` or `referenceplanesystemz2=0` specifies:
    - x: Channel direction
    - z: Direction normal to the MIS interface
    - y: In-plane with the MIS interface but normal to the channel direction
  - `referenceplanesystemz1=1` or `referenceplanesystemz2=1` specifies:
    - y: Channel direction
    - z: Direction normal to the MIS interface
    - x: In-plane with the MIS interface but normal to the channel direction
- For a MIS interface in the yz plane close to `referenceplanecoordinatex1` or `referenceplanecoordinatex2`:
  - `referenceplanesystemx1=0` or `referenceplanesystemx2=0` specifies:
    - y: Channel direction
    - x: Direction normal to the MIS interface
    - z: In-plane with the MIS interface but normal to the channel direction
  - `referenceplanesystemx1=1` or `referenceplanesystemx2=1` specifies:
    - z: Channel direction
    - x: Direction normal to the MIS interface
    - y: In-plane with the MIS interface but normal to the channel direction

For the simulation of a planar MIS transistor, using the `waferori` and `coordinatesystem` parameters is sufficient. Instead of using `waferori`, you can set `autoorientation=1` to detect automatically the crystallographic wafer or surface orientation. In this case, `waferori` is overwritten by the automatically detected orientation.

For other applications or for FinFETs with <100> channel orientation, you can use the `referenceplanesystem*` parameters to define the local coordinate system where the

## **Appendix A: Physical Model Interface Models**

### Parameters

crystallographic surface orientation is detected automatically. For that, set autoorientation=3.

---

## **Using Parameters**

The following examples illustrate how to use the parameters for different orientations and coordinate systems.

### **Example 1**

Planar MISFET with (100) wafer orientation and device coordinate system where x=channel direction, y=wafer normal direction, and z=device width direction:

Use default parameter values.

### **Example 2**

Planar MISFET with (100) wafer orientation and device coordinate system where x=channel direction, z=wafer normal direction, and y=device width direction, specify:

```
coordinatesystem=1
```

### **Example 3**

Planar MISFET with (110) wafer orientation and device coordinate system where x=channel direction, z=wafer normal direction, and y=device width direction, specify either:

```
coordinatesystem=1  
autoorientation=1
```

or:

```
coordinatesystem=1  
waferori=1
```

### **Example 4**

FinFET with (100) wafer orientation, <110> channel orientation, and device coordinate system where x=channel direction, y=wafer normal direction, and z=fin width direction, specify:

```
autoorientation=2
```

### **Example 5**

FinFET with (100) wafer orientation, <110> channel orientation, and device coordinate system where x=channel direction, z=wafer normal direction, and y=fin width direction, specify:

```
coordinatesystem=1  
autoorientation=2
```

## Appendix A: Physical Model Interface Models

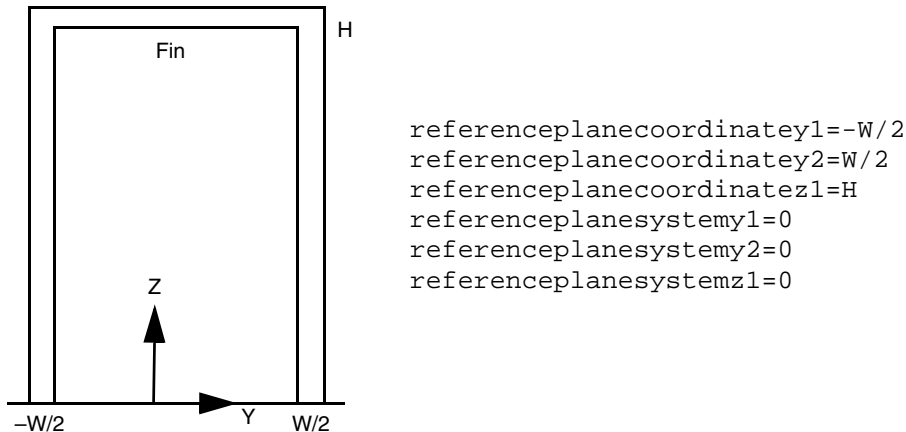
### Parameter Interface

#### Example 6

FinFET with (100) wafer orientation, <100> channel orientation, and device coordinate system where x=channel direction, z=wafer normal direction, and y=fin width direction, specify:

```
coordinatesystem=1
autoorientation=3
referenceplanesystemy1=0
referenceplanesystemy2=0
referenceplanesystemz1=0
referenceplanecoordinatey1=-@W/2.0@
referenceplanecoordinatey2=@W/2.0@
referenceplanecoordinatez1=@H@
```

Figure 56 Cross section of a FinFET structure normal to the channel direction with height ( $H$ ) and width ( $W$ ); the origin of the coordinate system is at  $y=0$  and  $z=0$



---

### Parameter Interface

The `MCmob` and `SBmob` models have a parameter interface that allows you to change all the coefficients of the fit and interpolation functions. In this way, you can define the mobility response to mechanical stress using the Sentaurus Device parameter file. For historical reasons, the syntax of the interface differs for `MCmob` and `SBmob`. [Parameter Interface and Equations of SBmob Model on page 112](#) explains the parameter interface of `SBmob` and its related implementations and equations.

Some settings must be specified in the Sentaurus Device command file. The `Type` parameter defines the device type: NMOS (`Type=0`) or PMOS (`Type=1`). The `Kanda` option switches on the Kanda model (see the *Sentaurus™ Device User Guide*).

## Appendix A: Physical Model Interface Models

### Parameter Interface

Additional parameter files and explanations are available on request. Contact TCAD Support (see [Contacting Your Local TCAD Support Team Directly](#)) or Engineering & Consulting ([tcad-services@synopsys.com](mailto:tcad-services@synopsys.com)).

---

## Parameter Interface and Equations of SBmob Model

The following polynomial describes the mobility response to the uniaxial stress components  $s_{xx}$ ,  $s_{yy}$ , and  $s_{zz}$ :

$$\frac{\Delta\mu}{\mu} = a_6 \cdot s_i^1 + a_5 \cdot s_i^2 + a_4 \cdot s_i^3 + a_3 \cdot s_i^4 + a_2 \cdot s_i^5 + a_1 \cdot s_i^6 \quad (4)$$

where  $i$  is  $xx$ ,  $yy$ , or  $zz$ . [Equation 4](#) considers one stress component only and sets the other two stress components to zero.

The parameter interface allows you to define the coefficients of the polynomials for the mobility response to uniaxial stress. [Table 17](#) lists most of these coefficients. Those not listed can be derived from information in the table.

*Table 17 Coefficients of polynomials for mobility response to uniaxial stress*

Coefficient	Description
aunics100c1106h	Coefficient $a_6$ of the hole mobility response to stress in the channel direction for (100) surface orientation and <110> channel direction. The other five coefficients are named as follows: <ul style="list-style-type: none"><li>• aunics100c1105h</li><li>• aunics100c1104h</li><li>• aunics100c1103h</li><li>• aunics100c1102h</li><li>• aunics100c1101h</li></ul>
aunins100c1101h	Coefficient $a_1$ of the hole mobility response to the stress normal to the MIS interface for (100) surface orientation and <110> channel direction.
auniws100c1001h	Coefficient $a_1$ of the hole mobility response to stress in the width direction of the device for (100) surface orientation and <100> channel direction.
auniws100c1101h	Coefficient $a_1$ of the hole mobility response to stress in the width direction of the device for (100) surface orientation and <110> channel direction.
auniws110c1001h	Coefficient $a_1$ of the hole mobility response to stress in the width direction of the device for (110) surface orientation and <100> channel direction.
auniws110c1101h	Coefficient $a_1$ of the hole mobility response to stress in the width direction of the device for (110) surface orientation and <110> channel direction.

## Appendix A: Physical Model Interface Models

### Parameter Interface

All  $a_i$  coefficients are mole fraction dependent. You can define the mole fraction dependency in the parameter file using the following syntax (default: 11 mole fraction positions at 0, 0.1, 0.2, 0.3, 0.4, 0.5, 0.6, 0.7, 0.8, 0.9, and 1.0):

$$a_i = (0, 1, 2, 3, 4, 5, 6, 7, 8, 9, 10) \text{ (arbitrary values are used here)}$$

To improve interpolation for high stress and for cases where the mobility response becomes independent of the stress or behaves linearly, additional coefficients for the mobility response to uniaxial stress are introduced. In the parameter file, these coefficients have the same name and syntax as the parameters for the  $a_i$  coefficients but have higher numbers (see [Table 18](#)).

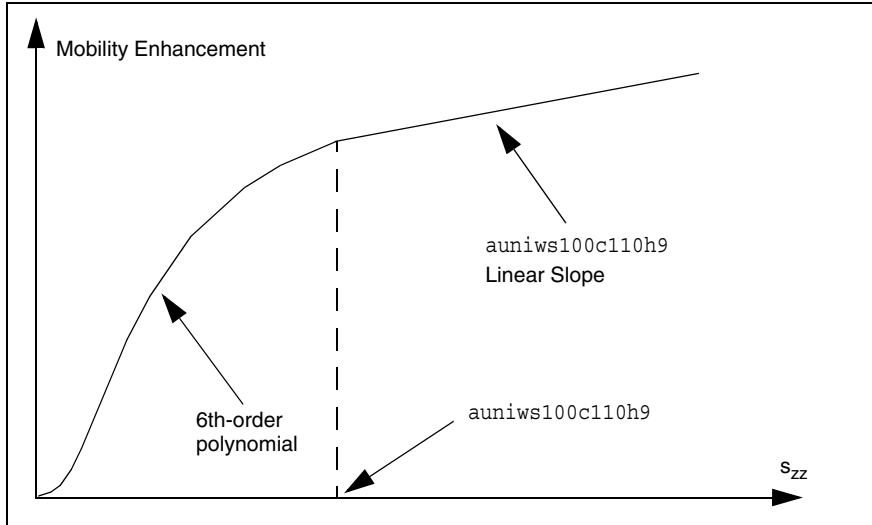
*Table 18 Additional coefficients of polynomials for mobility response to uniaxial stress*

Coefficient	Description
auniws100c1107h	Sets the negative stress value in GPa for the switch between the 6th-order polynomial and linear slope for the hole mobility response to stress in the width direction of the device for (100) surface orientation and <110> channel direction (see <a href="#">Figure 57 on page 114</a> ).
auniws100c1108h	Sets the slope in 1/Pa for the linear slope for stress values less than auniws100c1107h for the hole mobility response to stress in the width direction of the device for (100) surface orientation and <110> channel direction (see <a href="#">Figure 57</a> ).
auniws100c1109h	Sets the positive stress value in GPa for the switch between the 6th-order polynomial and linear slope for the hole mobility response to stress in the width direction of the device for (100) surface orientation and <110> channel direction (see <a href="#">Figure 57</a> ).
auniws100c11010h	Sets the slope in 1/Pa for the linear slope for stress values greater than auniws100c1109h for the hole mobility response to stress in the width direction of the device for (100) surface orientation and <110> channel direction (see <a href="#">Figure 57</a> ).

## Appendix A: Physical Model Interface Models

PMI for Calculating the Sheet Resistance

Figure 57 Use of the ai parameters in fitting uniaxial stress curves



---

## PMI for Calculating the Sheet Resistance

For the calculation of sheet resistance, you can use the Sentaurus Device PMI `sheetresistance`. In this approach, Sentaurus Device solves the Poisson equation or the complete set of drift-diffusion equations using an arbitrary doping profile as input. Then, the PMI calculates the sheet resistance using [Equation 5](#):

$$R_s = \frac{1}{e \cdot \int_0^t \mu_n \cdot n \cdot dx} \quad \text{in } \Omega/\text{square} \quad (5)$$

All mobility models that are available in Sentaurus Device can be used together with this PMI.  $R_s$  is written as a Sentaurus Workbench design-of-experiments parameter into the log file of Sentaurus Device and can be used by Sentaurus Workbench for further analysis. The input syntax for the Sentaurus Device command file is:

```
CurrentPlot {
    PMIModel (
        Name = "sheetresistance"
        rs_name = "sheetres"
        # BoxMin = (-1.0) BoxMax = (0.05)    # With this command, you can
                                                # change the integration interval,
                                                # for example, in cases where an
                                                # adjustment of the integration depth
                                                # is necessary.
    )
}
```

where `sheetres` is the name of the design-of-experiments parameter (default: `Rs_sim`).